doi.org/10.26434/chemrxiv.12854813.v1

Visible-Light-Promoted Metal-Free Ammoxidation of C(sp3)-H bonds

Kathiravan Murugesan, Karsten Donabauer, Burkhard Koenig

Submitted date: 24/08/2020 • Posted date: 24/08/2020

Citation information: Murugesan, Kathiravan; Donabauer, Karsten; Koenig, Burkhard (2020): Visible-Light-Promoted Metal-Free Ammoxidation of C(sp3)-H bonds. ChemRxiv. Preprint. https://doi.org/10.26434/chemrxiv.12854813.v1

The metal-free activation of C(sp^3)-H bonds to value-added products is of paramount importance in organic synthesis. Herein, we report the use of the commercially available organic dye 2,4,6-triphenylpyrylium tetrafluoroborate (TPP) for the conversion of methylarenes to the corresponding aryl nitriles via a photo process. Applying this methodology, a variety of cyanobenzenes have been synthesized in good to excellent yield under metal- and cyanide-free conditions. We demonstrate the scope of the method with over 50 examples including late-stage functionalization of drug molecules (celecoxib) and complex structures such as L-menthol, amino acids and cholesterol derivatives. Further, the presented synthetic protocol is applicable for gram-scale reactions. In addition to methylarenes, selected examples for the cyanation of aldehydes, alcohols and oximes are demonstrated as well. Detailed mechanistic investigations have been carried out using time-resolved luminescence quenching studies, control experiments and NMR- spectroscopic as well as kinetic studies, all supporting the proposed catalytic cycle.

File list (2)

Visible-Light-Promoted Metal-Free Ammoxidation of C(sp^3)-H bonds

Kathiravan Murugesan[a], Karsten Donabauer[a], and Burkhard König*[a]

[a]Faculty of Chemistry and Pharmacy, University of Regensburg, Germany.

KEYWORDS. Photoredox catalysis, nitriles, C-H functionalization, methylarenes, ammoxidation.

ABSTRACT: The metal-free activation of C(sp^3)-H bonds to value-added products is of paramount importance in organic synthesis. Herein, we report the use of the commercially available organic dye 2,4,6-triphenylpyrylium tetrafluoroborate (TPP) for the conversion of methylarenes to the corresponding aryl nitriles via a photo process. Applying this methodology, a variety of cyanobenzenes have been synthesized in good to excellent yield under metal- and cyanide-free conditions. We demonstrate the scope of the method with over 50 examples including late-stage functionalization of drug molecules (celecoxib) and complex structures such as L-menthol, amino acids and cholesterol derivatives. Further, the presented synthetic protocol is applicable for gram-scale reactions. In addition to methylarenes, selected examples for the cyanation of aldehydes, alcohols and oximes are demonstrated as well. Detailed mechanistic investigations have been carried out using time-resolved luminescence quenching studies, control experiments and NMR- spectroscopic as well as kinetic studies, all supporting the proposed catalytic cycle.

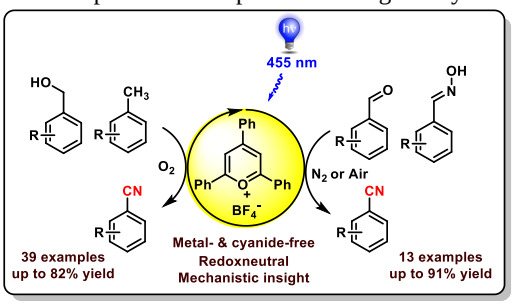

INTRODUCTION

Transition-metal based catalysts have an indispensable role in several chemical reactions,[1] industrial production,[1a-e, 1h] fine and bulk chemical synthesis.[1t] However, due to their high price,[2] less abundance[3] and toxicity,[4] the interest in using alternative metal-free catalysts is growing within the scientific community, especially for the late-stage functionalization of inert C(sp^3)-H bonds.[5] During the last two decades, several transition-metal based catalysts[1q, 6] have been developed for the activation of C-H bonds in sp^3 centres via thermal and photochemical pathways.[1q, 6] One of the most important transformations is the conversion of petroleum by-products into fine chemicals,[1a, 1b] e.g. the synthesis of benzonitrile from toluene.[1b, 1c] Industrially, benzonitrile is produced by ammoxidation of toluene using a transition-metal catalyst (vanadium) and applying a high NH_3 and O_2 pressure at 300-500 °C.[1b, 1c] Although the industrial ammoxidation process is an atom economic and sustainable route for the synthesis of nitriles starting from the unfunctionalized CH_3 group, but several functional groups are not tolerated due to the high reaction temperature and pressure.[1b, 1c] The nitrile moiety is an essential functional group in various drugs and bioactive compounds,[7] as well as an important building block for the preparation of fine and bulk chemicals, such as amines, carboxylic acids, amides and esters.[8] In conventional approaches, nitriles have been synthesized using the Sandmeyer reaction,[9] Rosenmund-von Braun reaction[10] and halide/CN exchange.[11] Further, transition-metal and photoredox catalyzed ammoxidations of aldehydes have been reported.[12] A few examples for the synthesis of nitriles from sp^2 C-H bonds via photocatalysis were reported by Nicewicz[13] and others.[14] However, the above-mentioned methods often suffer from several drawbacks, such as the use of transition metals leading to metal residue waste, high temperature, low selectivity or the generation of toxic cyanide. [11]

The direct conversion of methylarenes to nitriles in a one-step procedure is highly desired, but one-pot protocols to prepare nitriles from toluene are underdeveloped.[15] Wang et al. reported[15a] a Palladium-catalyzed cyanation of methylarenes in 2013, using an over stoichiometric amount of *t*BuONO and NHPI at 70 °C.

Scheme 1. Industrial ammoxidation process

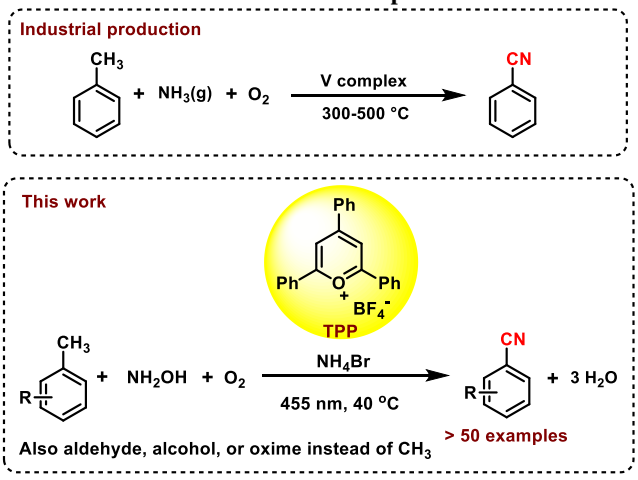

Recently, Kang and co-workers[15b] reported a similar strategy to Wang, where $AlCl_3$ was used as Lewis acid for the conversion of the oxime intermediates to nitriles at 80 °C. Major drawbacks of the reported methods are the harsh reaction conditions together with the use of hazardous reagents and transition metals.

In principle, a greener way to produce nitriles is by an oxidation process using molecular oxygen or simply air. Interestingly, a few examples to synthesize nitriles from alcohols[16] or amines[17] employing oxygen as oxidant are known to date.

However, the reported methods mainly rely on transition metal catalysts and applying harsh reaction conditions (> 100 °C).

We envisioned that an alternative metal- and cyanide-free methylarene to nitrile protocol could be developed by using a visible-light-assisted ammoxidation approach. Several challenges need to be addressed for this aim, such as the desired, yet difficult oxidation of the methylarene substrate (e.g. $E_{1/2}$ = +2.36 V vs SCE for toluene),[18] especially in case of electron deficient substituents, opposed to a more facile oxidation of ammonia ($E_{1/2}$ = + 0.63 V vs SCE),[19] and the prevention of an over oxidation of the methylarenes to the carboxylic acid. Herein we describe the use of the commercially available organic dye 2,4,6-triphenylpyrylium tetrafluoroborate (TPP)[20] for the synthesis of nitriles from methylarenes. In addition to this, a detailed mechanistic investigations was carried out to support our mechanistic hypothesis. All experimental results and spectroscopic analyses support the proposed catalytic cycle. To the best of our knowledge, this is the first example for a photocatalytic ammoxidation of methylarenes using abundant feedstock materials, ammonium salts and molecular oxygen without the use of metals and toxic reagents.

RESULTS AND DISCUSSION

At the start of our investigation, we tested different commercially available organic dyes for the desired transformation (Table 1).

Table 1. Organic dye photocatalysts in the ammoxidation of methyl 4-methylbenzoate to methyl 4-cyanobenzoate.

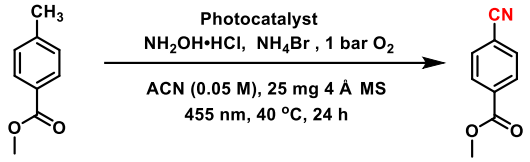

Entry	Photocatalyst (PC)	Ammonia source	Yield of **2** (%)
1[a]	PC-1	$NH_2OH•HCl$	26
2[a]	PC-2	$NH_2OH•HCl$	15
3[a]	PC-3	$NH_2OH•HCl$	35
4[a]	**PC-4**	**$NH_2OH•HCl$**	**76**
5[a]	PC-5	$NH_2OH•HCl$	12
6[a]	PC-6	$NH_2OH•HCl$	14
7[a]	PC-4	$NH_4(OAc)_2$	NR
8[a]	PC-4	Aq. NH_3	NR
9[a]	PC-4	$HCOONH_4$	NR
10[a]	PC-4	7N NH_3 in MeOH	NR

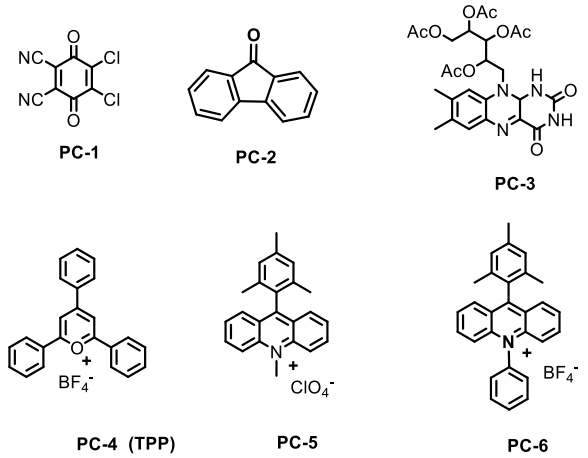

Reaction conditions: [a]0.1 mmol substrate, 20 mol% PC, 3 eq. ammonia source, 2.5 eq. NH_4Br, 25 mg 4 Å MS, 1 bar O_2, 2 mL acetonitrile (0.05 M), 455 nm, 40 °C, 24 h, yields were determined by GC using n-decane as standard.

The initial screening revealed DDQ and 9-fluorenone as ineffective catalysts for this reaction giving a yield of 26% and 15%, respectively (Table 1, entries 1-2). Interestingly, the use of RFTA led to a moderate yield of 35% (Table 1, entry 3), while the more sensitive photocatalyst TPP (PC-4) ($E_{1/2}$ = + 2.3 V),[21] yielded 76% of methyl 4-cyanobenzoate (Table 1, entry 4). Surprisingly, employing acridinium photocatalysts ($E_{1/2}$ = + 2.28 V)[1u] resulted in poor yields of 12% and 14%, respectively (Table 1, entries 5-6). Further, different ammonium salts were screened for the cyanation of methylarenes. Notably, merely hydroxylamine hydrochloride gave the desired product 2, while all other tested ammonium sources, such as ammonium acetate, aqueous ammonia, ammonium formate and methanolic ammonia failed to render the desired product (Table 1, entries 7-10). Possible reasons for this observations are that the oxidation of simple ammonia ($E_{1/2}$ = + 0.63 V vs SCE) might be faster than the required oxidation of the substrate and the potential degradation of PC-4 in the presence of a base or nucleophiles.

Kinetic investigations. After having identified a potential photocatalyst (PC-4, TPP), kinetic investigations on this system were performed, examining the effect of (a) reaction time, (b) concentration of the catalyst, (c) temperature, (d) hydroxylamine to substrate ratio, (e) ammonium bromide concentration, and (f) wavelength (Fig. 1). Regarding the reaction time (Fig. 1a), 30% of the starting material was converted after 2 h, with the major product being the oxime intermediate **3** (16%) and only small amounts of product (**2**). After 8 h, the starting material was almost completely converted. At this time, the oxime (**3**) concentration is beginning to decrease slowly, while the yield of the desired product **2** is steadily increasing.

Varying the catalyst loading (Fig. 1b), the starting material was predominant with 2 mol%. For 5 mol% catalyst, product **2**, **3** and starting material **1** were almost at an equal level (28-38%) and the maximum product yield of 76% was obtained when the photocatalyst loading was raised to 20 mol%. The reaction temperature had a significant effect on the product yield, as shown in Fig. 1(c). At 0 °C, product **2** together with **3** were observed in 42% and 38%, respectively. The oxime to

nitrile conversion was increased by elevating the reaction temperature, revealing 40 °C as the optimum. The absence or low concentration of hydroxylamine hydrochloride led to an increased amount of by-product **4** (Fig. 1d), whereas a loading of 3 eq. gave the product in a good yield. A catalytic amount of ammonium bromide was sufficient for the complete conversion of starting material. However, to reach the maximum yield an excess of ammonium bromide is required (Fig. 1e). When investigating the effect of different wavelength, we found that 365 nm and 455 nm LEDs are efficient light sources for this transformation (Fig. 1f).

In addition to this, the role of different solvents and additives were examined (Supporting Information, Table S1 and S2). Acetonitrile was identified as the ideal solvent, together with NH_4Br as the optimal additive (Supporting Information, Table S1 and S2). Crucially, control experiments revealed the necessity of light, photocatalyst, O_2 and $NH_2OH.HCl$ for the formation of the desired product (Supporting Information, Table S3, entries 2-4 and 7). However, in the absence of an additive or molecular sieves the desired product was observed as well, albeit in a low yield of 25

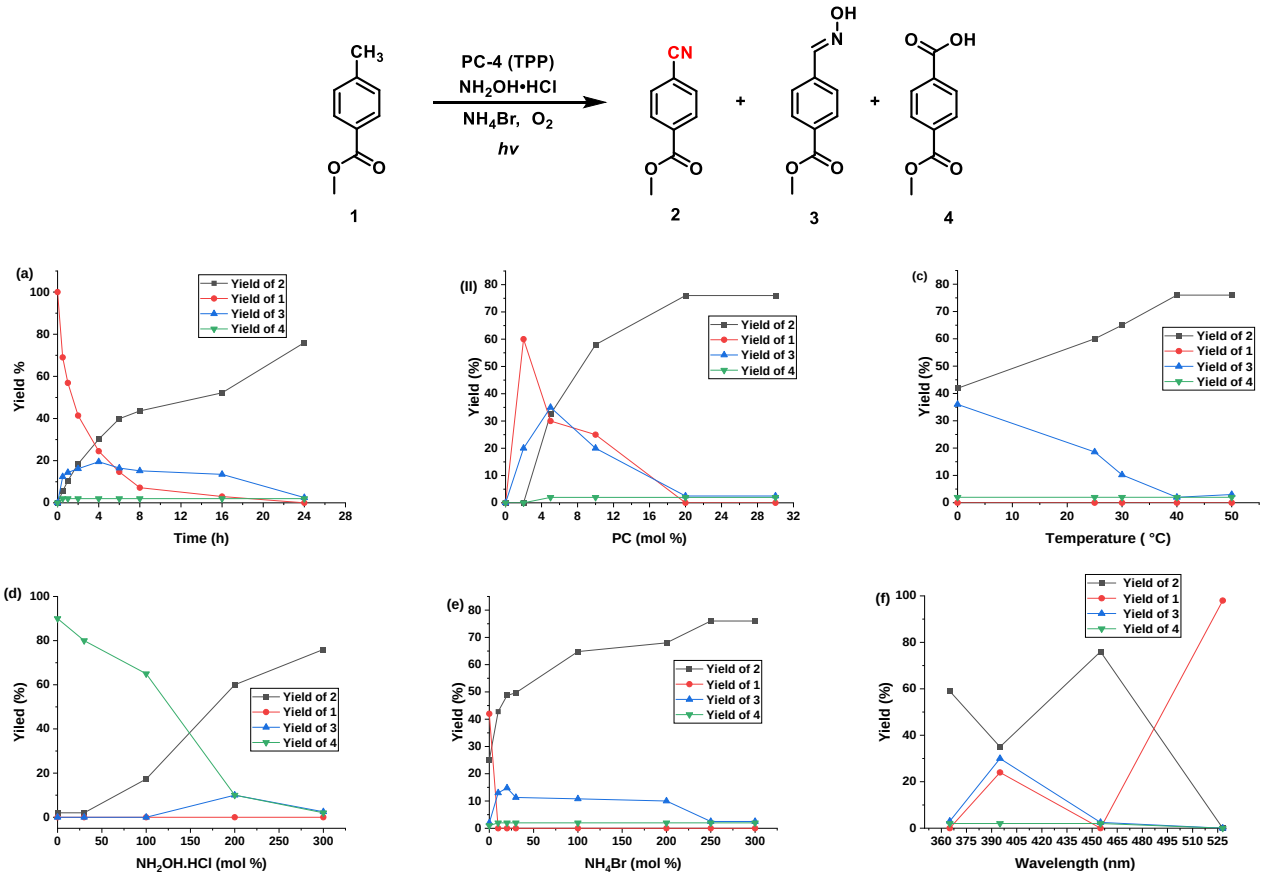

Fig. 1: Kinetic investigation on the photocatalytic ammoxidation**.** (a) Yield vs time, (b) yield vs concentration of TPP, (c) yield vs temperature, (d) yield vs mol% of NH_2OH•HCl, (e) yield vs mol% of NH_4Br, (f) yield vs wavelength. Reaction conditions: For Fig. 1(a): 0.1 mmol substrate, 20 mol% PC, 3 eq. NH_2OH•HCl, 2.5 eq. NH_4Br, 25 mg 4 Å MS, 1 bar O_2, 2 mL acetonitrile (0.05 M), 455 nm, 40 °C, 0-24 h. Fig. 1(b): 0.1 mmol substrate, 2-20 mol% PC, 3 eq. NH_2OH•HCl, 2.5 eq. NH_4Br, 25 mg 4 Å MS, 1 bar O_2, 2 mL acetonitrile (0.05 M), 455 nm, 40 °C, 24 h. Fig. 1(c): 0.1 mmol substrate, 20 mol% PC, 3 eq. NH_2OH•HCl, 2.5 eq. NH_4Br, 25 mg 4 Å MS, 1 bar O_2, 2 mL acetonitrile (0.05 M), 455 nm, 0-40 °C, 24 h. Fig. 1(d): 0.1 mmol substrate, 20 mol% PC, 0.3-3 eq. NH_2OH•HCl, 2.5 eq. NH_4Br, 25 mg 4 Å MS, 1 bar O_2, 2 mL acetonitrile (0.05 M), 455 nm, 40 °C, 24 h. Fig. 1(d): 0.1 mmol substrate, 20 mol% PC, 3 eq. NH_2OH•HCl, 0.1-2.5 eq. NH_4Br, 25 mg 4 Å MS, 1 bar O_2, 2 mL acetonitrile (0.05 M), 455 nm, 40 °C, 24 h. Fig. 1(e): 0.1 mmol substrate, 20 mol% PC, 3 eq. NH_2OH•HCl, 2.5 eq. NH_4Br, 25 mg 4 Å MS, 1 bar O_2, 2 mL acetonitrile (0.05 M), 365-528 nm, 40 °C, 24 h. Yields were determined by GC using n-decane as standard.

and 51%, respectively (Supporting Information, Table S3, entries 5-6).

Mechanistic hypothesis. The initial kinetic studies suggest that the oxime is one of the key intermediates, as its depletion is accompanied by the formation of the product. Further, the control experiment yielding no product in the absence of O_2 indicates that the oxime might be formed from the corresponding aldehyde. Based on this we envisioned following catalytic cycle (Cycle A): the substrate ($E_{1/2}$ ($1/1^{\bullet+}$) = + 2.45 V vs SCE, supporting information) is oxidised by the excited photocatalyst ($E_{1/2}$ ($PC\text{-}4^{+}$*/ $PC\text{-}4^{\bullet}$) = + 2.3 V Vs SCE) via electron transfer, generating radical cation **II** and the reduced photocatalyst species ($PC\text{-}4^{\bullet}$). The photocatalytic cycle is closed by the oxidation of the reduced photocatalyst with O_2, giving a superoxide anion ($O_2^{\bullet-}$). Intermediate **II** loses a proton to form the more stable benzylic radical (**III**), which combines with

the superoxide anion to peroxide derivative **V** after protonation. Elimination of water from **V** leads to the corresponding aldehyde intermediate (**VI**). Intermediate **VI** can yield oxime **VII** upon condensation with NH_2OH•HCl, which can be converted into the desired nitrile in a second cycle (Fig. 2, Cycle A'). In this cycle, the oxime (**VII**) is oxidised to **VIII** via reductive quenching of PC-4* followed by elimination of water to give intermediate **IX**. The reduced PC undergoes SET with **IX** to render the desired product **X**, closing the photocatalytic cycle and completing a redox-neutral process.

The presence of NH_4Br is crucial to obtain a satisfactory yield. Thus, another catalytic cycle may be operative, yielding the same reaction product (Fig. 2, Cycle B). Bromide anions are known hydrogen atom transfer (HAT) catalysts.[23] In presence of visible-light, the excited PC can oxidise Br^- to generate the $Br^•$ radical, which is capable to abstract the H-atom from the methylarene to yield a benzyl radical (**III**) and HBr. The combination of superoxide anion and **III** yields intermediate **IV**, which deprotonates HBr to regenerate the Br^- while generating intermediate **V**. After its formation, **V** follows the same mechanistic pathway as described above (Cycle A and A').

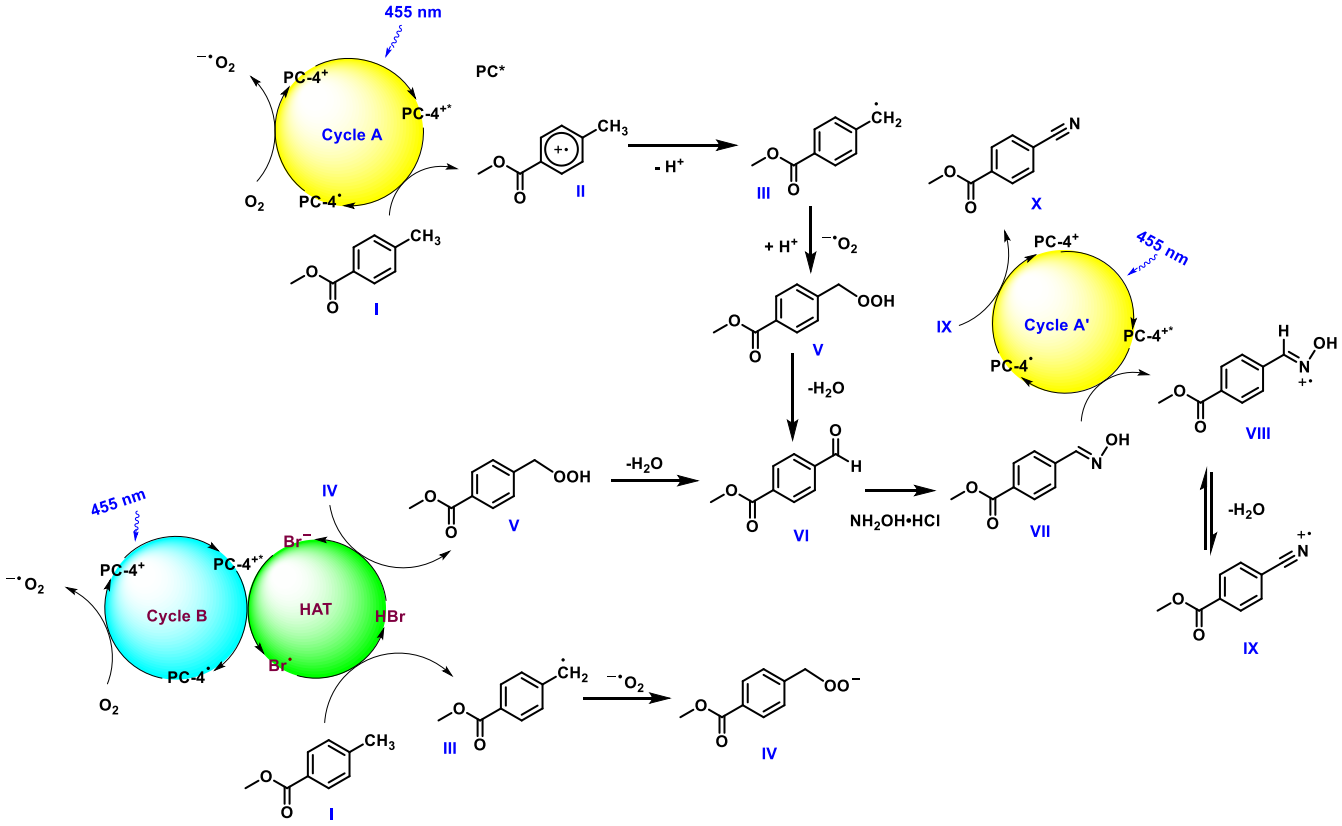

Fig. 2: Proposed catalytic cycles for the ammoxidation of methylarenes.

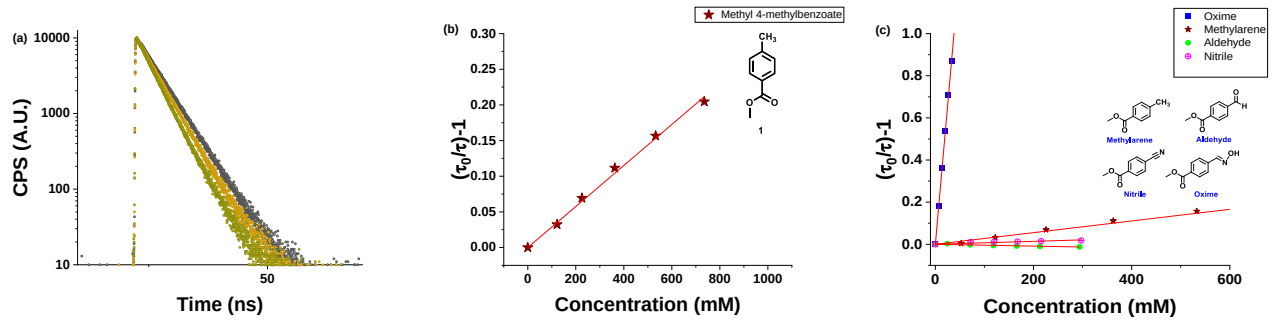

Fig. 3: Quenching studies. Fig. 3(a) Time-resolved luminescence quenching decay of methyl 4-methylbenzoate with TPP; Fig. 3(b) Stern-Volmer plot for the TPP with methyl 4-methylbenzoate; Fig. 3(c) Stern-Volmer plot for the comparison of different substances with TPP.

To support this proposed hypothesis, we performed several mechanistic experiments, starting with spectroscopic investigations. Time-resolved luminescence quenching experiments indicated that methyl 4-methylbenzoate (**1**) can be oxidized by the excited TPP (PC-4) (Fig. 3), as a slight decrease of the luminescence lifetime with increasing concentration of **1** was observed (Fig. 3a). The corresponding Stern-Volmer plot

showed a linear correlation between the quencher concentration and the luminescence lifetime (Fig. 3b)

Scheme 2. Mechanistic experiments to support the proposed catalytic hypothesis

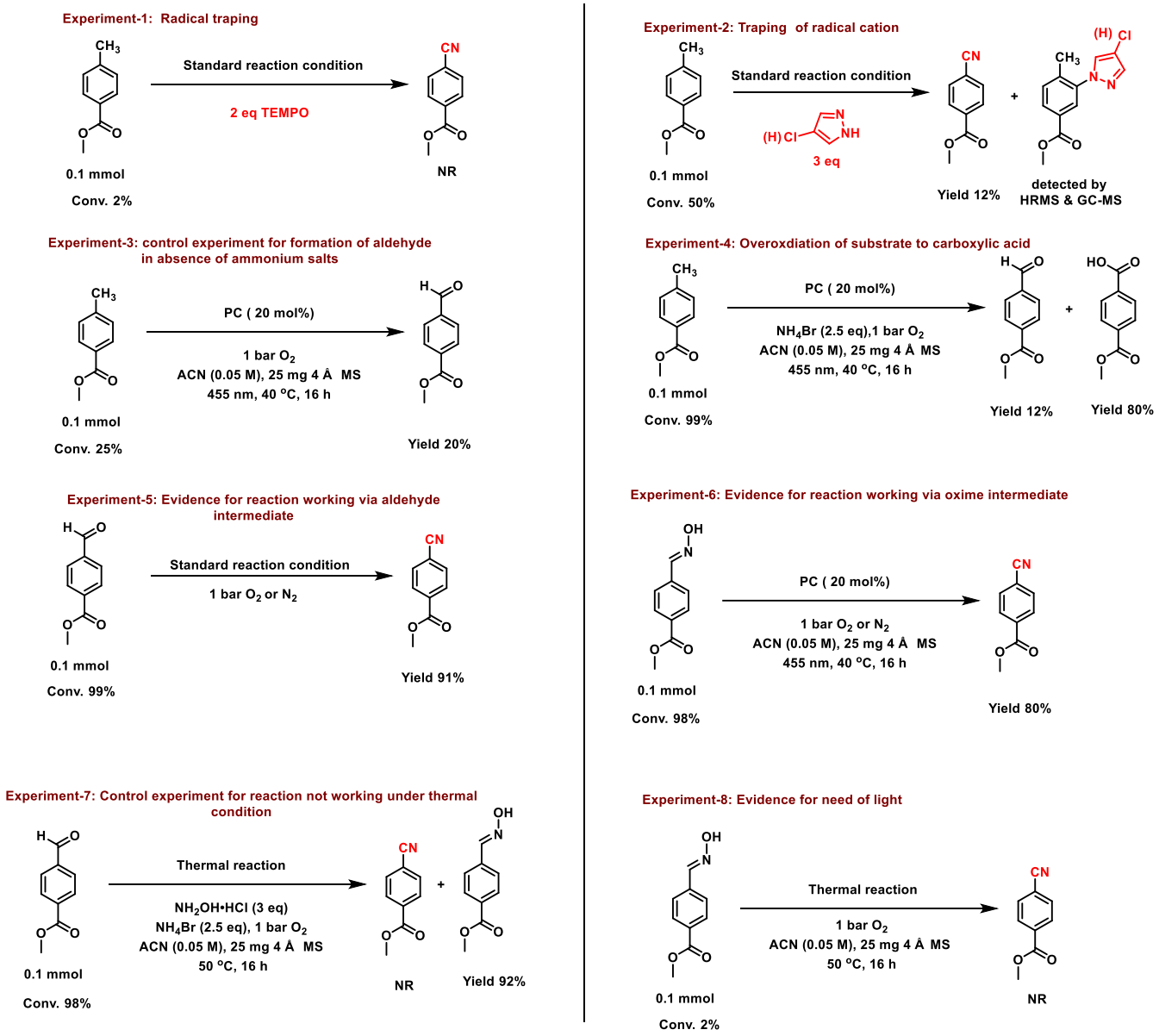

Yields were determined by GC using n-decane as standard

Further, the quenching of the starting material (**1**) was compared to the product (**2**) and the two crucial proposed intermediates methyl 4-formylbenzoate and methyl 4-((hydroxyimino)methyl)benzoate (**3**) under the same conditions. The starting material (**1**) was identified as a more efficient quencher than the corresponding aldehyde intermediate and nitrile product. On the other hand, the oxime intermediate (**3**) showed a superior quenching to methyl 4-methylbenzoate (**1**) (Fig. 3c), illustrating the possible interaction of the excited photocatalyst with the oxime intermediate under the applied reaction condition (Cycle A'). The quenching efficiencies of NH_2OH•HCl and NH_4Br were investigated as well, with the former exhibiting a poorer quenching than the later one (Supporting Information, Fig. S3), which reveals that Cycle B can be active as well. Comparing the luminescence lifetime quenching of NH_4Br and the methyl 4-methylbenzoate starting material (**1**), NH_4Br seems to decrease the lifetime more effectively (Supporting Information, Fig. S4). However, an electron-rich (4-methyl anisole) instead of an electron-deficient (**1**) substrate proved to be a more potent quencher as well (Supporting Information, Fig. S6), showing similar quenching ability as NH_4Br. Thus, based on the time-resolved luminescence quenching experiments, both proposed catalytic cycles A and B can be operative, with their respective importance

likely being dependent on the electronic nature of the starting material.

Next, several mechanistic control experiments were performed to directly or indirectly detect reaction intermediates vital for the mechanistic process. Further, selected stable intermediates were used as starting materials for the formation of the final product under specific reaction conditions to establish the mechanistic pathways more clearly (Scheme 2). The model reaction was performed under standard reaction condition in presence of TEMPO, yielding no product, which indicates a radical pathways (Scheme 2, Experiment-1). Further, the radical cation intermediate (Fig. 2, **II**) could be trapped in the presence of pyrazole or 4-cholorpyrazole as nucleophiles under standard reaction condition, in a similar reaction as reported by Nicewicz,[22] supporting its formation (Scheme 2, Experiment-2). Looking at the more stable intermediates, the methylarene is proposed to be oxidized to the corresponding aldehyde first (Fig. 2, **VI**). This was confirmed by performing the model reaction in absence of both ammonium salts (to avoid the formation of the oxime), providing the corresponding aldehyde as product in 20% GC yield (Scheme 2, experiment-3), with an incomplete starting material conversion of 25%. In contrast, a full conversion was observed when NH_4Br was added (Experiment 4, Scheme 2), showcasing its crucial role, likely due to the thus opened alternative Br^- HAT-pathway[6h, 23] (Cycle B, Fig. 2). The main product in this case was the corresponding carboxylic acid (80%) resulting from an over-oxidation of the aldehyde (12%). With no observable nitrile formation, the experiment further suggests, that NH_2OH•HCl is the main nitrogen source. It is proposed to rapidly form the oxime from the aldehyde, avoiding its oxidation to the carboxylate.

The generation of an aldehyde and oxime intermediate was further supported by using those as starting materials for the synthesis of the final nitrile product (Scheme 2, Experiment 5 and 6). In both cases, the product was formed with a yield of 91% and 80%, respectively. Additionally, the conversion of the aldehyde or oxime to the nitrile did not proceed under solely thermal condition in the absence of light (Scheme 2, Experiment 7 and 8), supporting the proposed catalytic cycle A'. To further indicate the necessity of more than one photon for the formation of one product molecule, the product yield dependent on the irradiation intensity was observed as well (Supporting Information, Fig. S12).[24]

In order to follow the mechanistic pathway in more detail, NMR studies were performed analysing the reaction mixture after defined time intervals (Fig. 4). The signal corresponding to the methyl ester (-$COOCH_3$) of the starting material (**1**) shows a singlet resonance at δ 3.84 ppm in the ^{1}H-NMR spectrum, while the oxime (**3**) gives a singlet at δ 3.87, and nitrile (**2**) a singlet at δ 3.91, allowing for a facile distinction between the species of interest. At the beginning, the depletion of the starting material is accompanied by the increase of the oxime intermediate as well as nitrile product, with all three compounds being clearly observable at the same time after 4 h of irradiation. Further increasing the reaction time leads to the

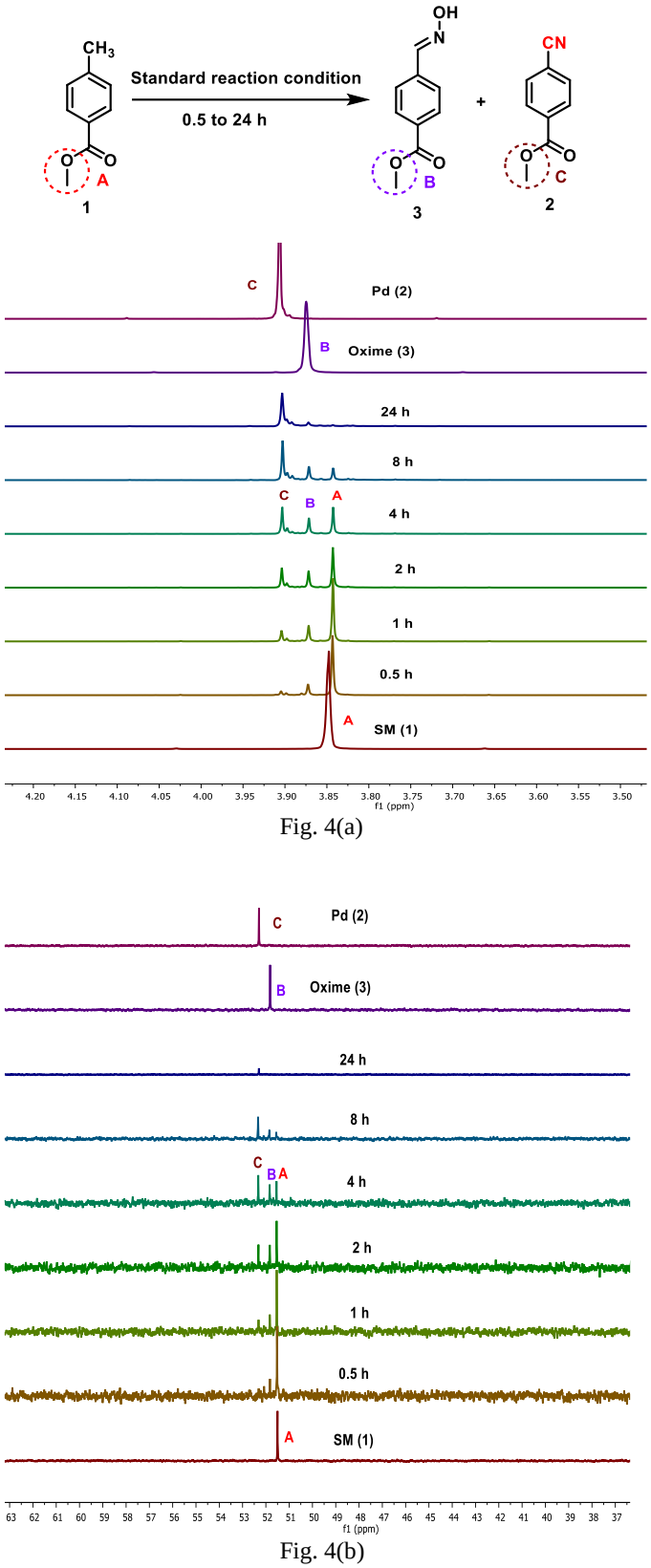

Fig. 4(a)

Fig. 4(b)

Fig. 4: NMR investigation. Fig. 4(a) ^{1}H NMR and Fig. 4(b) ^{13}C NMR.

(almost) full conversion of the starting material and the oxime with the dominant signal being the product peak.

Scheme 3. Substrate scope for synthesis of functionalized cycanobenzenes

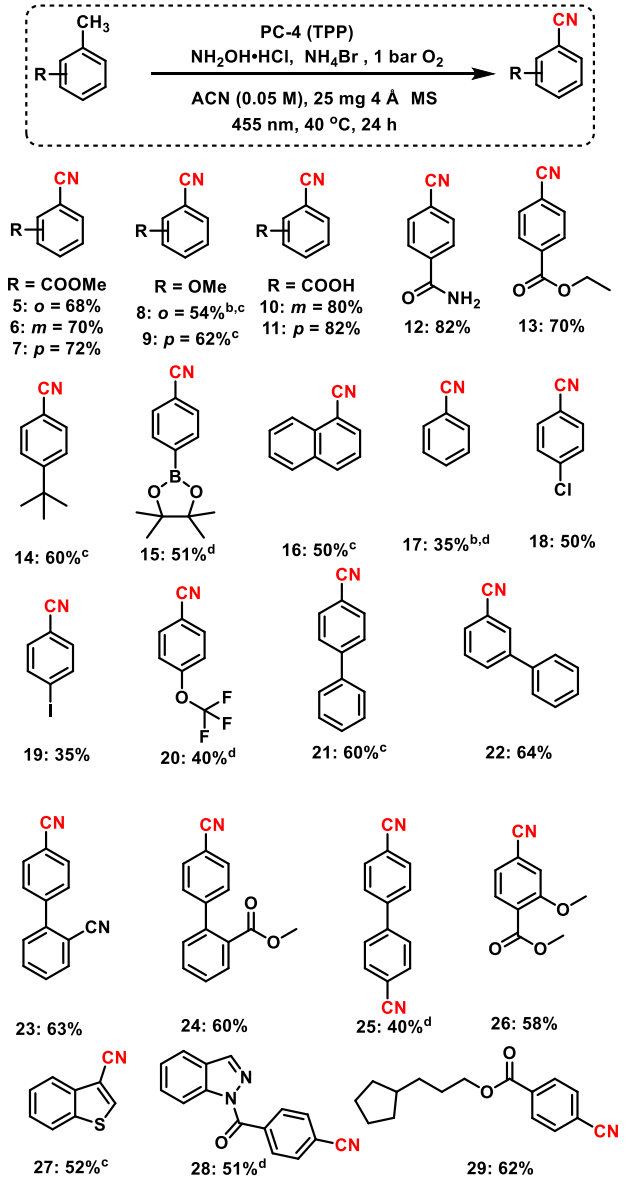

Reaction conditions: [a]0.1 mmol substrate, 20 mol% PC, 3 eq. $NH_2OH•HCl$, 2.5 eq. NH_4Br, 25 mg 4 Å MS, 1 bar O_2, 2 mL acetonitrile (0.05 M), 455 nm, 40 °C, 24 h, isolated yields. [b]GC yields using n-decane as standard. [c]same as 'a' using 1 eq. of PTSCl. [d]same as 'a ' 48 h instead of 24 h.

A similar tendency was observed in the ^{13}C-NMR for the corresponding methyl ester carbon (Fig. 4b), all together further supporting the formation of the oxime as crucial intermediate to render the nitrile.

Collectively, the spectroscopy investigation, control experiments and kinetic investigation all support the proposed photocatalytic cycles. In addition, the catalyst deactivation pathway also studied under the standard reaction conditions, suggesting 2,4,6-triphenylpyridine as the degradation product, which could further be observed in the scale-up batch as minor by-product supported by HRMS (Supporting Information, Scheme-S1).

Scheme 4. Late-stage functionalization of challenging and drug-like molecules

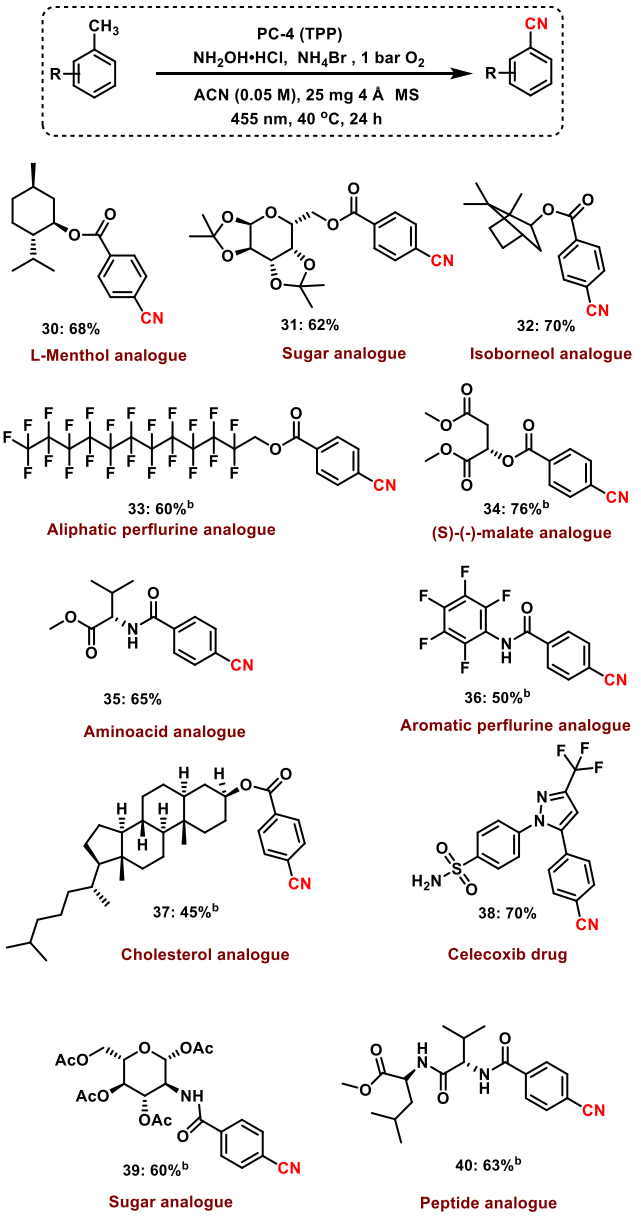

Reaction conditions: [a]0.1 mmol substrate, 20 mol% PC, 3 eq. $NH_2OH•HCl$, 2.5 eq. NH_4Br, 25 mg 4 Å MS, 1 bar O_2, 2 mL acetonitrile (0.05 M), 455 nm, 40 °C, 24 h, isolated yields. [b]same as 'a ' 48 h instead of 24 h.

With the successful conditions in hand, we explored the C(sp^3)-H functionalization of different methylarenes (Scheme 3 and 4). Substrates bearing electron-donating and -withdrawing groups, as well as heterocycles, gave the respective products in good to excellent yields (Scheme 3, **5-29**). Functional groups such as carboxylic acid, ester, amide, halogens, cyanide and boronic ester were untouched during the reaction (Scheme 3, **5-13**, **15**, **18-20** and **23-24**). Applying this methodology, a dinitrile could also be synthesized in a one-pot procedure with a moderate yield (Scheme 3, **25**).

Scheme 5. Gram-scale synthesis

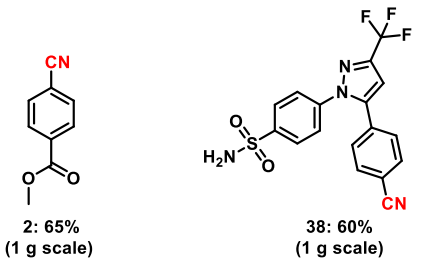

Reaction conditions: [a]1 g substrate, 20 mol% PC, 3 eq. NH_2OH•HCl, 2.5 eq. NH_4Br, 25 mg 4 Å MS for 0.1 mmol, 1 bar O_2, acetonitrile (0.05 M), 455 nm, 40 °C, 36 h, isolated yields.

Structurally complex, bioactive- and drug- molecules could be employed for a selective cyanation as well, rendering the desired product in good to excellent yields up to 76% (Scheme 4). Delightfully, substrates bearing multiple oxygen atoms, which are usually not stable under photochemical conditions in the presence of oxygen, are viable, too.[25] Using the developed protocol, sugar derivatives **31** and **39** were obtained in 62% and 60% yield, respectively. Further, more challenging substrates such as cholesterol, isoborneol, amino acid and peptide derivatives gave the corresponding products in 45-70% yield. Interestingly, anti-inflammatory drug (Celecoxib) gave the desired product in 70% yield. For the example of a bulk-scale preparation, compound **2** and Celecoxib were cyanated in a 1 g scale to give the desired product in 65 and 60% yield respectively (Scheme 5).

After the screening of methylarenes, we were interested to apply this methodology using alcohols, aldehydes and oximes as starting materials for the synthesis of aromatic nitriles as well (Scheme 6). Similar to methylarenes, alcohols, aldehydes and oximes gave good to excellent yields up to 91%. Notably, isophthalaldehyde (**49**) was cyanided twice to isophthalonitrile in 78% yield. Sterically crowded 2,6-dichlorobenzaldehyde (**52**) was a viable substrate, too, giving 2,6-dichlorobenzonitrile (DCBN) in 82% yield, which is used as herbicide and regarded as a potential intermediate for pesticides and agrochemicals.

Scheme 6. Synthesis of nitriles from alcohols, aldehydes, and oximes

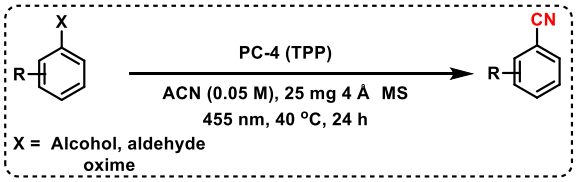

From alcohols

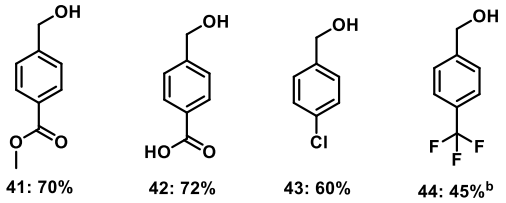

From aldehydes

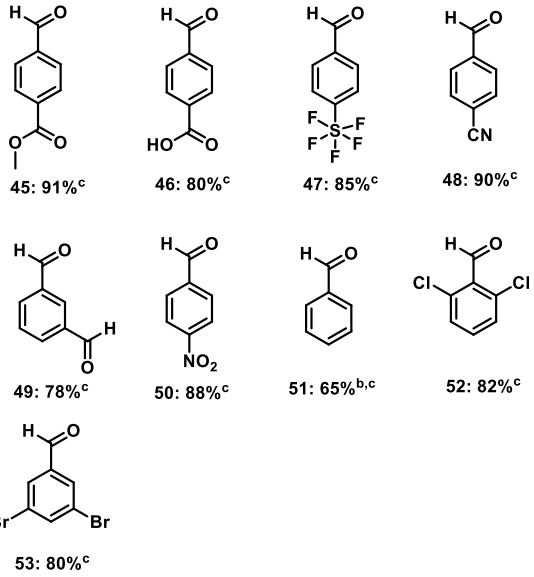

From oximes

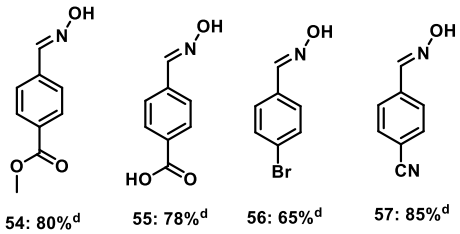

Reaction conditions: [a]0.1 mmol substrate, 20 mol% PC, 3 eq. NH_2OH•HCl, 2.5 eq. NH_4Br, 25 mg 4 Å MS, 1 bar O_2, 2 mL acetonitrile (0.05 M), 455 nm, 40 °C, 24 h, isolated yields of nitriles. [b]GC yields of nitriles using n-decane as standard. [c]0.1 mmol substrate, 20 mol% PC, 3 eq. NH_2OH•HCl, 25 mg 4 Å MS, N_2, 2 mL acetonitrile (0.05 M), 455 nm, 40 °C, 24 h, isolated yields of nitriles. [d]0.1 mmol substrate, 20 mol% PC, 25 mg 4 Å MS, N_2, 2 mL acetonitrile (0.05 M), 455 nm, 40 °C, 24 h, isolated yields of nitriles.

CONCLUSION

In conclusion, we present the first metal- and cyanide-free visible-light-induced photocatalytic ammoxidation of C(sp^3)-H bonds using an abundant ammonia source and molecular oxygen. A detailed mechanistic investigation was carried out to support the proposed mechanistic hypothesis including various spectroscopy experiments. Applying this methodology, more than 50 aromatic and heteroaromatic substrates, as well as steroids and existing drug molecules containing methyl groups

could be converted to the nitrile in good to excellent yields. In addition to this, the method could be executed on gram scale and alcohols, aldehydes and oximes could be used as starting materials for their conversion to nitriles in up to 91% yield in the same manner.

AUTHOR INFORMATION

Corresponding Author

*Corresponding authors:

Burkhard König (burkhard.koenig@chemie.uni-regensburg.de)

.

ACKNOWLEDGMENT

This work was supported by the German Science Foundation (DFG, KO 1537/18-1). This project has received funding from the European Research Council (ERC) under the European Union's Horizon 2020 Research and Innovation Programme (grant agreement No. 741623). We thank Dr. Rudolf Vasold for GC-MS measurements and Regina Hoheisel for Cyclic Voltammetry measurements.

REFERENCES

1. (a) Franck, H.-G.; Stadelhofer, J. W., Production of benzene, toluene and xylenes. In *Industrial Aromatic Chemistry: Raw Materials · Processes · Products*, Springer Berlin Heidelberg: Berlin, Heidelberg, 1988; pp 99-131, doi:10.1007/978-3-642-73432-8_4. (b) Otamiri, J. C., *Ammoxidation of Toluene Over V_2O_5 and Cuprate Perovskite Catalysts*. Lund: University.: 1990, . (c) Takao Maki, K. T., Benzoic Acid and Derivatives. In *Ullmann's Encyclopedia of Industrial Chemistry*, 2000, doi:10.1002/14356007.a03_555. (d) Chiusoli, G. P.; Maitlis, P. M., *Metal-catalysis in Industrial Organic Processes*. RSC Publishing: 2008, . (e) Magano, J.; Dunetz, J. R., Large-Scale Applications of Transition Metal-Catalyzed Couplings for the Synthesis of Pharmaceuticals. *Chem. Rev.* **2011,** *111*, 2177-2250, doi:10.1021/cr100346g. (f) Negishi, E.-i., Magical Power of Transition Metals: Past, Present, and Future (Nobel Lecture). *Angew. Chem., Int. Ed.* **2011,** *50*, 6738-6764, doi:doi:10.1002/anie.201101380. (g) Hoffmann, N., Chemical Photocatalysis. Edited by Burkhard König. *Angew. Chem., Int. Ed.* **2013,** *52*, 11456-11456, doi:10.1002/anie.201307399. (h) Medlock, J.; Bonrath, W., Applications of Transition Metal Catalysis in Drug Discovery and Development. An Industrial Perspective. Edited by Matthew L. Crawley and Barry M. Trost. *Angew. Chem., Int. Ed.* **2013,** *52*, 5435-5435, doi:10.1002/anie.201302033. (i) Prier, C. K.; Rankic, D. A.; MacMillan, D. W. C., Visible Light Photoredox Catalysis with Transition Metal Complexes: Applications in Organic Synthesis. *Chem. Rev.* **2013,** *113*, 5322-5363, doi:10.1021/cr300503r. (j) Gadge, S. T.; Gautam, P.; Bhanage, B. M., Transition Metal-Catalyzed Carbonylative C-H Bond Functionalization of Arenes and C(sp3)-H Bond of Alkanes. *Chem. Rec.* **2016,** *16*, 835-856, doi:10.1002/tcr.201500280. (k) Skubi, K. L.; Blum, T. R.; Yoon, T. P., Dual Catalysis Strategies in Photochemical Synthesis. *Chem. Rev.* **2016,** *116*, 10035-10074, doi:10.1021/acs.chemrev.6b00018. (l) Gui, Y.-Y.; Chen, X.-W.; Zhou, W.-J.; Yu, D.-G., Arylation of Amide and Urea C(sp3)–H Bonds with Aryl Tosylates Generated In Situ from Phenols. *Synlett* **2017,** *28*, 2581-2586, doi:10.1055/s-0036-1589126. (m) Zhou, W. J.; Cao, G. M.; Shen, G.; Zhu, X. Y.; Gui, Y. Y.; Ye, J. H.; Sun, L.; Liao, L. L.; Li, J.; Yu, D. G., Visible-Light-Driven Palladium-Catalyzed Radical Alkylation of C-H Bonds with Unactivated Alkyl Bromides. *Angew. Chem., Int. Ed.* **2017,** *56*, 15683-15687, doi:10.1002/anie.201704513. (n) Alig, L.; Fritz, M.; Schneider, S., First-Row Transition Metal (De)Hydrogenation Catalysis Based On Functional Pincer Ligands. *Chem. Rev.* **2018,** *119*, 2681-2751, doi:10.1021/acs.chemrev.8b00555. (o) Karimov, R. R.; Hartwig, J. F., Transition-Metal-Catalyzed Selective Functionalization of C(sp3)−H Bonds in Natural Products. *Angew. Chem., Int. Ed.* **2018,** *57*, 4234-4241, doi:10.1002/anie.201710330. (p) Beaumier, E. P.; Pearce, A. J.; See, X. Y.; Tonks, I. A., Modern applications of low-valent early transition metals in synthesis and catalysis. *Nat. Rev. Chem.* **2019,** *3*, 15-34, doi:10.1038/s41570-018-0059-x. (q) Gandeepan, P.; Müller, T.; Zell, D.; Cera, G.; Warratz, S.; Ackermann, L., 3d Transition Metals for C–H Activation. *Chem. Rev.* **2019,** *119*, 2192-2452, doi:10.1021/acs.chemrev.8b00507. (r) Milligan, J. A.; Phelan, J. P.; Badir, S. O.; Molander, G. A., Alkyl Carbon–Carbon Bond Formation by Nickel/Photoredox Cross-Coupling. *Angew. Chem., Int. Ed.* **2019,** *58*, 6152-6163, doi:10.1002/anie.201809431. (s) Yu, X.-Y.; Chen, J.-R.; Xiao, W.-J., Visible Light-Driven Radical-Mediated C–C Bond Cleavage/Functionalization in Organic Synthesis. *Chem. Rev.* **2020**, doi:10.1021/acs.chemrev.0c00030. (t) Spargo, P. L., Transition Metals for Organic Synthesis: Building Blocks and Fine Chemicals. Second Revised and Enlarged Edition. (2-Volume Set.) Edited by Matthias Beller and Carsten Bolm. Wiley-VCH: Weinheim. 2004. 662 pp. (Vol. 1), 652 pp (Vol. 2). *Org. Process Res. Dev.* **2005,** *9*, 1017-1018, doi:10.1021/op050145w. (u) Marzo, L.; Pagire, S. K.; Reiser, O.; König, B., Visible-Light Photocatalysis: Does It Make a Difference in Organic Synthesis? *Angew. Chem., Int. Ed.* **2018,** *57*, 10034-10072, doi:10.1002/anie.201709766

2. (a) Precious metals management (pmm). www.platinum.matthey.com. (b) Metals market prices, forecasts & analysis. . www.metalprices.com.

3. Hans Wedepohl, K., The composition of the continental crust. *Geochim. Cosmochim. Acta* **1995,** *59*, 1217-1232, doi:https://doi.org/10.1016/0016-7037(95)00038-2

4. Egorova, K. S.; Ananikov, V. P., Toxicity of Metal Compounds: Knowledge and Myths. *Organometallics* **2017,** *36*, 4071-4090, doi:10.1021/acs.organomet.7b00605

5. (a) Nicewicz, D. A.; Nguyen, T. M., Recent Applications of Organic Dyes as Photoredox Catalysts in Organic Synthesis. *ACS Catal.* **2014,** *4*, 355-360, doi:10.1021/cs400956a. (b) Qin, Y.; Zhu, L.; Luo, S., Organocatalysis in Inert C–H Bond Functionalization. *Chem. Rev.* **2017,** *117*, 9433-9520, doi:10.1021/acs.chemrev.6b00657. (c) Shamsabadi, A.; Chudasama, V., Recent advances in metal-free aerobic C–H activation. *Organic & Biomolecular Chemistry* **2019,** *17*, 2865-2872, doi:10.1039/C9OB00339H. (d) Zhang, Y.; Schilling, W.; Riemer, D.; Das, S., Metal-free photocatalysts for the oxidation of non-activated alcohols and the oxygenation of tertiary amines performed in air or oxygen. *Nat. Protoc* **2020,** *15*, 822-839, doi:10.1038/s41596-019-0268-x. (e) Zhang, Y.; Schilling, W.; Das, S., Metal-Free Photocatalysts for C−H Bond Oxygenation Reactions with Oxygen as the Oxidant. *ChemSusChem* **2019,** *12*, 2898-2910, doi:10.1002/cssc.201900414

6. (a) Perry, I. B.; Brewer, T. F.; Sarver, P. J.; Schultz, D. M.; DiRocco, D. A.; MacMillan, D. W. C., Direct arylation of strong aliphatic C–H bonds. *Nature* **2018,** *560*, 70-75, doi:10.1038/s41586-018-0366-x. (b) Sarver, P. J.; Bacauanu, V.; Schultz, D. M.; DiRocco, D. A.; Lam, Y.-h.; Sherer, E. C.; MacMillan, D. W. C., The merger of decatungstate and copper catalysis to enable aliphatic C(sp3)–H trifluoromethylation. *Nat. Chem.* **2020,** *12*, 459-467, doi:10.1038/s41557-020-0436-1. (c) Rand, A. W.; Yin, H.; Xu, L.; Giacoboni, J.; Martin-Montero, R.; Romano, C.; Montgomery, J.; Martin, R., Dual Catalytic Platform for Enabling sp3 α C–H Arylation and Alkylation of Benzamides. *ACS Catal.* **2020,** *10*, 4671-4676, doi:10.1021/acscatal.0c01318. (d) Janssen-Müller, D.; Sahoo, B.; Sun, S.-Z.; Martin, R., Tackling Remote sp3 C−H Functionalization via Ni-Catalyzed "chain-walking" Reactions. *Isr. J. Chem.* **2020,** *60*, 195-206, doi:10.1002/ijch.201900072. (e) Jia, J.; Kancherla, R.; Rueping, M.; Huang, L., Allylic C(sp3)–H alkylation via synergistic organo- and photoredox catalyzed radical addition to imines. *Chem. Sci.,* **2020,** *11*, 4954-4959, doi:10.1039/D0SC00819B. (f) Huang, H.-M.; Bellotti, P.; Glorius, F., Transition metal-catalysed allylic functionalization reactions involving radicals. *Chem. Soc. Rev.* **2020**, doi:10.1039/D0CS00262C. (g) Schwarz, J. L.; Kleinmans, R.; Paulisch, T. O.; Glorius, F., 1,2-Amino Alcohols via Cr/Photoredox Dual-Catalyzed Addition of α-Amino Carbanion Equivalents to Carbonyls. *J. Am. Chem. Soc.* **2020,** *142*, 2168-2174, doi:10.1021/jacs.9b12053. (h) Shields, B. J.; Doyle, A. G., Direct C(sp3)–H Cross Coupling Enabled by Catalytic Generation of Chlorine Radicals. *J. Am. Chem. Soc.* **2016,** *138*, 12719-12722, doi:10.1021/jacs.6b08397. (i) Berger, A. L.; Donabauer, K.; König, B., Photocatalytic carbanion generation from C–H bonds – reductant free Barbier/Grignard-type reactions. *Chem. Sci.,* **2019,** *10*, 10991-10996, doi:10.1039/C9SC04987H. (j) Capaldo, L.; Quadri, L. L.; Ravelli, D., Photocatalytic hydrogen atom transfer: the philosopher's stone for late-stage functionalization? *Green Chem.* **2020,** *22*, 3376-3396, doi:10.1039/D0GC01035A. (k) Laudadio, G.; Deng, Y.; van der Wal, K.; Ravelli, D.; Nuño, M.; Fagnoni, M.; Guthrie, D.; Sun, Y.; Noël, T., C(sp3)–H functionalizations of light hydrocarbons using decatungstate photocatalysis in flow. **2020,** *369*, 92-96, doi:10.1126/science.abb4688 %J Science. (l) Capaldo, L.; Merli, D.; Fagnoni, M.; Ravelli, D., Visible Light Uranyl Photocatalysis: Direct C–H to C–C Bond Conversion. *ACS Catal.* **2019,** *9*, 3054-3058, doi:10.1021/acscatal.9b00287. (m) Masuda, Y.; Ishida, N.; Murakami, M., Light-Driven Carboxylation of o-Alkylphenyl Ketones with CO2. *J. Am. Chem. Soc.* **2015,** *137*, 14063-14066, doi:10.1021/jacs.5b10032. (n) Donabauer, K.; Murugesan, K.; Rozman, U.; Crespi, S.; König, B., Photocatalytic Reductive Radical-Polar Crossover for a Base-Free Corey-Seebach Reaction. *n/a*, doi:10.1002/chem.202003000. (o) Meng, Q.-Y.; Schirmer, T. E.; Berger, A. L.; Donabauer, K.; König, B., Photocarboxylation of Benzylic C–H Bonds. *J. Am. Chem. Soc.* **2019,** *141*, 11393-11397, doi:10.1021/jacs.9b05360

7. (a) Fleming, F. F.; Yao, L.; Ravikumar, P. C.; Funk, L.; Shook, B. C., Nitrile-Containing Pharmaceuticals: Efficacious Roles of the Nitrile Pharmacophore. *J. Med. Chem.* **2010,** *53*, 7902-7917, doi:10.1021/jm100762r. (b) F. Fleming, F., Nitrile-containing natural products. *Nat. Prod. Rep.* **1999,** *16*, 597-606, doi:10.1039/A804370A

8. Paquette, L. A., Book Review: Comprehensive Organic Transformations. By R. C. Larock. *Angew. Chem. Int. Ed* **1990,** *29*, 435-435, doi:10.1002/anie.199004351

9. Hodgson, H. H., The Sandmeyer Reaction. *Chem. Rev.* **1947,** *40*, 251-277, doi:10.1021/cr60126a003

10. Rosenmund, K. W.; Struck, E., Das am Ringkohlenstoff gebundene Halogen und sein Ersatz durch andere Substituenten. I. Mitteilung: Ersatz des Halogens durch die Carboxylgruppe. *Berichte der deutschen chemischen Gesellschaft (A and B Series)* **1919,** *52*, 1749-1756, doi:10.1002/cber.19190520840

11. (a) Mowry, D. T., The Preparation of Nitriles. *Chem. Rev.* **1948,** *42*, 189-283, doi:10.1021/cr60132a001. (b) Anbarasan, P.; Schareina, T.; Beller, M., Recent developments and perspectives in palladium-catalyzed cyanation of aryl halides: synthesis of benzonitriles. *Chem. Soc. Rev.* **2011,** *40*, 5049-5067, doi:10.1039/C1CS15004A

12. (a) Dornan, L. M.; Cao, Q.; Flanagan, J. C. A.; Crawford, J. J.; Cook, M. J.; Muldoon, M. J., Copper/TEMPO catalysed synthesis of nitriles from aldehydes or alcohols using aqueous ammonia and with air as the oxidant. *Chem. Commun.* **2013,** *49*, 6030-6032, doi:10.1039/C3CC42231C. (b) Murugesan, K.; Senthamarai, T.; Sohail, M.; Sharif, M.; Kalevaru, N. V.; Jagadeesh, R. V., Stable and reusable nanoscale Fe2O3-catalyzed aerobic oxidation process for the selective synthesis of nitriles and primary amides. *Green Chem.* **2018,** *20*, 266-273, doi:10.1039/c7gc02627g. (c) Kelly, C. B.; Lambert, K. M.; Mercadante, M. A.; Ovian, J. M.; Bailey, W. F.; Leadbeater, N. E., Access to Nitriles from

Aldehydes Mediated by an Oxoammonium Salt. *Angew. Chem., Int. Ed.* **2015,** *54*, 4241-4245, doi:10.1002/anie.201412256. (d) Nandi, J.; Witko, M. L.; Leadbeater, N. E., Combining Oxoammonium Cation Mediated Oxidation and Photoredox Catalysis for the Conversion of Aldehydes into Nitriles. *Synlett* **2018,** *29*, 2185-2190, doi:10.1055/s-0037-1610272. (e) Verma, F.; Shukla, P.; Bhardiya, S. R.; Singh, M.; Rai, A.; Rai, V. K., Visible light-induced direct conversion of aldehydes into nitriles in aqueous medium using Co@g-C3N4 as photocatalyst. *Catal. Commun.* **2019,** *119*, 76-81, doi:https://doi.org/10.1016/j.catcom.2018.10.031. (f) Singh, P.; Shee, M.; Shah, S. S.; Singh, N. D. P., Photocatalytic Conversion of Benzyl Alcohols/Methyl Arenes to Aryl Nitriles via H-Abstraction by Azide Radical. *Chemistry* **2020,** *n/a*, doi:10.1002/chem.202001332

13. McManus, J. B.; Nicewicz, D. A., Direct C–H Cyanation of Arenes via Organic Photoredox Catalysis. *J. Am. Chem. Soc.* **2017,** *139*, 2880-2883, doi:10.1021/jacs.6b12708

14. (a) Alam, T.; Rakshit, A.; Begum, P.; Dahiya, A.; Patel, B. K., Visible-Light-Induced Difunctionalization of Styrenes: Synthesis of N-Hydroxybenzimidoyl Cyanides. *Org. Lett.* **2020,** *22*, 3728-3733, doi:10.1021/acs.orglett.0c01235. (b) Ghosh, I.; Khamrai, J.; Savateev, A.; Shlapakov, N.; Antonietti, M.; König, B., Organic semiconductor photocatalyst can bifunctionalize arenes and heteroarenes. *Science* **2019,** *365*, 360-366, doi:10.1126/science.aaw3254 %J Science

15. (a) Shu, Z.; Ye, Y.; Deng, Y.; Zhang, Y.; Wang, J., Palladium(II)-Catalyzed Direct Conversion of Methyl Arenes into Aromatic Nitriles. *Angew. Chem., Int. Ed.* **2013,** *52*, 10573-10576, doi:10.1002/anie.201305731. (b) Liu, J.; Zheng, H.-X.; Yao, C.-Z.; Sun, B.-F.; Kang, Y.-B., Pharmaceutical-Oriented Selective Synthesis of Mononitriles and Dinitriles Directly from Methyl(hetero)arenes: Access to Chiral Nitriles and Citalopram. *J. Am. Chem. Soc.* **2016,** *138*, 3294-3297, doi:10.1021/jacs.6b00180. (c) Zhou, W.; Zhang, L.; Jiao, N., Direct Transformation of Methyl Arenes to Aryl Nitriles at Room Temperature. *Angew. Chem., Int. Ed.* **2009,** *48*, 7094-7097, doi:10.1002/anie.200903838

16. (a) Oishi, T.; Yamaguchi, K.; Mizuno, N., Catalytic Oxidative Synthesis of Nitriles Directly from Primary Alcohols and Ammonia. *Angew. Chem., Int. Ed.* **2009,** *48*, 6286-6288, doi:10.1002/anie.200900418. (b) Jagadeesh, R. V.; Junge, H.; Beller, M., Green synthesis of nitriles using non-noble metal oxides-based nanocatalysts. *Nat commun.* **2014,** *5*, 4123, doi:10.1038/ncomms5123. (c) Preger, Y.; Root, T. W.; Stahl, S. S., Platinum-Based Heterogeneous Catalysts for Nitrile Synthesis via Aerobic Oxidative Coupling of Alcohols and Ammonia. *ACS Omega* **2018,** *3*, 6091-6096, doi:10.1021/acsomega.8b00911. (d) Yin, W.; Wang, C.; Huang, Y., Highly Practical Synthesis of Nitriles and Heterocycles from Alcohols under Mild Conditions by Aerobic Double Dehydrogenative Catalysis. *Org. Lett.* **2013,** *15*, 1850-1853, doi:10.1021/ol400459y

17. (a) Kim, J.; Stahl, S. S., Cu/Nitroxyl-Catalyzed Aerobic Oxidation of Primary Amines into Nitriles at Room Temperature. *ACS Catal.* **2013,** *3*, 1652-1656, doi:10.1021/cs400360e. (b) Pavel, O. D.; Goodrich, P.; Cristian, L.; Coman, S. M.; Pârvulescu, V. I.; Hardacre, C., Direct oxidation of amines to nitriles in the presence of ruthenium-terpyridyl complex immobilized on ILs/SILP. *Catal. Sci. Technol.* **2015,** *5*, 2696-2704, doi:10.1039/C5CY00011D

18. Roth, H. G.; Romero, N. A.; Nicewicz, D. A., Experimental and Calculated Electrochemical Potentials of Common Organic Molecules for Applications to Single-Electron Redox Chemistry. *Synlett* **2016,** *27*, 714-723, doi:10.1055/s-0035-1561297

19. Habibzadeh, F.; Miller, S. L.; Hamann, T. W.; Smith, M. R., Homogeneous electrocatalytic oxidation of ammonia to N_2 under mild conditions. *Proc. Natl. Acad. Sci. U.S.A.* **2019,** *116*, 2849-2853, doi:10.1073/pnas.1813368116 %J Proceedings of the National Academy of Sciences

20. Miranda, M. A.; Garcia, H., 2,4,6-Triphenylpyrylium Tetrafluoroborate as an Electron-Transfer Photosensitizer. *Chem. Rev.* **1994,** *94*, 1063-1089, doi:10.1021/cr00028a009

21. S. Jayanthi, S.; Ramamurthy, P., Photoinduced electron transfer reactions of 2,4,6-triphenylpyrylium: solvent effect and charge-shift type of systems. *PCCP* **1999,** *1*, 4751-4757, doi:10.1039/A904727A

22. Romero, N. A.; Margrey, K. A.; Tay, N. E.; Nicewicz, D. A., Site-selective arene C-H amination via photoredox catalysis. *Science* **2015,** *349*, 1326-1330, doi:10.1126/science.aac9895 %J Science

23. Capaldo, L.; Ravelli, D., Hydrogen Atom Transfer (HAT): A Versatile Strategy for Substrate Activation in Photocatalyzed Organic Synthesis. *Eur. J. Org. Chem.* **2017,** *2017*, 2056-2071, doi:10.1002/ejoc.201601485

24. Chatterjee, A.; Konig, B., Birch-Type Photoreduction of Arenes and Heteroarenes by Sensitized Electron Transfer. *Angew. Chem., Int. Ed.* **2019,** *58*, 14289-14294, doi:10.1002/anie.201905485

25. (a) Yang, H.; Zhang, X.; Zhou, L.; Wang, P., Development of a Photolabile Carbonyl-Protecting Group Toolbox. *J. Org. Chem.* **2011,** *76*, 2040-2048, doi:10.1021/jo102429g. (b) Thevenet, D.; Neier, R., An Efficient Photoinduced Deprotection of Aromatic Acetals and Ketals. *HCA* **2011,** *94*, 331-346, doi:10.1002/hlca.201000333

Visible-Light-Promoted Metal-Free Ammoxidation of C(sp^3)-H bonds

Kathiravan Murugesan, Karsten Donabauer, and Burkhard König *

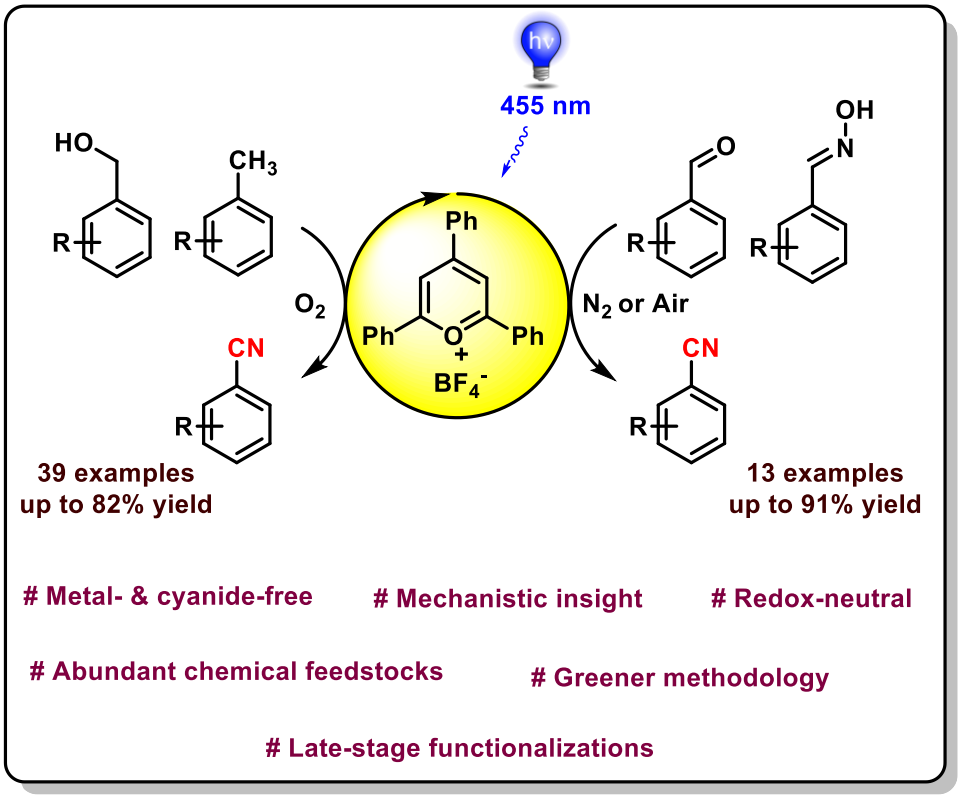
hν
455 nm
HO
R
CH3
R
O2
Ph
Ph
O
Ph
BF4-
N2 or Air
O
R
OH
N
R
CN
R
CN
R
39 examples
up to 82% yield
13 examples
up to 91% yield
Metal- & cyanide-free
Mechanistic insight
Redox-neutral
Abundant chemical feedstocks
Greener methodology
Late-stage functionalizations

Visible-Light-Promoted Metal-Free Ammoxidation of C(sp^3)-H bonds

Kathiravan Murugesan[a], Karsten Donabauer[a] and Burkhard König[a]*

[a]Faculty of Chemistry and Pharmacy, University of Regensburg, Germany

*Correspondence: burkhard.koenig@ur.de

Table of contents

1. General information

All required fine chemicals were purchased from commercial suppliers (abcr, Acros, Alfa Aesar, Fluka, Fluorochem, Merck, Sigma Aldrich, TCI) and were used directly without purification unless stated otherwise. All air and moisture sensitive reactions were carried out under nitrogen atmosphere using standard Schlenk manifold technique. Extra dry anhydrous acetonitrile was purchased from Acros organics.

All NMR spectra were measured at room temperature using a Bruker Avance 300 (300 MHz for ^{1}H, 75 MHz for ^{13}C, 282 MHz for ^{19}F) or a Bruker Avance 400 (400 MHz for ^{1}H, 101 MHz for ^{13}C, 376 MHz for ^{19}F)[1] NMR spectrometer. All chemical shifts are reported in δ-scale as parts per million [ppm] (multiplicity, coupling constant *J*, number of protons) relative to the solvent residual peaks as the internal standard.[2] Coupling constants *J* are given in Hertz [Hz]. Abbreviations used for signal multiplicity: ^{1}H-NMR: b = broad, s = singlet, d = doublet, t = triplet, q = quartet, p = quintet, and m = multiplet.

GC measurements were performed on a GC 7890 from Agilent Technologies. Data acquisition and evaluation was done with Agilent ChemStation Rev.C.01.04. GC/MS measurements were performed on a 7890A GC system from Agilent Technologies with an Agilent 5975 MSD Detector. Data acquisition and evaluation was done with MSD ChemStation E.02.02.1431. A capillary column HP-5MS/30 m x 0.25 mm/0.25 μM film and helium as carrier gas (flow rate of 1 mL/min) were used. The injector temperature (split injection: 40:1 split) was 280 °C, detection temperature 300 °C (FID). GC measurements were made and investigated *via* integration of the signal obtained. The GC oven temperature program was adjusted as follows: initial temperature 40 °C was kept for 3 minutes, the temperature was increased at a rate of 15 °C/min over a period of 16 minutes until 280 °C was reached and kept for 5 minutes, the temperature was again

increased at a rate of 25 °C/min over a period of 48 seconds until the final temperature (300 °C) was reached and kept for 5 minutes. *n*-Decane was used as an internal standard.

Analytical TLC was performed on silica gel coated aluminium sheets (Merck, TLC Silica gel 60 F_{254}). Compounds were visualized by exposure to UV-light (254 or 366 nm) or by dipping the plates in staining solutions (permanganate stain, bromocresol green stain, ceric ammonium molybdate stain) followed by heating. Purification by column chromatography was performed with silica gel 60 M (40-63 μm, 230-440 mesh, Merck) or with a pre-packed Biotage® Snap Ultra HP-Sphere™ 25 *u*m column on a Biotage® Isolera™ Spektra One device. All mixed solvent eluents are reported as v/v solutions.

High resolution mass spectrometry (HRMS) were performed at the Central Analytical Laboratory of the University of Regensburg. Mass spectra were recorded on a Finnigan MAT 95, ThermoQuest Finnigan TSQ 7000, Finnigan MAT SSQ 710 A or Agilent Q-TOF 6540 UHD instrument and a Waters Acquity UPLC system equipped with Waters PDA, sample manager, sample organiser, column oven and Waters Xevo QTOF mass spectrometer. Photoreactions in regular scale were irradiated with blue LEDs (OSRAM Oslon SSL 80 royal-blue, λ = 455 nm (± 15), average radiant flux 232 ± 23 mW, 2.9 V, 350 mA) or green LEDs (λ = 535 nm, average radiant flux, 29 ± 5 mW) and were exposed to light from the flat bottom side of the vial. The temperature of the reaction mixtures was controlled by a water-cooling circuit consisting of an aluminium cooling block connected to a thermostat (Fig. S1). An exemplary reaction in larger scale was carried out in a custom-built glass reactor which upon vigorous stirring generates a thin film of the reaction mixture between the reaction vessel and an attached cold finger. The reaction vessel was surrounded by blue LED arrays (OSRAM Oslon SSL 80 LT-2010, λ = 451 nm, 700 mA) generating a total radiant flux of 12 W (Fig. S2). Luminescence measurements were performed on a Horiba® Scientific FluoroMax-4 instrument using the above-mentioned quartz cells. Luminescence lifetime measurements were performed on a Horiba® Scientific DeltraPro™ fluorescence lifetime system using a 452 nm laser diode from Horiba® Scientific DeltaDiode™ as excitation source and above-mentioned quartz cells. The instrument response function (IRF) was determined prior to measurements by using colloidal silica (LUDOX®) in water.

CV measurements were performed with the three-electrode potentiostat galvanostat PGSTAT302N from Metrohm Autolab using a glassy carbon working electrode, a platinum wire

counter electrode, a silver wire as a reference electrode and TBATFB 0.1 M as supporting electrolyte. The control of the measurement instrument, the acquisition and processing of the cyclic voltammetric data were performed with the software Metrohm Autolab NOVA 1.10.4. The measurements were carried out as follows: a 0.1 M solution of TBATFB in acetonitrile was added to the measuring cell and the solution was degassed by argon purge for 5 min. After recording the baseline the electroactive compound was added (0.01 M) and the solution was again degassed a stream of argon for 5 min. The cyclic voltammogram was recorded with one to three scans. Afterwards ferrocene (2.20 mg, 12.0 μmol) was added to the solution which was again degassed by argon purge for 5 min and the final measurement was performed with three scans.

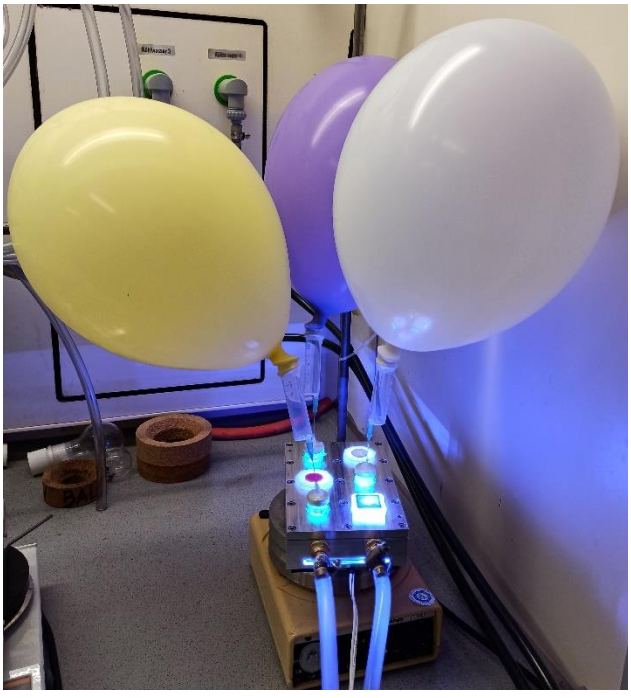

Fig. S1: Typical set-up for small scale synthesis

Fig. S2: Custom-built glass reactor for upscaling of the photocatalytic ammoxidation reaction.

2. Synthetic procedure

2.1 General procedure for the synthesis of methylarenes

Methylarenes were synthesized according to a literature procedure.[3]

General conditions: To a stirred solution of 4-methyl benzoyl chloride (7.5 mmol, 1.5 eq) in DCM (10 mL) and added an alcohol or amine nucleophile (5 mmol 1.0 eq), DMAP (0.5 mmol, 0.1 eq) and Et_3N (10 mmol, 2.0 eq) in DCM (10 mL). The reaction was allowed to stir overnight at room temperature. Then, the mixture was quenched upon addition of NH_4Cl (aq. 10%), and extracted with DCM (3x). The organic phase was washed with brine, concentrated and purified by silica gel flash chromatography to give the corresponding substituted methylarenes. If the HCl salt of the amine nucleophile was employed, 4 eq of Et_3N were used.

2.2 General procedure for the synthesis of oximes

Oximes were synthesized according to a literature procedure.[4]

A 100 mL round bottom flask equipped with a magnetic stirring bar was loaded with NH_2OH•HCl (1.2 eq for 1.0 g of substrate) in water (25 mL), followed by the addition of $NaHCO_3$ (1.75 eq for 1.0 g of substrate) at 0° C. A solution of the corresponding aldehyde (1.0 g, 1 eq) in MeOH was added to the above mixture and stirred at RT for 6h. The reaction progress was monitored by TLC (PE:EA). After completion of the reaction, MeOH was removed under reduced pressure. The precipitated solid was filtered off, washed with water and dried under high vacuum. The thus obtained product was used for following steps without further purification.

2.3 General procedure for the synthesis of nitriles from methylarenes or alcohols

A 5 mL crimp cap vial equipped with a magnetic stirring bar was loaded with TPP (20 μmol, 8.0 mg, 20 mol%), NH_2OH•HCl (0.3 mmol, 20.7 mg, 3 eq), NH_4Br (0.25 mmol, 25.0 mg, 2.5 eq), 4 Å molecular sieves (25 mg), the corresponding methylarene or alcohol (0.1 mmol, 1 eq.) and dry ACN (2 mL, 0.05M). In doing so, all solid compounds were added before capping the vial, whereas all liquid compounds were added *via* syringe after setting the capped vial under an O_2 atmosphere (highly viscous liquids were added before capping the vial as well). The reaction mixture was stirred under 1 bar of O_2 using an O_2-filled balloon and under light irradiation using a 455 nm (± 15 nm) LED for 24 h at 40 °C using a cryostat. Four reaction batches were combined, filtered and concentrated under reduced pressure. The crude product was

purified by automated flash column chromatography using a petrolether/ethyl acetate mixture. Note: in order to get better yields, dry acetonitrile and freshly activated 4 Å molecular sieves are mandatory.

2.4 General procedure for the synthesis of nitriles from aldehydes

A 5 mL crimp cap vial equipped with a magnetic stirring bar was loaded with TPP (20 μmol, 8.0 mg, 20 mol%), NH_2OH•HCl (0.3 mmol, 20.7 mg, 3 eq), NH_4Br (0.25 mmol, 25.0 mg, 2.5 eq), 4 Å molecular sieves (25 mg), the corresponding aldehyde (0.1 mmol, 1 eq.) and dry ACN (2 mL, 0.05M). In doing so, all solid compounds were added before capping the vial, whereas all liquid compounds were added *via* syringe after setting the capped vial under N_2 atmosphere (highly viscous liquids were added before capping the vial as well). The reaction mixture was stirred under light irradiation using a 455 nm (± 15 nm) LED for 24 h at 40 °C using a cryostat. Four reaction batches were combined, filtered and concentrated under reduced pressure. The crude product was purified by automated flash column chromatography using a petrolether/ethyl acetate mixture.

2.5 General procedure for the synthesis of nitriles from oximes

A 5 mL crimp cap vial equipped with a magnetic stirring bar was loaded with TPP (20 μmol, 8.0 mg, 20 mol%), 4 Å molecular sieves (25 mg), the corresponding oxime (0.1 mmol, 1 eq.) and dry ACN (2 mL, 0.05M). In doing so, all solid compounds were added before capping the vial, whereas all liquid compounds were added *via* syringe after setting the capped vial under a N_2 atmosphere (highly viscous liquids were added before capping the vial as well). The reaction mixture was stirred under light irradiation using a 455 nm (± 15 nm) LED for 24 h at 40 °C using a cryostat. Four reaction batches were combined, filtered and concentrated under reduced pressure. The crude product was purified by automated flash column chromatography using a petrolether/ethyl acetate mixture.

2.6 General procedure for gram scale reactions

A 200 mL glass reactor equipped with a magnetic stirring bar was loaded with TPP (20 mol% for 1 g of substrate), NH_2OH•HCl (3 eq for 1 g of substrate), NH_4Br (2.5 eq for 1 g of substrate), 4 Å molecular sieves (25 mg for 0.1 mmol of substrate), the corresponding methylarene (1 g, 1 eq.) and dry ACN (0.05 M). In doing so, all solid compounds were added first to the glass reactor, whereas all liquid compounds were added at the end under O_2 or air atmosphere. The reaction setup was connected to two balloons holding

each 1 bar of oxygen (please see Fig. S2) and the mixture was stirred under light irradiation using a 455 nm (± 15 nm) LED for 36 h at 40 °C using a cryostat. The reaction progress was monitored by GC-FID. After the completion of the reaction, the reaction mixture was filtered over a celite bed and concentrated under reduced pressure. The crude product was purified by automated flash column chromatography using a petrolether/ethyl acetate mixture.

3. Reaction optimization

Table S1. Screening of different solvents

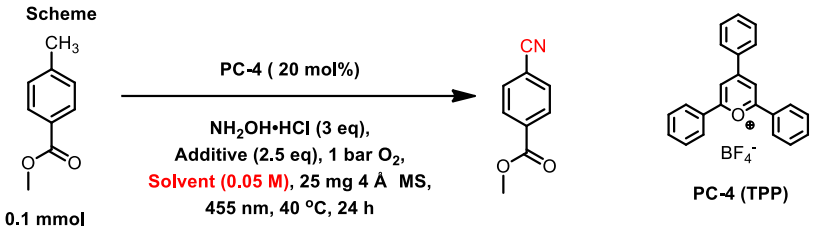

Entry	Solvent (0.05M conc.)	Yield of product (%)
1	**ACN**	**76**
2	Benzene	22
3	DMF	NR
4	DMSO	NR
5	DCM	3
6	TFE	12
7	Acetic acid	NR
8	ACN (0.1 M)	63
9	ACN (0.2 M)	39
10	ACN + 100 µL H_2O (without molecular sieves)	10

Reaction conditions: [a]0.1 mmol substrate, 20 mol% PC, 3 eq. NH_2OH•HCl, 2.5 eq. NH_4Br, 25 mg 4 Å MS, 1 bar O_2, 2 mL solvent (0.05 M), 455 nm, 40 °C, 24 h, GC yields using n-decane as standard.

Table S2. Screening of different additives

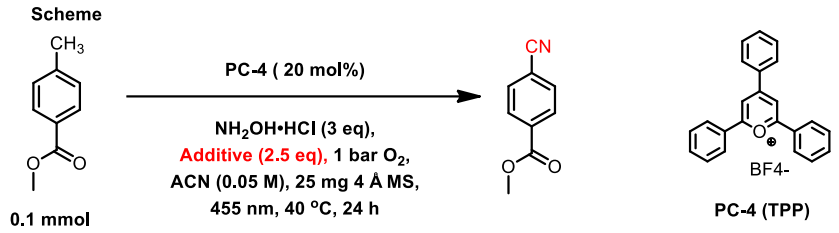

Entry	Ammonia source (3 eq)	Additive(2.5 eq)	Yield of product (%)
1	$NH_2OH•HCl$	NH_4Br	76
2	$NH_2OH•HCl$	TBABr	10
3	$NH_2OH•HCl$	$Sc(OTf)_3$	35
4	$NH_2OH•HCl$	TFA	10
5	$NH_2OH•HCl$	NH_4F	4
6	$NH_2OH•HCl$	NH_4Cl	32
7	$NH_2OH•HCl$	NH_4I	NR
8	$NH_2OH•HCl$	CBr_4	33
9	$NH_2OH•HCl$	KBr	36

Reaction conditions: [a]0.1 mmol substrate, 20 mol% PC, 3 eq. $NH_2OH•HCl$, 2.5 eq. additive, 25 mg 4 Å MS, 1 bar O_2, 2 mL acetonitrile (0.05 M), 455 nm, 40 °C, 24 h, GC yields using n-decane as standard.

Table S3. Control experiments

Scheme

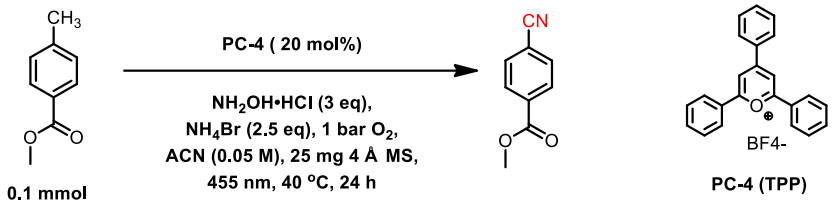

Entry	PC-4 (20 mol%)	Light (455 nm)	$NH_2OH•HCl$ (3 eq)	NH_4Br (2.5 eq)	4 Å MS (25 mg)	O_2 (1 bar)	Yield of product (%)
1	**YES**	**YES**	**YES**	**YES**	**YES**	**YES**	**76**
2	NO	YES	YES	YES	YES	YES	1
3	YES	NO	YES	YES	YES	YES	NR
4	YES	YES	NO	YES	YES	YES	2
5	YES	YES	YES	NO	YES	YES	25
6	YES	YES	YES	YES	NO	YES	51
7	YES	YES	YES	YES	YES	NO	NR

Reaction conditions: [a]0.1 mmol substrate, 20 mol% PC, 3 eq. $NH_2OH•HCl$, 2.5 eq. NH_4Br, 25 mg 4 Å MS, 1 bar O_2, 2 mL acetonitrile (0.05 M), 455 nm, 40 °C, 24 h, GC yields using n-decane as standard.

4. Mechanistic Investigation

4.1 Time-resolved Luminescence Quenching studies

A linear correlation between concentration of quencher [Q] and $\tau_0 \times \tau^{-1}$ indicates a dynamic luminescence quenching. The luminescence lifetime was recorded in dry ACN using a quartz cuvette (1×1 cm) with septum screw cap. The cuvette was degassed *in vacuo* and backfilled with N_2 (5×) before the stock solution of quencher and the catalyst solution were added *via* syringe. For excitation of the sample, a 452 nm laser diode was used and an optical longpass filter (cut-on wavelength 500 nm) was installed before the detection unit. The time range for the measurement was set to 100 ns. The experimental data were fitted with a mono-exponential function. For liquid sample added as such for solid sample concertation solution in ACN was used. In case of $NH_2OH.HCl$ and NH_4Br 1 mmol was taken in 1 mL ACN and stirred at 40° C for 15 minutes then passed through the filter pad and clear solution was used for quenching studies.

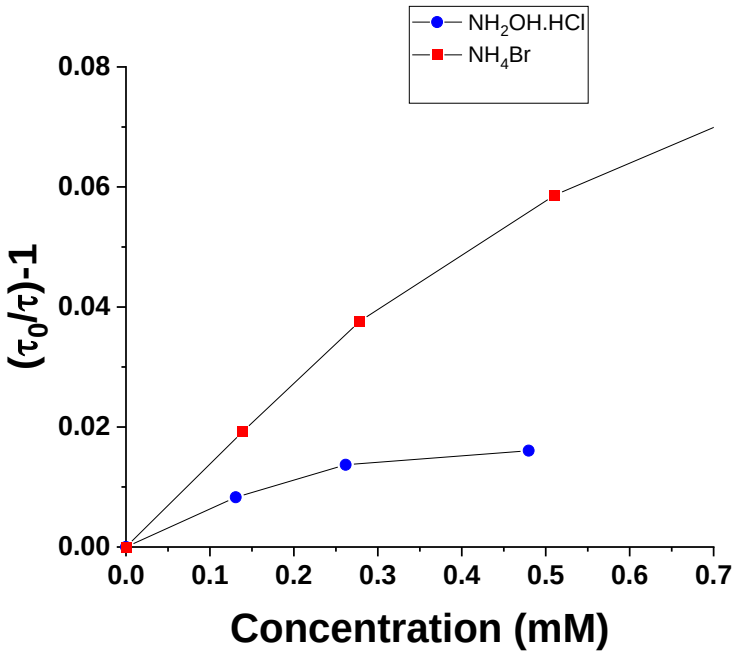

Fig. S3: Stern-Volmer plot developed with data obtained from time-resolved quenching experiments of TPP (PC-4) with NH_2OH•HCl and NH_4Br.

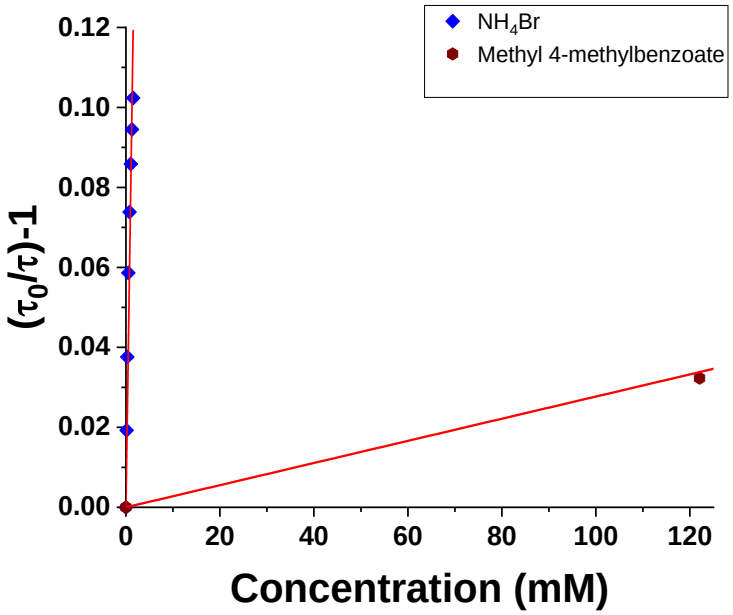

Fig. S4: Stern-Volmer plot developed with data obtained from time-resolved quenching experiments of TPP (PC-4) with methyl 4-methylbenzoate and NH_4Br.

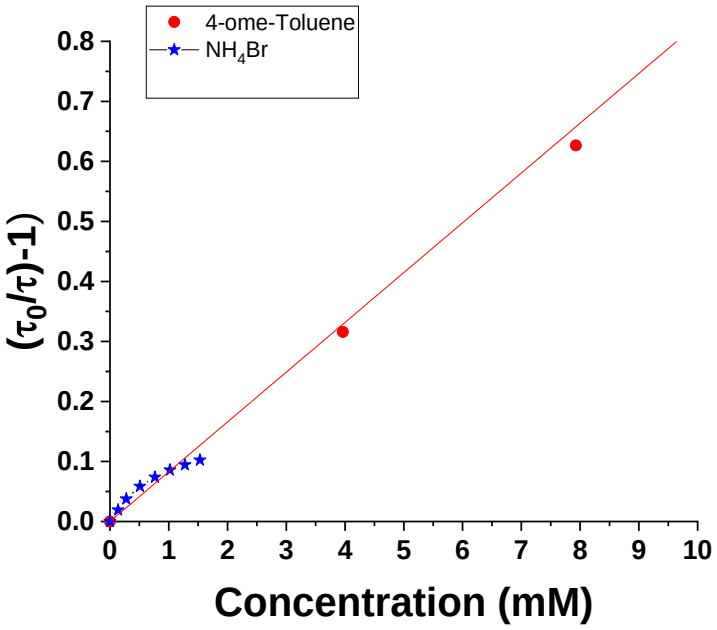

Fig. S5: Stern-Volmer plot developed with data obtained from time-resolved quenching experiments of TPP (PC-4) with 4-methoxy toluene and NH_4Br.

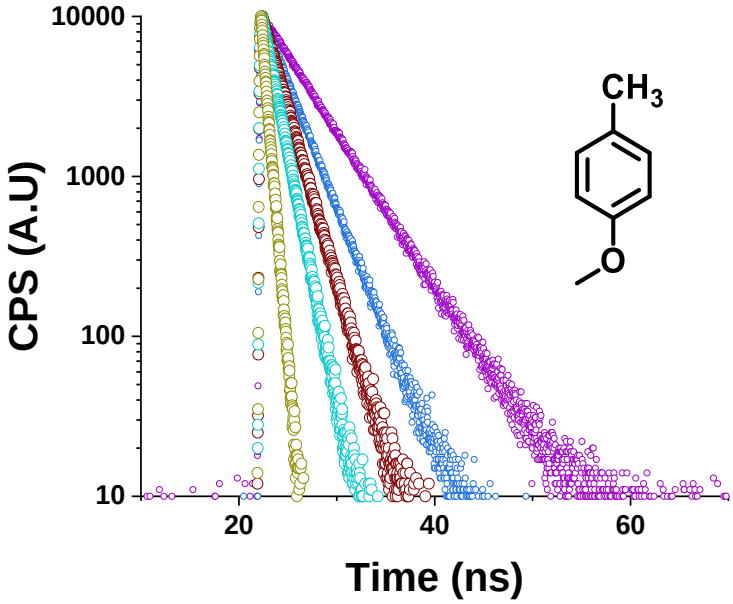

Fig. S6: Luminescence decay of 4-methoxy toluene with TPP (PC-4). The lifetime was determined by employing an exponential fit function.

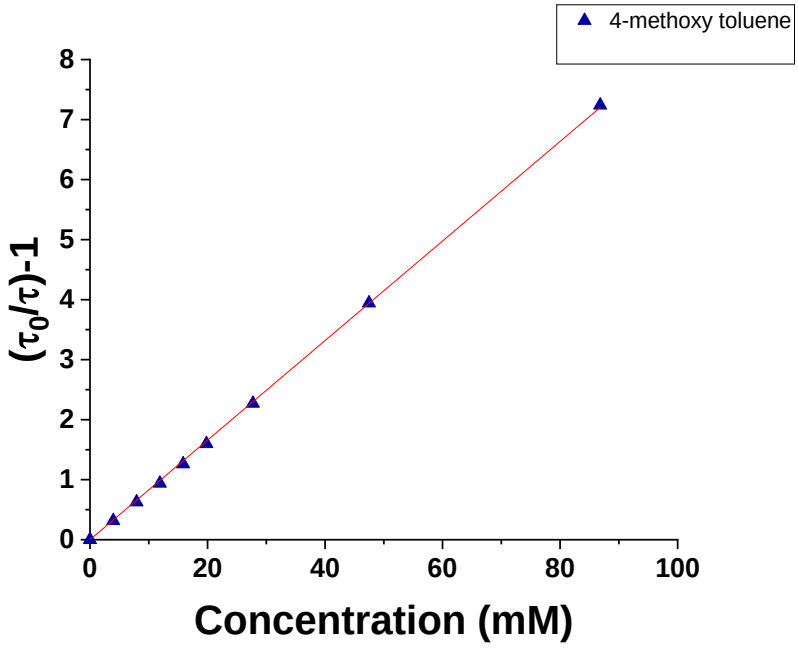

Fig. S7: Stern-Volmer plot developed with data obtained from time-resolved quenching experiments of TPP (PC-4) with 4-methoxy toluene.

4.2 Trapping experiments[5]

Experiment-2a: Traping of radical cation

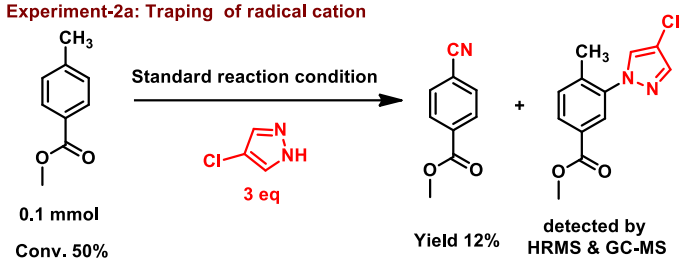

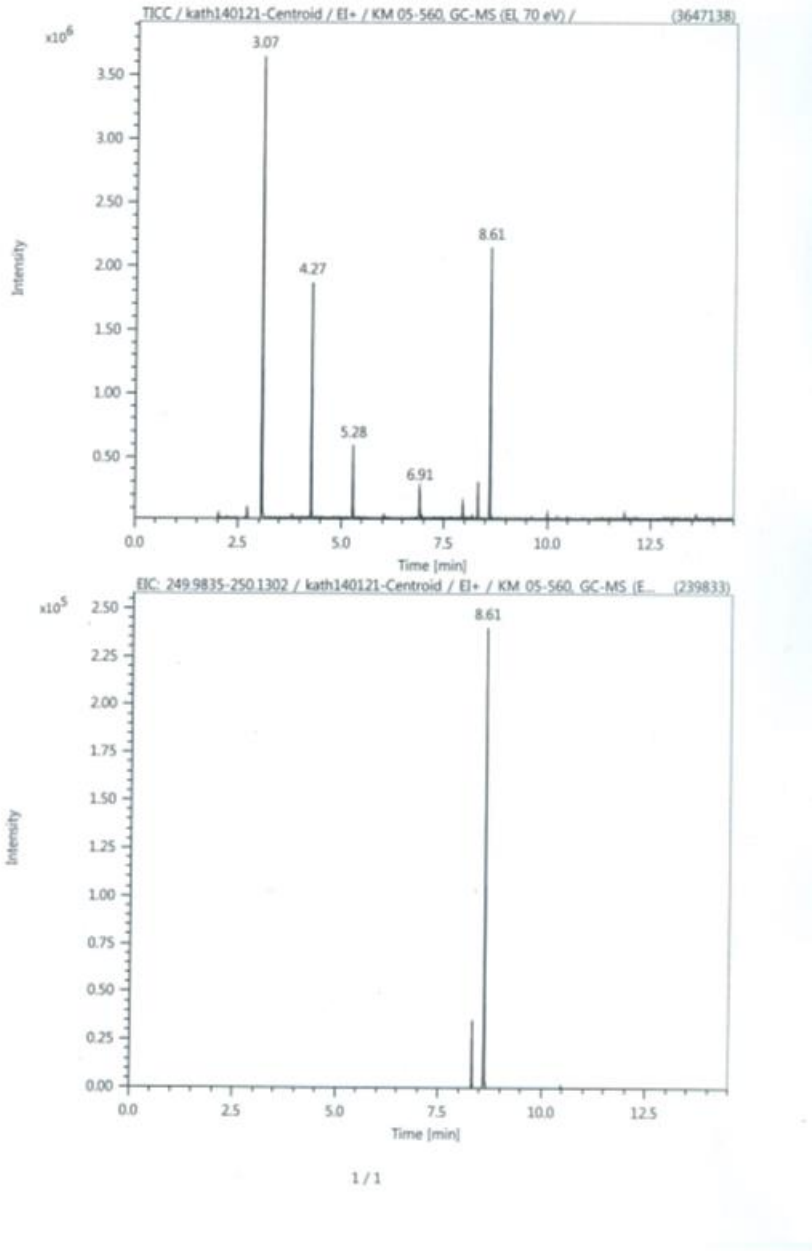

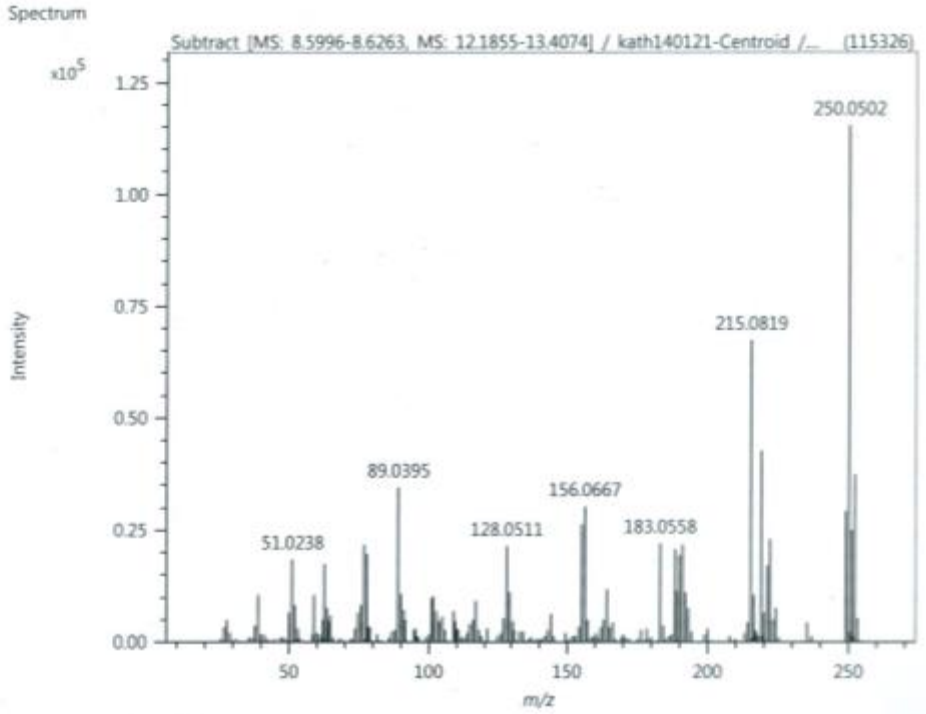

Elemental Composition

Parameters	
Tolerance:	15.00 ppm
Electron:	Odd/Even
Charge:	+1
DBE:	-1.5 - 50.0

Elements:

Symbol	C	H	N	O	S	Cl	B	Br
Min	1	1	0	0	0	0	0	0
Max	100	100	3	3	0	3	0	0

Symbol	F
Min	0
Max	0

Results

Mass	Intensity	Formula	Calculated Mass	Mass Difference [mDa]	Mass Difference [ppm]	DBE
249.04264	29291.78	C12 H10 N2 O2 Cl	249.04253	0.11	0.45	8.5
		C9 H13 N3 O Cl2	249.04302	-0.38	-1.51	4.0
		C15 H7 N O3	249.04204	0.60	2.40	13.0
		C11 H15 O2 Cl2	249.04436	-1.72	-6.90	3.5
		C18 H5 N2	249.04472	-2.08	-8.36	17.5
		C8 H18 N O Cl3	249.04485	-2.21	-8.86	-1.0
250.05017	115325.67	C12 H11 N2 O2 Cl	250.05036	-0.19	-0.74	8.0
		C15 H8 N O3	250.04987	0.30	1.20	12.5
		C9 H14 N3 O Cl2	250.05084	-0.67	-2.69	3.5
		C11 H16 O2 Cl2	250.05219	-2.02	-8.06	3.0
		C18 H6 N2	250.05255	-2.38	-9.51	17.0

1 / 1

Fig. S8: GC-MS and HRMS spectra of 4-chloro pyrazole trapped product under standard reaction condition

Experiment-2b: Traping of radical cation

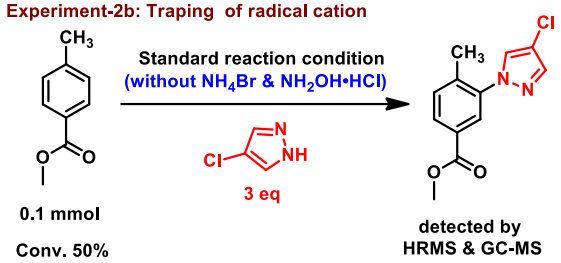

0.1 mmol

Conv. 50%

detected by
HRMS & GC-MS

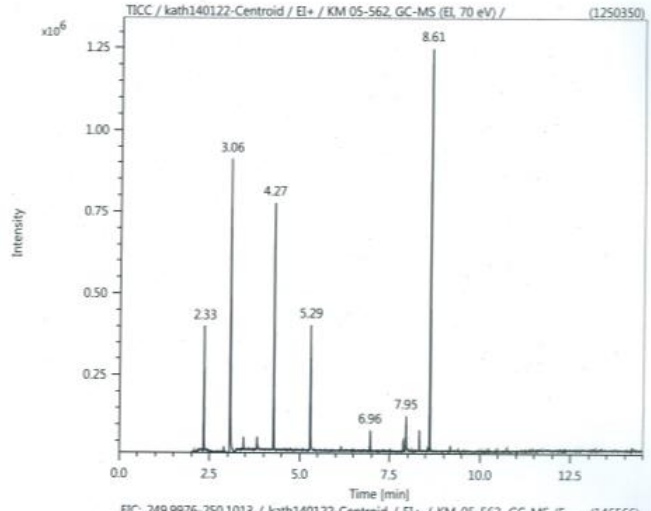

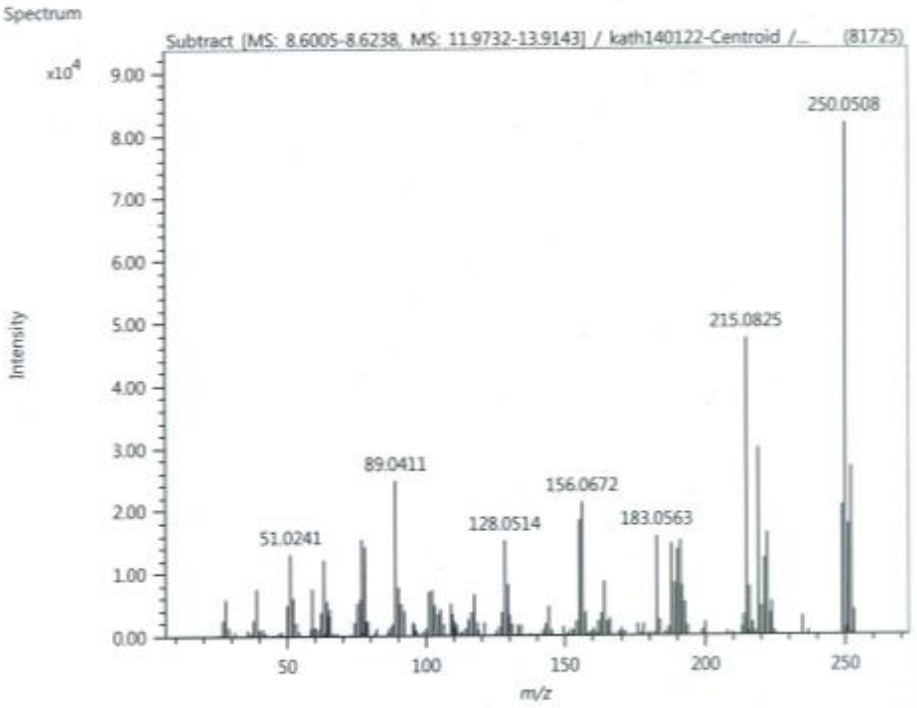

Elemental Composition

Parameters	
Tolerance:	15.00 ppm
Electron:	Odd/Even
Charge:	+1
DBE:	-1.5 - 50.0

Elements:

Symbol	C	H	N	O	S	Cl	B	Br
Min	1	1	0	0	0	0	0	0
Max	100	100	3	3	0	3	0	0

Symbol	F
Min	0
Max	0

Results

Mass	Intensity	Formula	Calculated Mass	Mass Difference [mDa]	Mass Difference [ppm]	DBE
249.04319	20812.63	C9 H13 N3 O Cl2	249.04302	0.17	0.70	4.0
		C12 H10 N2 O2 Cl	249.04253	0.66	2.66	8.5
		C15 H7 N O3	249.04204	1.15	4.61	13.0
		C11 H15 O2 Cl2	249.04436	-1.17	-4.69	3.5
		C18 H5 N2	249.04472	-1.53	-6.15	17.5
		C8 H18 N O Cl3	249.04485	-1.66	-6.65	-1.0
		C17 H10 Cl	249.04655	-3.36	-13.50	12.5
250.05078	81724.75	C9 H14 N3 O Cl2	250.05084	-0.06	-0.25	3.5
		C12 H11 N2 O2 Cl	250.05036	0.42	1.70	8.0
		C15 H8 N O3	250.04987	0.91	3.65	12.5
		C11 H16 O2 Cl2	250.05219	-1.41	-5.62	3.0

Fig. S9: GC-MS and HRMS spectra of 4-chloro pyrazole trapped product without NH_4Br and NH_2OH•HCl

Experiment-2c: Traping of radical cation

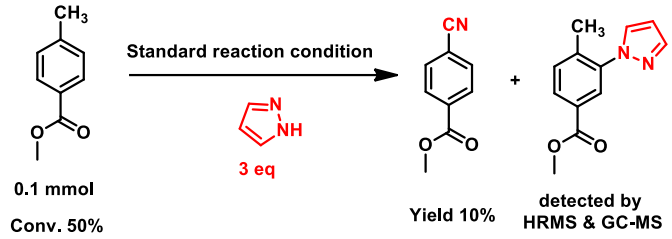

0.1 mmol

Conv. 50%

Yield 10%

detected by HRMS & GC-MS

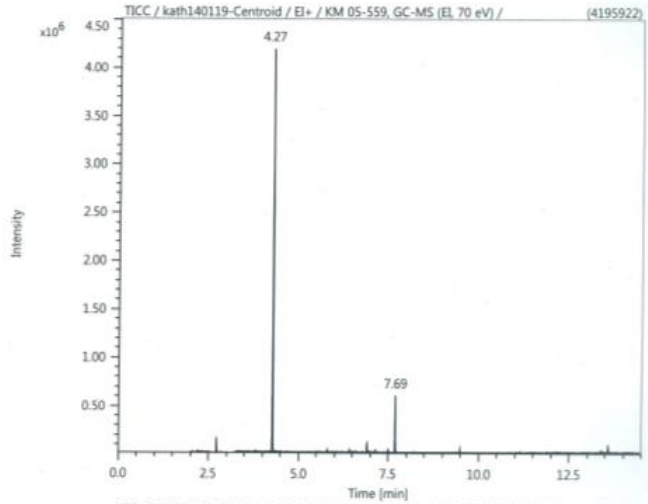

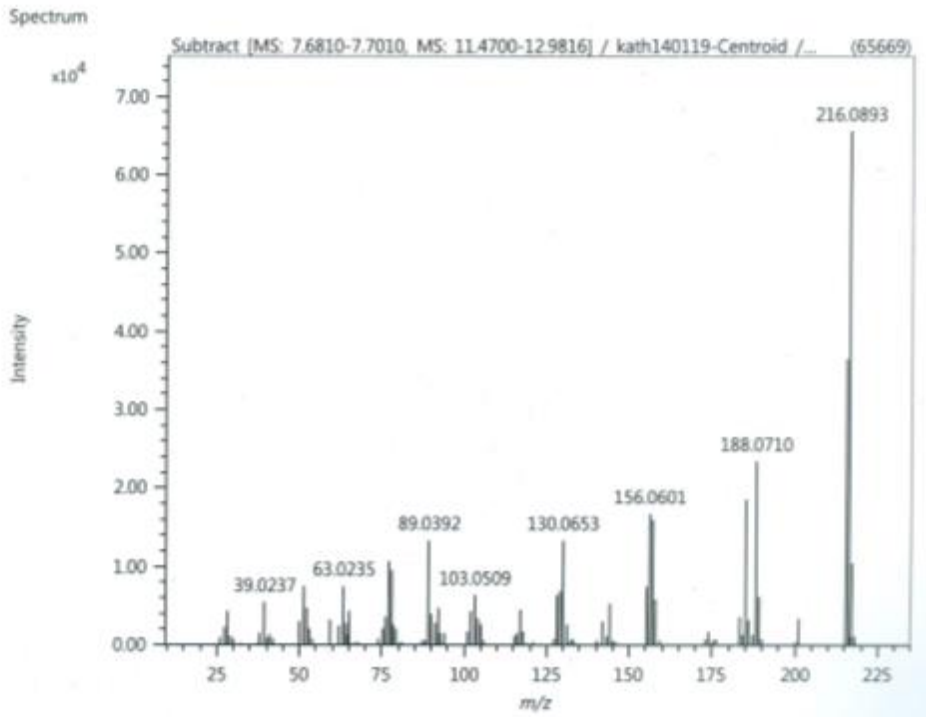

Elemental Composition

Parameters	
Tolerance:	15.00 ppm
Electron:	Odd/Even
Charge:	+1
DBE:	-1.5 - 50.0

Elements:

Symbol	C	H	N	O	S	Cl	B	Br
Min	1	1	0	0	0	0	0	0
Max	100	100	5	5	0	0	0	0

Symbol	F
Min	0
Max	0

Results

Mass	Intensity	Formula	Calculated Mass	Mass Difference [mDa]	Mass Difference [ppm]	DBE
215.08165	36668.71	C12 H11 N2 O2	215.08150	0.14	0.67	8.5
		C10 H9 N5 O	215.08016	1.49	6.91	9.0
		C9 H13 N O5	215.07882	2.82	13.13	4.0
216.08930	65669.14	C12 H12 N2 O2	216.08933	-0.03	-0.15	8.0
		C10 H10 N5 O	216.08799	1.31	6.06	8.5
		C9 H14 N O5	216.08665	2.65	12.25	3.5

Fig. S10: GC-MS and HRMS spectra of pyrazole trapped product under standard reaction condition

Experiment-2d: Traping of radical cation

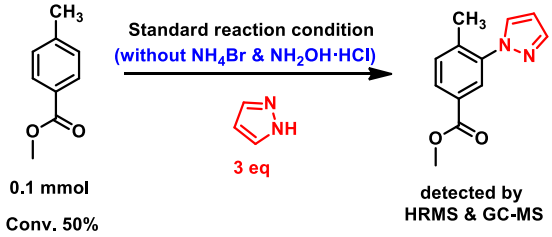

0.1 mmol

Conv. 50%

detected by
HRMS & GC-MS

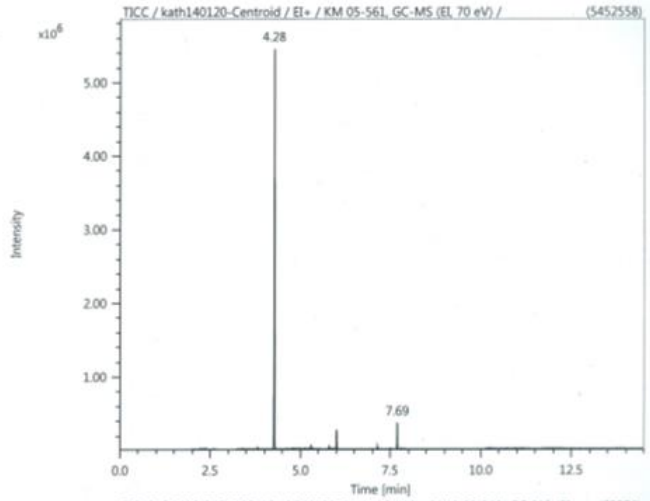

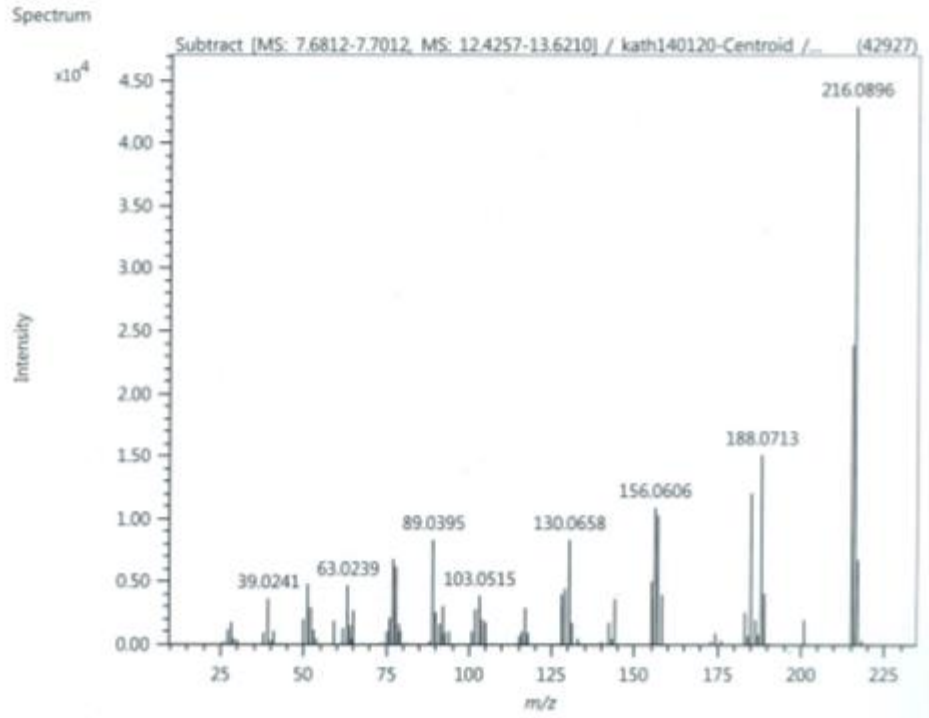

Elemental Composition

Parameters	
Tolerance:	15.00 ppm
Electron:	Odd/Even
Charge:	+1
DBE:	-1.5 - 50.0

Elements:

Symbol	C	H	N	O	S	Cl	B	Br
Min	1	1	0	0	0	0	0	0
Max	100	100	5	5	0	0	0	0

Symbol	F
Min	0
Max	0

Results

Mass	Intensity	Formula	Calculated Mass	Mass Difference [mDa]	Mass Difference [ppm]	DBE
215.08202	23973.43	C12 H11 N2 O2	215.08150	0.52	2.42	8.5
		C10 H9 N5 O	215.08016	1.86	8.66	9.0
		C9 H13 N O5	215.07882	3.20	14.88	4.0
216.08962	42926.57	C12 H12 N2 O2	216.08933	0.29	1.33	8.0
		C10 H10 N5 O	216.08799	1.63	7.55	8.5
		C9 H14 N O5	216.08665	2.97	13.74	3.5

1 / 1

Fig. S11: GC-MS and HRMS spectra of 4-chloro pyrazole trapped product without NH_4Br and NH_2OH•HCl

4.3 The product yield on irradiation density

The irradiation power of blue LED was adjusted in Photoreactor TAK 120 by turning the voltage or current knob. PowerMax USB-PS19Q Power Sensor was also used to verify the emitted light power.

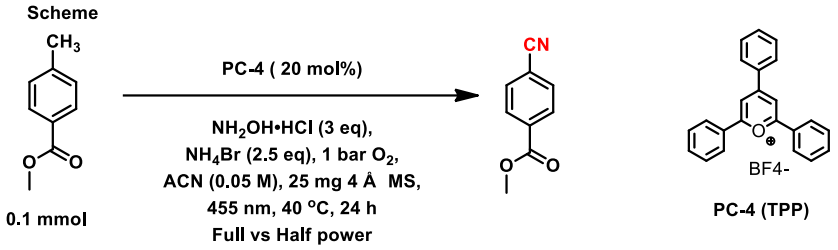

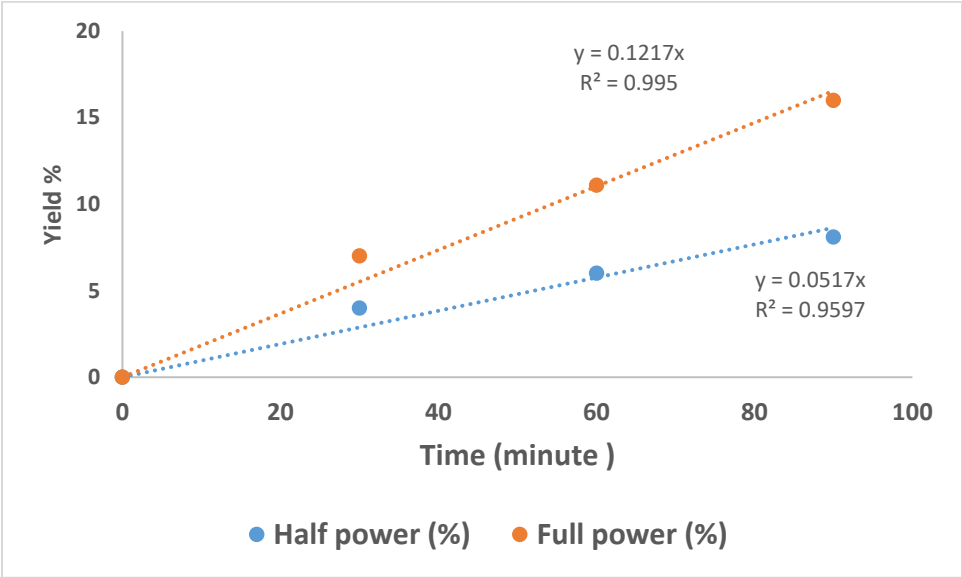

Fig. S12: Two, according to the standard reaction conditions (Section 2.3) identically prepared samples, containing methyl 4-methylbenzoate (1 equiv.), TPP (20 mol%), NH_4Br (2.5 eq.), NH_2OH•HCl (3 eq), 4 Å molecular sieves (25 mg) and 2 mL ACN, were irradiated with the same blue LED using different intensities. To exclude other influencing factors, such as, adverse effects of prolonged reaction time, the reactions were irradiated only for 90 minutes. After 30, 60 and 90 minutes, the irradiation was stopped for both reactions. Yields to the given time were determined by GC analysis using n-decane as internal standard. The slope showed a 2.3:1 (full power: half power) relation, which supports a mechanism involving more than one photon.

4.4 NMR studies

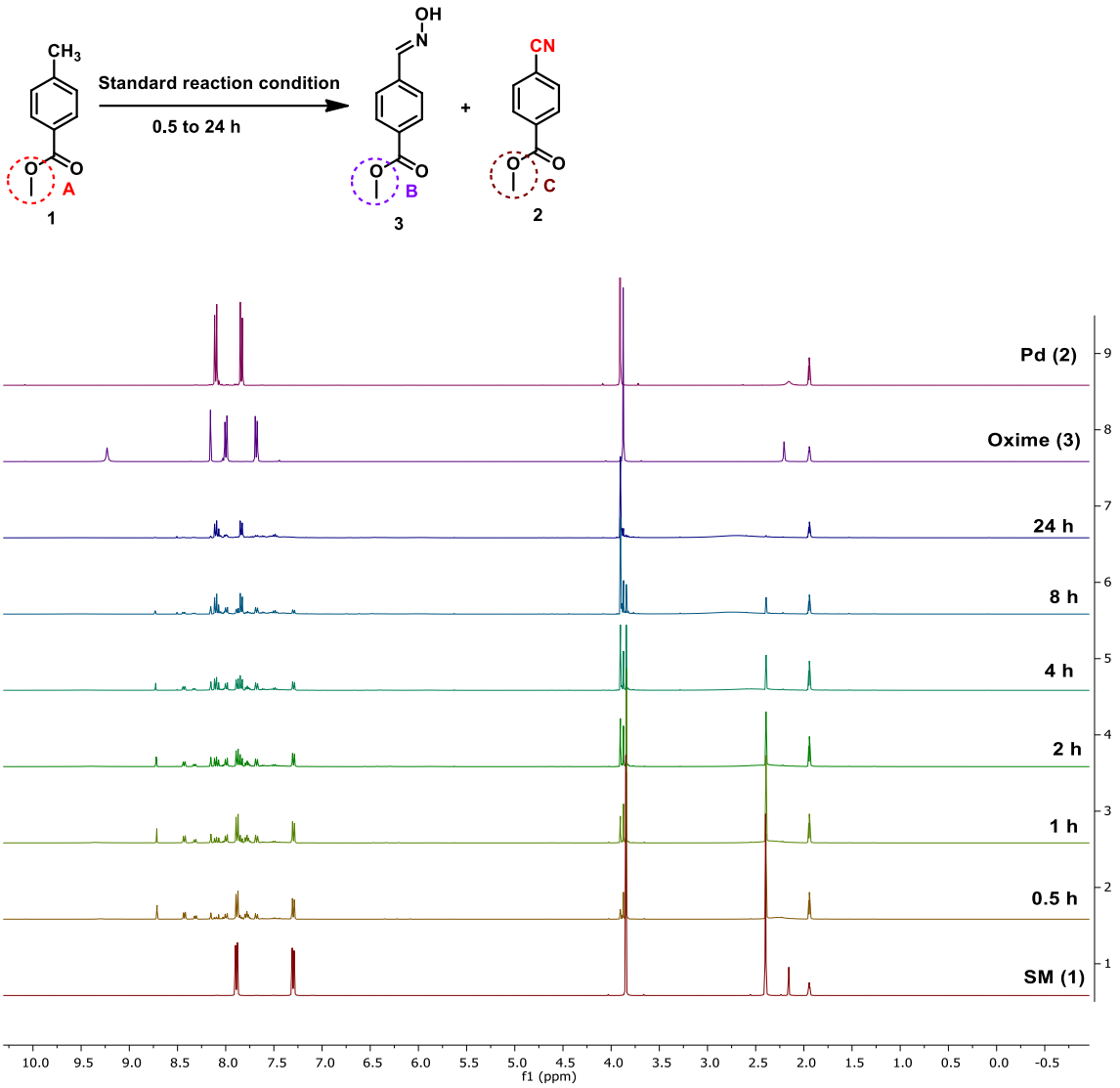

Fig. S13: ^{1}H NMR spectra for different time interval using CD_3CN as a solvent.

Reaction conditions: [a]0.1 mmol substrate, 20 mol% PC, 3 eq. NH_2OH•HCl, 2.5 eq. NH_4Br, 25 mg 4 Å MS, 1 bar O_2, 1 mL CD_3CN (0.1 M), 455 nm, 40 °C, 0.5-24 h. After each time interval, the reaction mixture was filtered through filter pad and the NMR of the solution was measured as such.

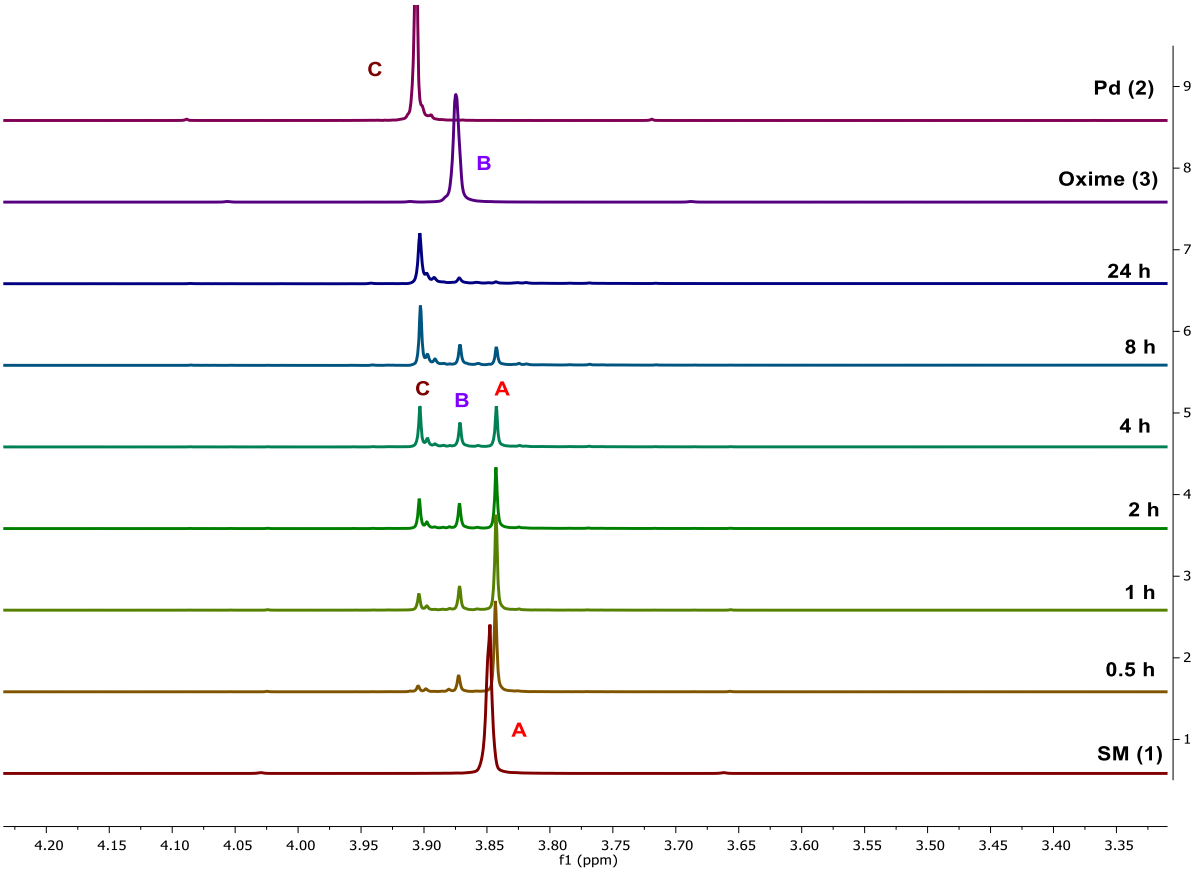

Fig. S13a: ^{1}H NMR spectra for different time interval using CD_3CN as a solvent.

Reaction conditions: [a]0.1 mmol substrate, 20 mol% PC, 3 eq. NH_2OH•HCl, 2.5 eq. NH_4Br, 25 mg 4 Å MS, 1 bar O_2, 1 mL CD_3CN (0.1 M), 455 nm, 40 °C, 0.5-24 h. After each interval reaction mixture was filtered through filtered pad and measured as such a for NMR analysis.

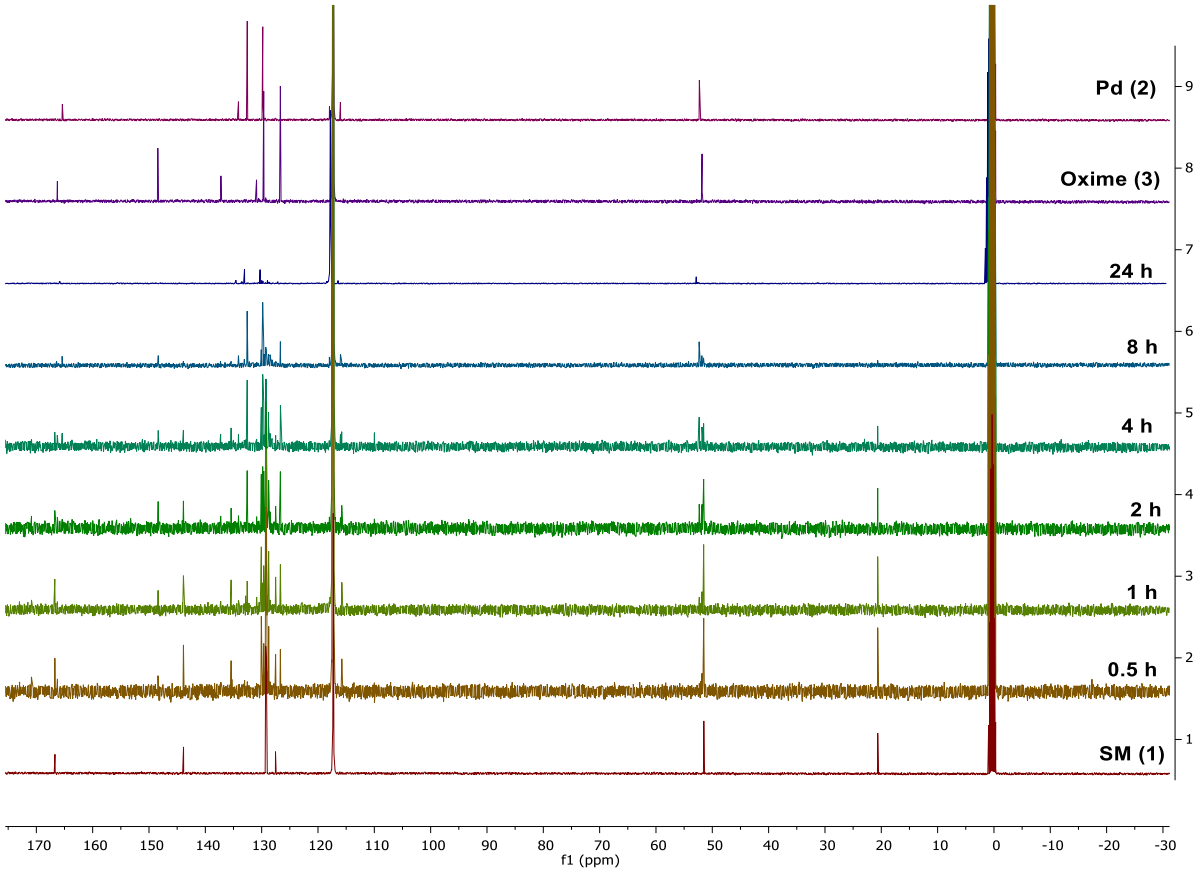

Fig. S14: ^{13}C NMR spectra for different time interval using CD_3CN as a solvent.

Reaction conditions: [a]0.1 mmol substrate, 20 mol% PC, 3 eq. NH_2OH•HCl, 2.5 eq. NH_4Br, 25 mg 4 Å MS, 1 bar O_2, 1 mL CD_3CN (0.1 M), 455 nm, 40 °C, 0.5-24 h. After each interval reaction mixture was filtered through filtered pad and measured as such a for NMR analysis.

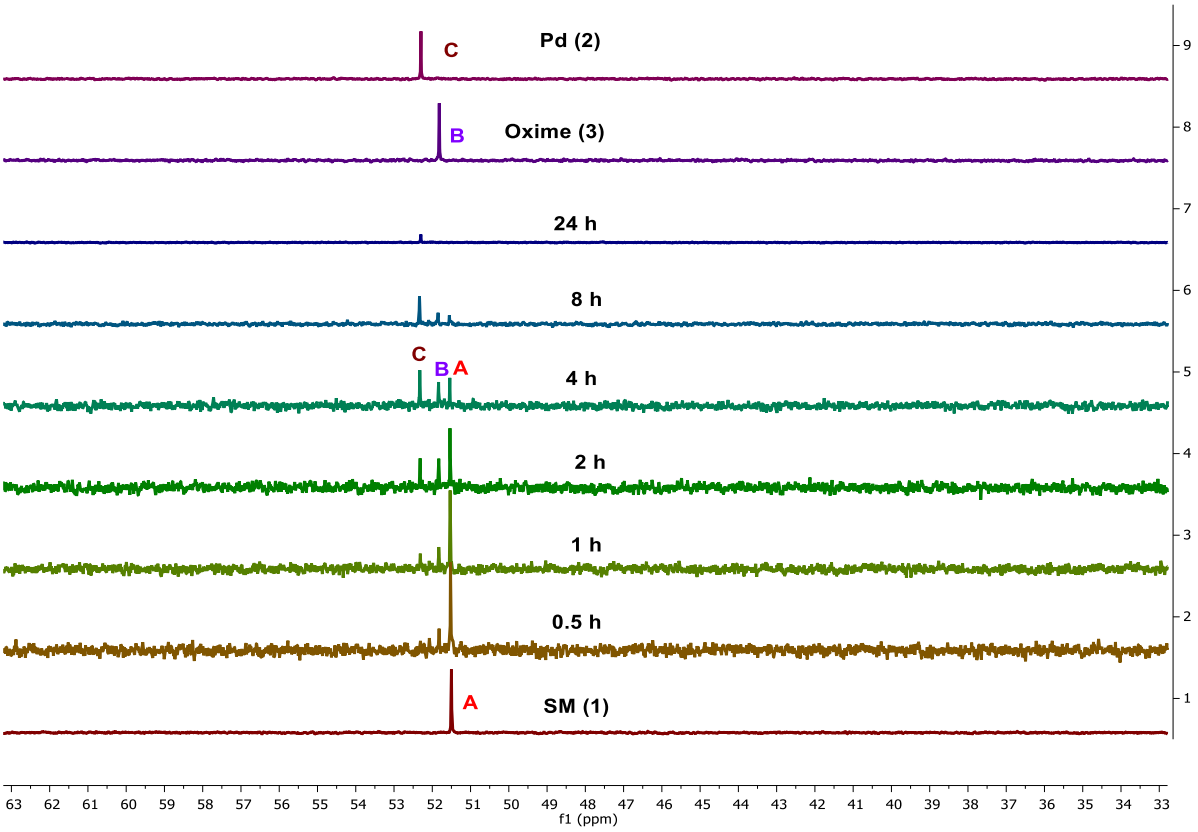

Fig. S14a: ^{13}C NMR spectra for different time interval using CD_3CN as a solvent.

Reaction conditions: [a]0.1 mmol substrate, 20 mol% PC, 3 eq. NH_2OH•HCl, 2.5 eq. NH_4Br, 25 mg 4 Å MS, 1 bar O_2, 1 mL CD_3CN (0.1 M), 455 nm, 40 °C, 0.5-24 h. After each interval reaction mixture was filtered through filtered pad and measured as such a for NMR analysis.

4.5 Catalyst deactivation

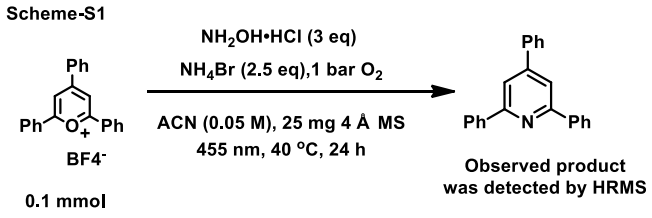

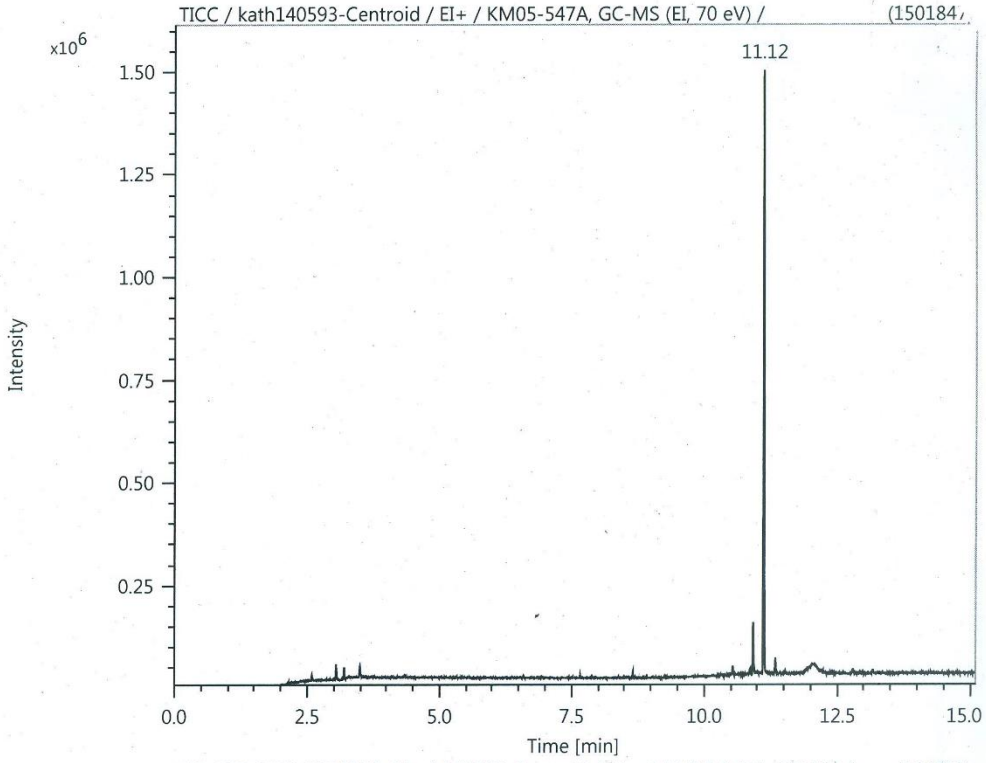
TICC / kath140593-Centroid / EI+ / KM05-547A, GC-MS (EI, 70 eV) /
(150184
x10^6
11.12
1.50
1.25
1.00
0.75
0.50
0.25
Intensity
0.0
2.5
5.0
7.5
10.0
12.5
15.0
Time [min]

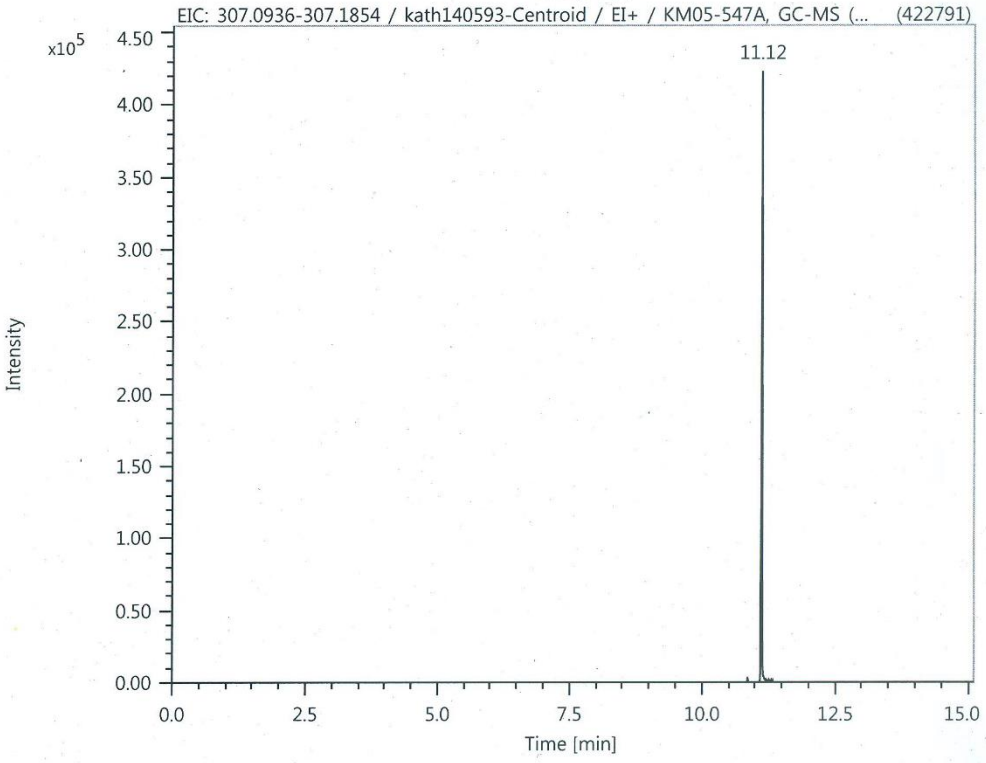
EIC: 307.0936-307.1854 / kath140593-Centroid / EI+ / KM05-547A, GC-MS (...
(422791)
x10^5
11.12
4.50
4.00
3.50
3.00
2.50
2.00
1.50
1.00
0.50
0.00
Intensity
0.0
2.5
5.0
7.5
10.0
12.5
15.0
Time [min]

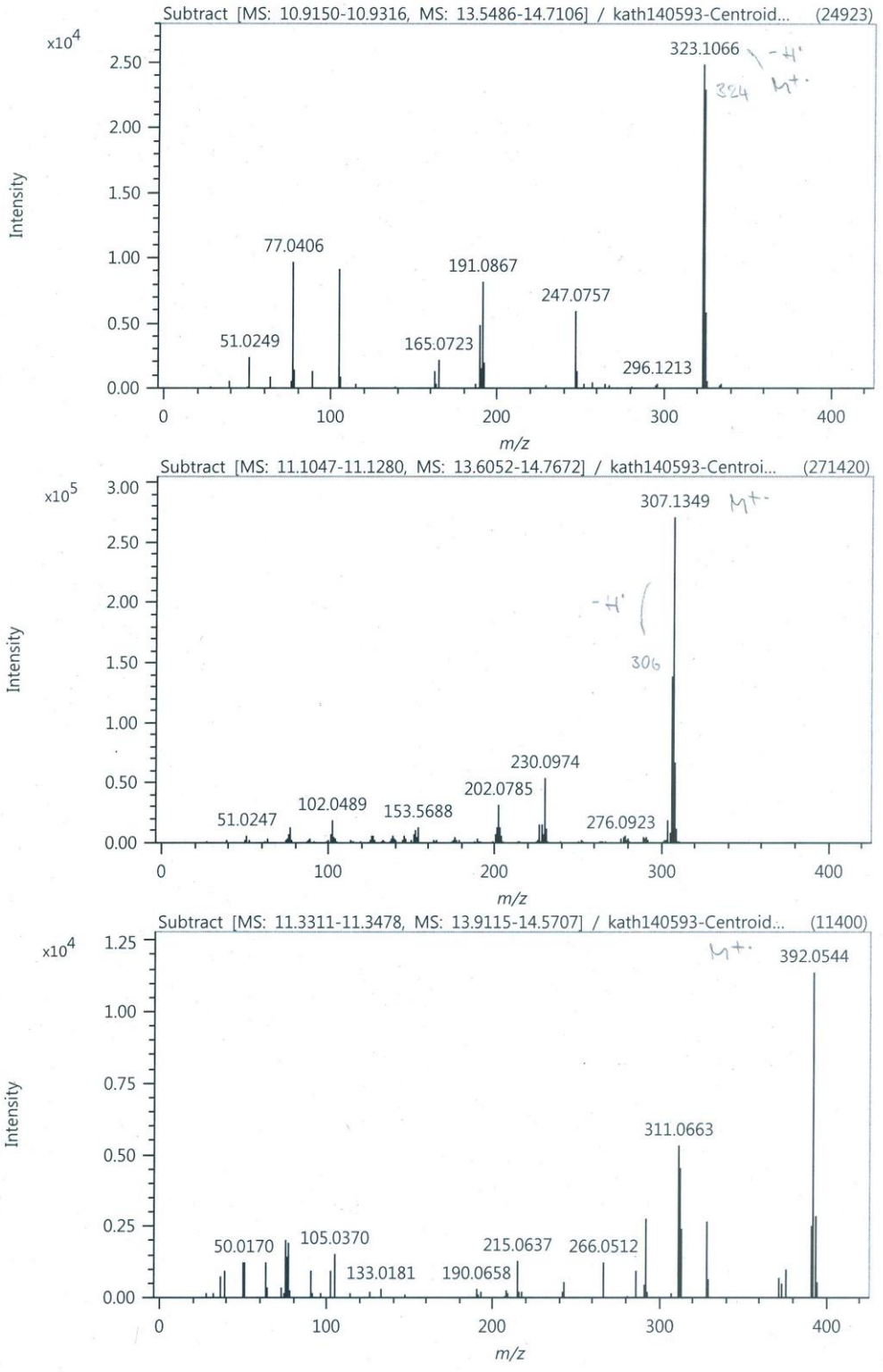
Subtract [MS: 10.9150-10.9316, MS: 13.5486-14.7106] / kath140593-Centroid... (24923)
x10^4
Intensity
323.1066
-H·
324
M+·
77.0406
191.0867
247.0757
51.0249
165.0723
296.1213
m/z
Subtract [MS: 11.1047-11.1280, MS: 13.6052-14.7672] / kath140593-Centroi... (271420)
x10^5
307.1349
M+·
-H·
306
230.0974
202.0785
102.0489
153.5688
51.0247
276.0923
m/z
Subtract [MS: 11.3311-11.3478, MS: 13.9115-14.5707] / kath140593-Centroid... (11400)
x10^4
M+·
392.0544
311.0663
50.0170
105.0370
133.0181
190.0658
215.0637
266.0512
m/z

Spectrum

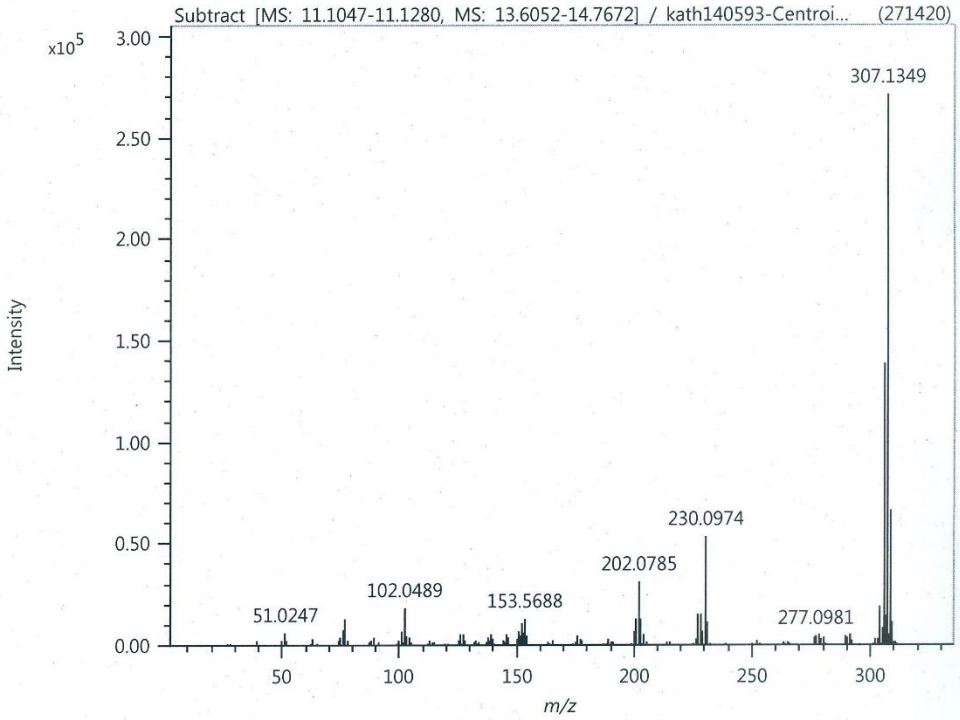

Elemental Composition

Parameters	
Tolerance:	10.00 ppm
Electron:	Odd/Even
Charge:	+1
DBE:	-1.5 - 50.0

Elements:

Symbol	C	H	N	O	Si	Cl	B	Br
Min	1	1	0	0	0	0	0	0
Max	100	100	5	0	0	0	0	0

Symbol	I
Min	0
Max	0

Results

Mass	Intensity	Formula	Calculated Mass	Mass Difference [mDa]	Mass Difference [ppm]	DBE
306.12766	138800.25	C23 H16 N	306.12773	-0.06	-0.20	16.5
307.13487	271419.63	C23 H17 N	307.13555	-0.68	-2.22	16.0

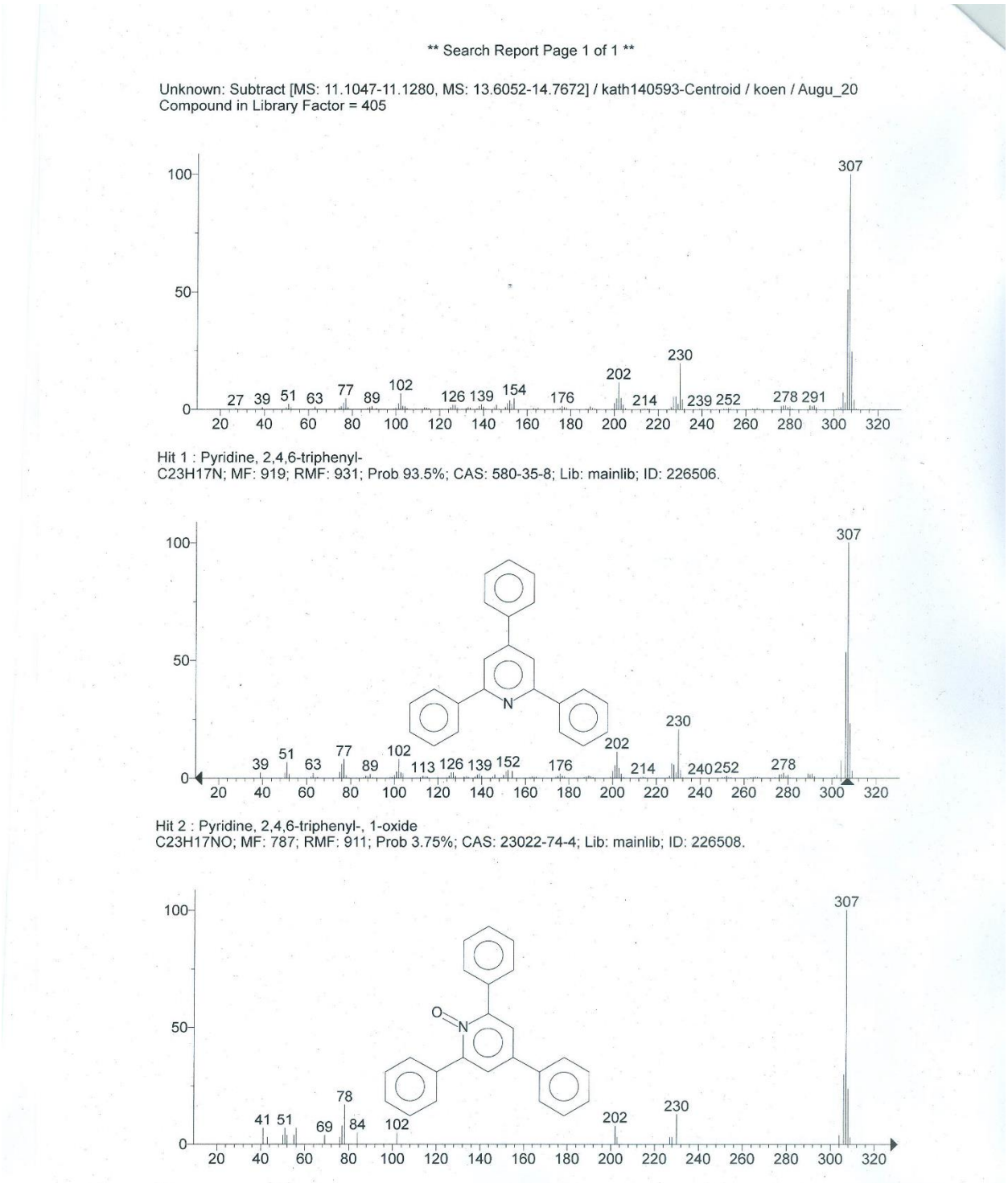

Fig. S15: HRMS and GC-MS spectra for catalyst deactivation

Reaction conditions: [a]0.1 mmol PC, 3 eq. NH_2OH•HCl, 2.5 eq. NH_4Br, 25 mg 4 Å MS, 1 bar O_2, 1 mL acetonitrile (0.05 M), 455 nm, 40 °C, 24 h.

4.5 Cyclic Voltammetry measurement

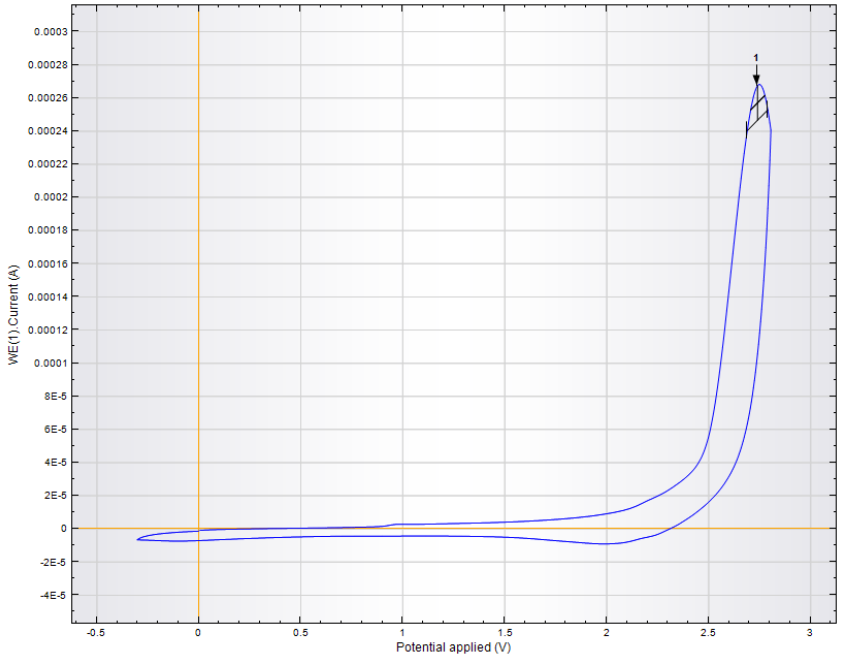

Index	Peak position
1	2.7393

Fig. S16: Cyclic voltammogram of methyl 4-methylbenzoate (**1**) in acetonitrile under argon. The peak at +2.74 V shows the oxidation of **1**. The measurement was performed with a scan rate of 50 mV/s and with TBATFB (0.1M) as supporting electrolyte.

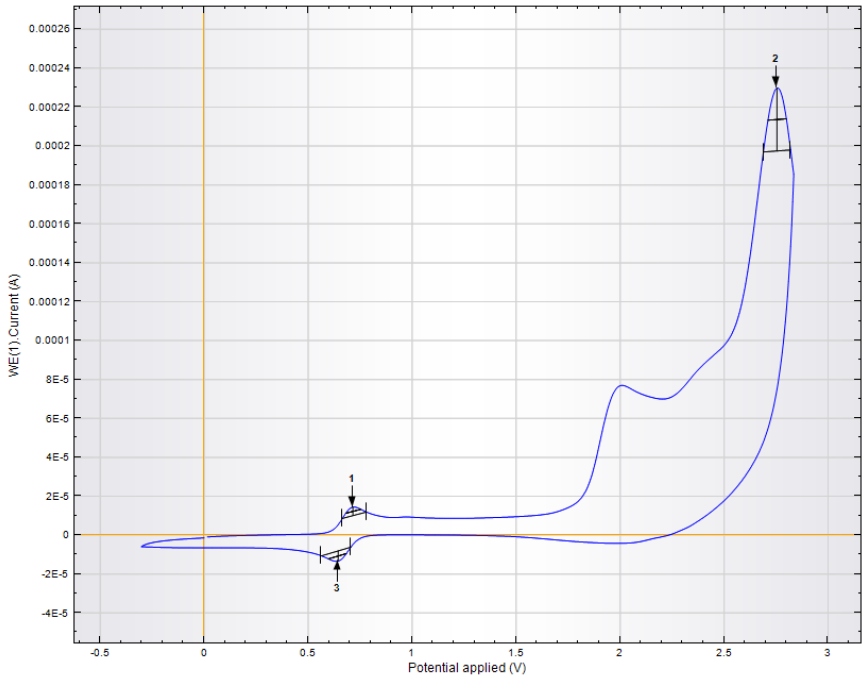

Index	Peak position
1	0.71503
2	2.7544
3	0.64453

Fig. S17: Cyclic voltammogram of methyl 4-methylbenzoate (**1**) in the presence of ferrocene as internal standard in acetonitrile under argon. The peak at +2.75 V shows the oxidation of **1**, whereas the reversible peak at +0.64 and +0.72 V corresponds to ferrocene. The measurement was performed with a scan rate of 50 mV/s and with TBATFB (0.1M) as supporting electrolyte.

With these values, the oxidation potential of **1** was calculated as follows:

$$E_{1/2}(\mathbf{1}^{\bullet+}/\mathbf{1}) = \left(2.754\,V - \frac{0.715\,V + 0.645\,V}{2}\right) vs.\ Fc^{+}/Fc = 2.07\,V\ vs.Fc^{+}/Fc$$

This value was converted from the ferrocene reference to the SCE[6]:

$$E_{1/2}(\mathbf{1}^{\bullet+}/\mathbf{1}) = (2.07\,V + 0.38\,V)\ vs.SCE = 2.45\,V\ vs.SCE$$

5. Characterization of prepared compounds

(1H-indazol-1-yl)(p-tolyl)methanone[7]

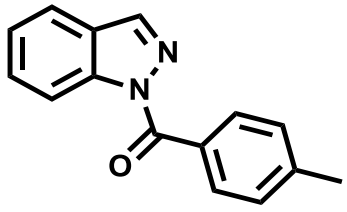

^{1}H NMR (400 MHz, Chloroform-*d*) δ 8.50 (dd, *J* = 8.4, 0.9 Hz, 1H), 8.12 (d, *J* = 0.8 Hz, 1H), 7.92 (d, *J* = 8.2 Hz, 2H), 7.69 (dd, *J* = 7.9, 1.0 Hz, 1H), 7.54 (ddd, *J* = 8.3, 7.1, 1.2 Hz, 1H), 7.32 (ddd, *J* = 8.0, 7.1, 0.9 Hz, 1H), 7.25 (d, *J* = 7.6 Hz, 2H), 2.38 (s, 3H). **^{13}C NMR (101 MHz, Chloroform-*d*)** δ 168.35 , 143.01 , 140.21 , 140.08 , 131.14 , 130.45 , 129.43 , 128.74 , 126.11 , 124.72 , 120.91 , 115.93 , 21.70 . **HRMS (EI)** (m/z): [M^+] ($C_{15}H_{12}N_2O^+$) calc. 236.0944; observed 236.0947. **Off-white solid.**

3-cyclopentylpropyl 4-methylbenzoate

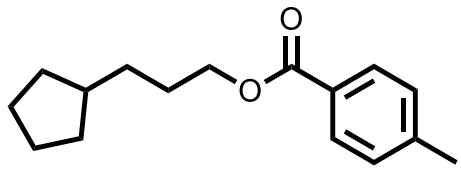

^{1}H NMR (400 MHz, Chloroform-*d*) δ 7.95 (d, *J* = 8.2 Hz, 2H), 7.25 (d, *J* = 8.0 Hz, 2H), 4.31 (t, *J* = 6.7 Hz, 2H), 2.42 (s, 3H), 1.87 – 1.72 (m, 5H), 1.68 – 1.40 (m, 6H), 1.18 – 1.02 (m, 2H). **^{13}C NMR (101 MHz, Chloroform-*d*)** δ 166.77 , 143.39 , 129.56 , 129.02 , 127.83 , 65.16 , 39.84 , 32.69 , 32.43 , 28.02 , 25.18 , 21.65 . **HRMS (APCI)** (m/z): [$M+H^+$] ([$C_{16}H_{22}O_2+H]^+$) calc. 247.1693; observed 247.1698. **Yellow oil.**

(1R,2S,5R)-2-isopropyl-5-methylcyclohexyl 4-methylbenzoate[8]

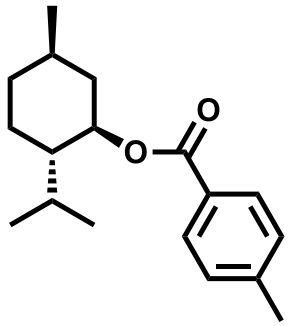

^{1}H NMR (400 MHz, Chloroform-*d*) δ 7.95 (d, *J* = 8.2 Hz, 2H), 7.25 (d, *J* = 7.9 Hz, 2H), 4.93 (td, *J* = 10.9, 4.4 Hz, 1H), 2.42 (s, 3H), 2.20 – 2.09 (m, 1H), 2.04 – 1.88 (m, 1H), 1.83 – 1.70 (m, 2H), 1.63 – 1.46 (m, 2H), 1.24 – 1.02 (m, 2H), 0.98 – 0.90 (m, 7H), 0.81 (d, *J* = 7.0 Hz, 3H). **^{13}C NMR (101 MHz, Chloroform-*d*)** δ 166.16 , 143.28 , 129.58 , 128.99 , 128.15 , 74.59 , 47.31 , 41.02 , 34.37 , 31.46 , 26.52 , 23.69 , 22.06 , 21.63 , 20.77 , 16.56 . **HRMS (APCI)** (m/z): [M+H^{+}] ([$C_{18}H_{26}O_2$+H]$^{+}$) calc. 275.2006; observed 275.2011. **Colorless oil.**

((3aR,5R,5aS,8aS,8bR)-2,2,7,7-tetramethyltetrahydro-3aH-bis([1,3]dioxolo)[4,5-b:4',5'-d]pyran-5-yl)methyl 4-methylbenzoate[9]

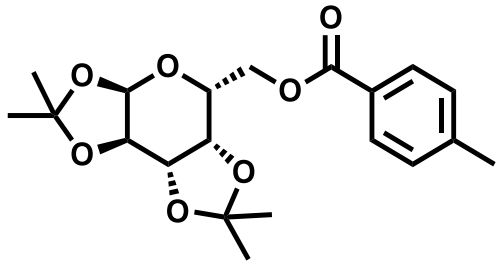

^{1}H NMR (400 MHz, Chloroform-*d*) δ 7.97 (d, *J* = 8.2 Hz, 2H), 7.25 (d, *J* = 8.0 Hz, 2H), 5.59 (d, *J* = 4.9 Hz, 1H), 4.68 (dd, *J* = 7.9, 2.5 Hz, 1H), 4.55 (dd, *J* = 11.5, 4.9 Hz, 1H), 4.47 – 4.33 (m, 3H), 4.25 – 4.16 (m, 1H), 2.43 (s, 3H), 1.54 (s, 3H), 1.50 (s, 3H), 1.38 (s, 3H), 1.36 (s, 3H). **^{13}C NMR (101 MHz, Chloroform-*d*)** δ 166.49 , 143.62 , 129.74 , 129.04 , 127.33 , 109.67 , 108.80 , 96.33 , 71.17 , 70.74 , 70.56 , 66.20 , 63.69 , 26.03 , 25.99 , 25.00 , 24.50 , 21.66 . **HRMS (ESI)** (m/z): [M+H^{+}] ([$C_{20}H_{26}O_7$+H]$^{+}$) calc. 379.1751; observed 379.1753. **Colorless gum.**

1,7,7-trimethylbicyclo[2.2.1]heptan-2-yl 4-methylbenzoate

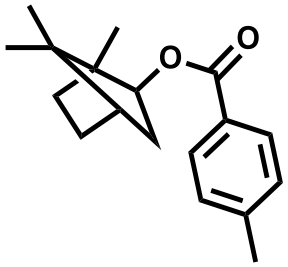

^{1}H NMR (400 MHz, Chloroform-*d*) δ 7.92 (d, *J* = 8.2 Hz, 2H), 7.25 (d, *J* = 7.8 Hz, 2H), 4.92 (dd, *J* = 7.1, 4.5 Hz, 1H), 2.42 (s, 3H), 1.99 – 1.69 (m, 4H), 1.68 – 1.57 (m, 1H), 1.30 – 1.18 (m, 2H), 1.14 (s, 3H), 0.95 (s, 3H), 0.91 (s, 3H). **^{13}C NMR (101 MHz, Chloroform-*d*)** δ 166.13 , 143.30 , 129.49 , 129.05 , 128.18 , 81.33 , 49.01 , 47.03 , 45.14 , 38.95 , 33.78 , 27.10 , 21.64 , 20.16 , 20.09 , 11.60 . **HRMS (APCI)** (m/z): $[M+H^+]$ ($[C_{18}H_{24}O_2+H]^+$) calc. 273.1849; observed 273.1852. **Colorless oil.**

2,2,3,3,4,4,5,5,6,6,7,7,8,8,9,9,10,10,11,11,12,12,12-tricosafluorododecyl 4-methylbenzoate

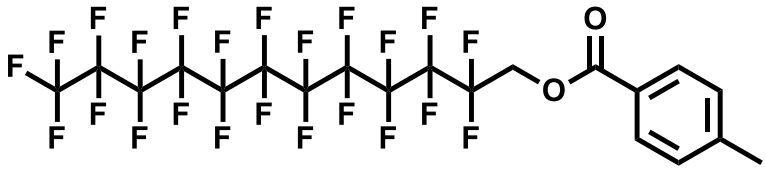

^{1}H NMR (400 MHz, Chloroform-*d*) δ 7.95 (d, *J* = 8.2 Hz, 2H), 7.27 (d, *J* = 8.3 Hz, 2H), 4.92 – 4.68 (m, 2H), 2.43 (s, 3H). **^{13}C NMR (101 MHz, Chloroform-*d*)** δ 164.96 , 144.84 , 130.03 , 129.35 , 125.57 , 59.96 , 21.74 . **^{19}F NMR (282 MHz, Chloroform-*d*)** δ -81.31 (t, *J* = 10.0 Hz, 3F), -119.58 – -120.10 (m, 2F), -121.95 – -122.72 (m, 12F), -123.02 – -123.47 (m, 2F), -123.49 – -124.17 (m, 2F), -126.40 – -127.02 (m, 2F). **HRMS (APCI)** (m/z): $[M+NH_4^+]$ ($[C_{20}H_9F_{23}O_2+NH_4]^+$) calc. 736.0574; observed 736.0589. **White solid.**

(S)-dimethyl 2-((4-methylbenzoyl)oxy)succinate

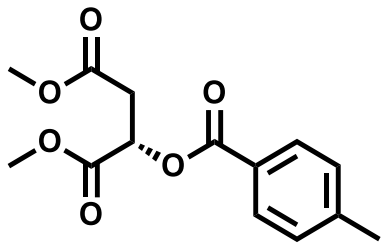

^{1}H NMR (400 MHz, Chloroform-*d*) δ 7.95 (d, *J* = 8.2 Hz, 2H), 7.25 (d, *J* = 8.0 Hz, 2H), 5.72 (dd, *J* = 6.9, 5.4 Hz, 1H), 3.79 (s, 3H), 3.73 (s, 3H), 3.04 (dd, *J* = 6.2, 1.8 Hz, 2H), 2.42 (s, 3H). **^{13}C NMR (101 MHz, Chloroform-*d*)** δ 169.62 , 169.50 , 165.51 , 144.30 , 129.99 , 129.15 , 126.31 , 68.60 , 52.73 , 52.20 , 36.21 , 21.72 . **HRMS (APCI)** (m/z): $[M+H^+]$ ($[C_{14}H_{16}O_6+H]^+$) calc. 281.1020; observed 281.1023. **Yellow oil.**

(S)-methyl 3-methyl-2-(4-methylbenzamido)butanoate[10]

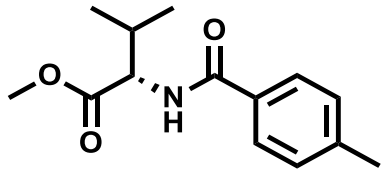

^{1}H NMR (400 MHz, Chloroform-*d*) δ 7.71 (d, *J* = 8.2 Hz, 2H), 7.25 (d, *J* = 8.0 Hz, 2H), 6.59 (d, *J* = 8.6 Hz, 1H), 4.79 (dd, *J* = 8.7, 4.9 Hz, 1H), 3.78 (s, 3H), 2.41 (s, 3H), 2.35 – 2.22 (m, 1H), 1.00 (dd, *J* = 9.2, 6.9 Hz, 6H). **^{13}C NMR (101 MHz, Chloroform-*d*)** δ 172.75 , 167.18 , 142.19 , 131.32 , 129.26 , 127.05 , 57.34 , 52.22 , 31.68 , 21.47 , 19.00 , 17.98 . **HRMS (ESI)** (m/z): $[M+H^+]$ ($[C_{14}H_{19}NO_3+H]^+$) calc. 250.1438; observed 250.1440. **White solid.**

(3S,5S,8R,9S,10S,13R,14S,17R)-10,13-dimethyl-17-((R)-6-methylheptan-2-yl)hexadecahydro-1H-cyclopenta[a]phenanthren-3-yl 4-methylbenzoate[11]

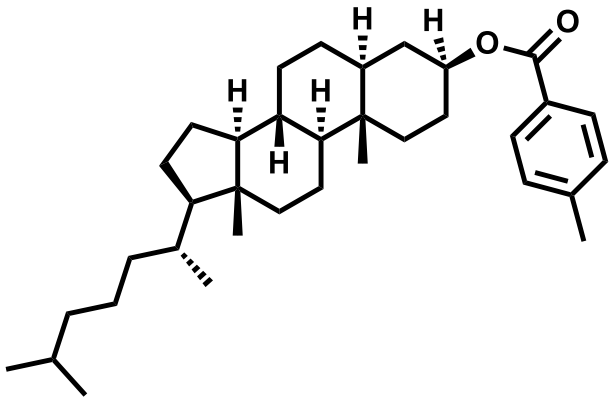

^{1}H NMR (400 MHz, Chloroform-*d*) δ 7.95 (d, *J* = 8.2 Hz, 2H), 7.25 (d, *J* = 8.0 Hz, 2H), 5.29 – 4.47 (m, 1H), 2.43 (s, 3H), 2.07 – 0.84 (m, 43H), 0.78 – 0.61 (m, 3H). **^{13}C NMR (101 MHz, Chloroform-*d*)** δ 166.21 , 143.22 , 129.54 , 128.94 , 128.24 , 74.15 , 56.44 , 56.29 , 54.26 , 44.73 , 42.61 , 40.01 , 39.53 , 36.83 , 36.18 , 35.82 , 35.54 , 35.52 , 34.17 , 32.03 , 28.67 , 28.02 , 27.62 , 26.23, 24.23 , 23.85 , 22.83 , 22.57 , 21.64 , 21.24 , 18.69 , 12.31 , 12.09 . **HRMS (APCI)** (m/z): $[M+H^+]$ ($[C_{35}H_{54}O_2+H]^+$) calc. 507.4197; observed 507.4210. **White solid.**

(2R,3S,4S,5R,6S)-6-(acetoxymethyl)-3-(4-methylbenzamido)tetrahydro-2H-pyran-2,4,5-triyl triacetate[12]

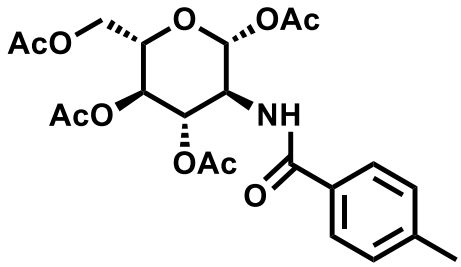

^{1}H NMR (400 MHz, Chloroform-*d*) δ 7.58 (d, *J* = 8.2 Hz, 2H), 7.19 (d, *J* = 8.0 Hz, 2H), 6.33 (d, *J* = 9.5 Hz, 1H), 5.79 (d, *J* = 8.8 Hz, 1H), 5.37 – 5.15 (m, 2H), 4.57 (dt, *J* = 10.4, 9.1 Hz, 1H), 4.29 (dd, *J* = 12.5, 4.7 Hz, 1H), 4.16 (dd, *J* = 12.5, 2.2 Hz, 1H), 3.86 (ddd, *J* = 9.8, 4.7, 2.2 Hz, 1H), 2.37 (s, 3H), 2.10 (s, 3H), 2.06 (s, 6H), 1.98 (s, 3H). **^{13}C NMR (101 MHz, Chloroform-*d*)** δ 171.54 , 170.69 , 169.62 , 169.25 , 167.21 , 142.55 , 130.69 , 129.39 , 126.93 , 92.88 , 73.15 , 72.73 , 67.77 , 61.76 , 53.22 , 21.45 , 20.86 , 20.75 , 20.63 , 20.60 . **HRMS (ESI)** (m/z): [M+H^{+}] ([$C_{22}H_{27}NO_{10}$+H]$^{+}$) calc. 466.1708; observed 466.1706. **White solid.**

(R)-methyl 4-methyl-2-((S)-3-methyl-2-(4-methylbenzamido)butanamido)pentanoate

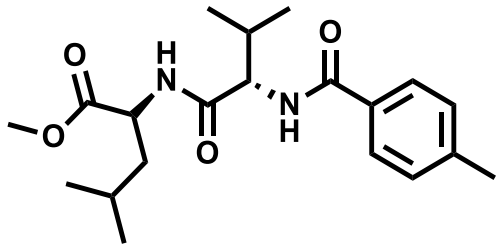

^{1}H NMR (400 MHz, Chloroform-*d*) δ 7.70 (d, *J* = 8.2 Hz, 2H), 7.22 (d, *J* = 7.4 Hz, 2H), 6.88 (d, *J* = 8.7 Hz, 1H), 6.81 (d, *J* = 7.8 Hz, 1H), 4.68 – 4.51 (m, 2H), 3.73 (s, 3H), 2.38 (s, 3H), 2.29 – 2.12 (m, 1H), 1.69 – 1.42 (m, 3H), 1.03 (dd, *J* = 8.2, 6.8 Hz, 6H), 0.84 (dd, *J* = 6.2, 4.9 Hz, 6H). **^{13}C NMR (101 MHz, Chloroform-*d*)** δ 173.11 , 171.34 , 167.31 , 142.20 , 131.23 , 129.23 , 127.12 , 58.49 , 52.24 , 50.92 , 41.07 , 31.75 , 24.80 , 22.65 , 21.81 , 21.47 , 19.15 , 18.37 . **HRMS (ESI)** (m/z): [M+H^{+}] ([$C_{20}H_{30}N_2O_4$+H]$^{+}$) calc. 363.2278; observed 363.2285. **White solid.**

(E)-methyl 4-((hydroxyimino)methyl)benzoate[4]

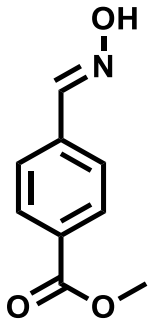

^{1}H NMR (400 MHz, Chloroform-*d*) δ 7.86 (s, 1H), 7.27 (d, *J* = 8.7 Hz, 2H), 6.66 (d, *J* = 8.7 Hz, 2H), 3.58 (s, 3H). **^{13}C NMR (101 MHz, Chloroform-*d*)** δ 161.10 , 149.92 , 128.56 , 124.56 , 114.27 , 113.96 , 55.36 . **White solid.** (Exchangeable OH-proton was not picked-up)

(E)-4-((hydroxyimino)methyl)benzoic acid[13]

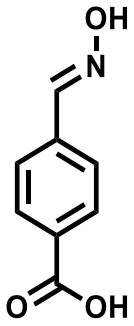

^{1}H NMR (400 MHz, DMSO-d_6) δ 13.03 (br s, 1H), 11.53 (s, 1H), 8.21 (s, 1H), 7.94 (d, *J* = 8.3 Hz, 2H), 7.69 (d, *J* = 8.3 Hz, 2H). **^{13}C NMR (101 MHz, DMSO-d_6)** δ 167.38 , 147.99 , 137.65 , 131.56 , 130.15 , 126.88 . **White solid.**

(E)-4-bromobenzaldehyde oxime[14]

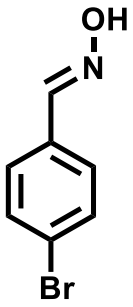

^{1}H NMR (400 MHz, DMSO-*d*$_6$) δ 11.35 (s, 1H), 8.12 (s, 1H), 7.59 (d, *J* = 8.6 Hz, 2H), 7.53 (d, *J* = 8.6 Hz, 2H). **^{13}C NMR (101 MHz, DMSO-*d*$_6$)** δ 147.68 , 132.82 , 132.16 , 128.75 , 122.86 . **White solid.**

(E)-4-((hydroxyimino)methyl)benzonitrile[15]

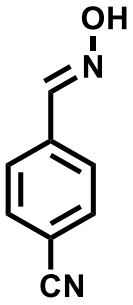

^{1}H NMR (400 MHz, DMSO-*d*$_6$) δ 11.72 (s, 1H), 8.23 (s, 1H), 7.85 (d, *J* = 8.4 Hz, 2H), 7.76 (d, *J* = 8.4 Hz, 2H). **^{13}C NMR (101 MHz, DMSO-*d*$_6$)** δ 147.57 , 138.08 , 133.14 , 127.47 , 119.16 , 111.83 . **White solid.**

methyl 2-cyanobenzoate[16]

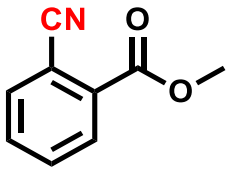

^{1}H NMR (400 MHz, Chloroform-*d*) δ 8.18 – 8.09 (m, 1H), 7.83 – 7.77 (m, 1H), 7.70 – 7.63 (m, 2H), 3.99 (s, 3H). **^{13}C NMR (101 MHz, Chloroform-*d*)** δ 164.51 , 134.82 , 132.72 , 132.50 , 132.42 , 131.19 , 117.53 , 112.95 , 52.87 . **Yellow solid.**

methyl 3-cyanobenzoate[17]

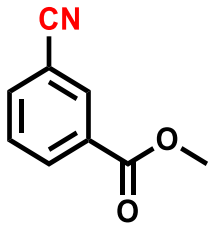

^{1}H NMR (400 MHz, Chloroform-*d*) δ 8.32 (td, *J* = 1.7, 0.6 Hz, 1H), 8.26 (dt, *J* = 8.0, 1.5 Hz, 1H), 7.83 (dt, *J* = 7.8, 1.4 Hz, 1H), 7.58 (td, *J* = 7.9, 0.7 Hz, 1H), 3.95 (s, 3H). **^{13}C NMR (101 MHz, Chloroform-*d*)** δ 165.09 , 135.98 , 133.65 , 133.27 , 131.44 , 129.46 , 117.88 , 112.99 , 52.72 . **White solid.**

methyl 4-cyanobenzoate[18]

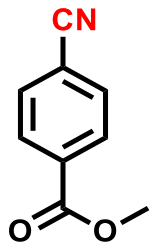

^{1}H NMR (400 MHz, Chloroform-*d*) δ 8.13 (d, *J* = 8.5 Hz, 2H), 7.74 (d, *J* = 8.4 Hz, 2H), 3.95 (s, 3H). **^{13}C NMR (101 MHz, Chloroform-*d*)** δ 165.43 , 133.94 , 132.24 , 130.11 , 117.97 , 116.42 , 52.74 . **White solid.**

4-methoxybenzonitrile[19]

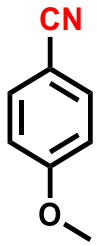

^{1}H NMR (400 MHz, Chloroform-*d*) δ 7.58 (d, *J* = 8.9 Hz, 2H), 6.95 (d, *J* = 8.8 Hz, 2H), 3.86 (s, 3H). **^{13}C NMR (101 MHz, Chloroform-*d*)** δ 162.86 , 134.00 , 119.24 , 114.77 , 104.00 , 55.57 . **White solid.**

3-cyanobenzoic acid[20]

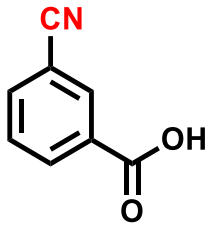

^{1}H NMR (400 MHz, DMSO-*d*$_6$) δ 8.27 (d, *J* = 1.7 Hz, 1H), 8.22 (dt, *J* = 7.9, 1.5 Hz, 1H), 8.08 (dt, *J* = 7.8, 1.5 Hz, 1H), 7.78 – 7.66 (m, 1H). **^{13}C NMR (101 MHz, DMSO-*d*$_6$)** δ 166.15 , 136.72 , 134.22 , 133.22 , 132.51 , 130.55 , 118.53 , 112.38 . **White solid.** (Exchangeable OH-proton was not picked-up)

4-cyanobenzoic acid[21]

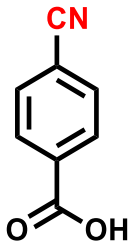

^{1}H NMR (400 MHz, DMSO-*d*$_6$) δ 13.55 (br s, 1H), 8.08 (d, *J* = 8.5 Hz, 2H), 7.98 (d, *J* = 8.4 Hz, 2H). **^{13}C NMR (101 MHz, DMSO-*d*$_6$)** δ 166.48 , 135.32 , 133.12 , 130.37 , 118.64 , 115.51 . **Off-white solid.**

4-cyanobenzamide[22]

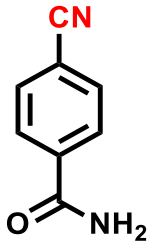

^{1}H NMR (400 MHz, DMSO-*d*$_6$) δ 8.19 (br s, 1H), 8.01 (d, *J* = 8.7 Hz, 2H), 7.93 (d, *J* = 8.4 Hz, 2H), 7.66 (br s, 1H). **^{13}C NMR (101 MHz, DMSO-*d*$_6$)** δ 166.90 , 138.75 , 132.84 , 128.71 , 118.83 , 114.10 . **White solid.**

ethyl 4-cyanobenzoate[23]

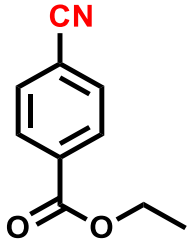

^{1}H NMR (400 MHz, Chloroform-*d*) δ 8.14 (d, *J* = 8.7 Hz, 2H), 7.74 (d, *J* = 8.7 Hz, 2H), 4.42 (q, *J* = 7.1 Hz, 2H), 1.41 (t, *J* = 7.1 Hz, 3H). **^{13}C NMR (101 MHz, Chloroform-*d*)** δ 164.96 , 134.32 , 132.19 , 130.08 , 118.03 , 116.30 , 61.84 , 14.26 . **White solid.**

4-(tert-butyl)benzonitrile[23]

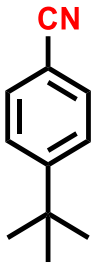

^{1}H NMR (400 MHz, Chloroform-*d*) δ 7.58 (d, *J* = 8.7 Hz, 2H), 7.48 (d, *J* = 8.5 Hz, 2H), 1.33 (s, 9H). **^{13}C NMR (101 MHz, Chloroform-*d*)** δ 156.66 , 131.98 , 126.19 , 119.17 , 109.33 , 35.29 , 30.97 . **Yellow oil.**

4-(4,4,5,5-tetramethyl-1,3,2-dioxaborolan-2-yl)benzonitrile[24]

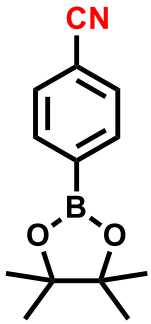

^{1}H NMR (400 MHz, Chloroform-*d*) δ 7.88 (d, *J* = 8.2 Hz, 2H), 7.64 (d, *J* = 8.3 Hz, 2H), 1.35 (s, 12H). **^{13}C NMR (101 MHz, Chloroform-*d*)** δ 135.11 , 135.10 , 131.15 , 118.88 , 114.56 , 84.52 , 24.89 . **White solid.**

1-naphthonitrile[25]

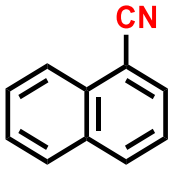

^{1}H NMR (400 MHz, Chloroform-*d*) δ 8.28 – 8.19 (m, 1H), 8.08 (dd, *J* = 8.4, 1.1 Hz, 1H), 7.91 (ddd, *J* = 7.1, 6.3, 1.1 Hz, 2H), 7.69 (ddd, *J* = 8.3, 6.9, 1.4 Hz, 1H), 7.62 (ddd, *J* = 8.2, 6.9, 1.3 Hz, 1H), 7.52 (dd, *J* = 8.3, 7.2 Hz, 1H). **^{13}C NMR (101 MHz, Chloroform-*d*)** δ 133.31 , 132.95 , 132.65 , 132.38 , 128.69 , 128.62 , 127.58 , 125.17 , 124.95 , 117.85 , 110.22 . **Off-white solid.**

4-chlorobenzonitrile[25]

^{1}H NMR (400 MHz, Chloroform-*d*) δ 7.60 (d, *J* = 8.6 Hz, 2H), 7.46 (d, *J* = 8.6 Hz, 2H). **^{13}C NMR (101 MHz, Chloroform-*d*)** δ 139.57 , 133.40 , 129.72 , 117.98 , 110.82 . **White solid.**

4-iodobenzonitrile[26]

^{1}H NMR (400 MHz, Chloroform-*d*) δ 7.85 (d, *J* = 8.4 Hz, 2H), 7.37 (d, *J* = 8.4 Hz, 2H). **^{13}C NMR (101 MHz, Chloroform-*d*)** δ 138.54 , 133.18 , 118.23 , 111.78 , 100.32. **Pale brown solid.**

4-(trifluoromethoxy)benzonitrile[23]

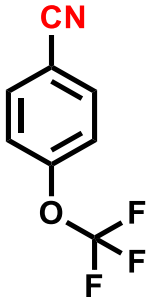

^{1}H NMR (400 MHz, Chloroform-*d*) δ 7.72 (d, *J* = 8.9 Hz, 2H), 7.32 (d, *J* = 8.0 Hz, 2H). **^{13}C NMR (101 MHz, Chloroform-*d*)** δ 152.21 (d, *J* = 1.9 Hz), 134.19 ,120.18 (q, *J* = 259.7 Hz), 121.23 , 117.65 , 110.85 . **^{19}F NMR (376 MHz, Chloroform-*d*)** δ -58.30 . **Yellow oil.**

methyl 4-cyano-2-methoxybenzoate[27]

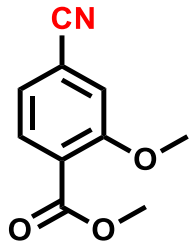

^{1}H NMR (400 MHz, Chloroform-*d*) δ 7.68 – 7.58 (m, 3H), 3.98 (s, 3H), 3.93 (s, 3H). **^{13}C NMR (101 MHz, Chloroform-*d*)** δ 165.50 , 161.12 , 135.49 , 133.74 , 121.65 , 115.61 , 112.03 , 105.84 , 56.36 , 52.78 . **HRMS (EI)** (m/z): [M^+] ($C_{10}H_9NO_3^+$) calc. 191.0576; observed 191.0578. **Yellow solid**.

[1,1'-biphenyl]-4-carbonitrile[26]

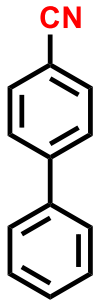

^{1}H NMR (400 MHz, Chloroform-*d*) δ 7.76 – 7.66 (m, 4H), 7.62 – 7.56 (m, 2H), 7.53 – 7.39 (m, 3H). **^{13}C NMR (101 MHz, Chloroform-*d*)** δ 145.70 , 139.20 , 132.62 , 129.14 , 128.68 , 127.76 , 127.25 , 118.96 , 110.95 . **White solid.**

[1,1'-biphenyl]-3-carbonitrile[26]

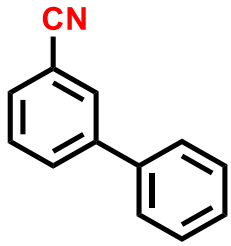

^{1}H NMR (400 MHz, Chloroform-*d*) δ 7.90 – 7.84 (m, 1H), 7.82 (dt, *J* = 7.8, 1.6 Hz, 1H), 7.64 (dt, *J* = 7.7, 1.4 Hz, 1H), 7.59 – 7.52 (m, 3H), 7.52 – 7.38 (m, 3H). **^{13}C NMR (101 MHz, Chloroform-*d*)** δ 142.48 , 138.91 , 131.51 , 130.74 , 130.71 , 129.62 , 129.15 , 128.41 , 127.11 , 118.87 , 112.99 . **Yellow gum.**

[1,1'-biphenyl]-2,4'-dicarbonitrile[28]

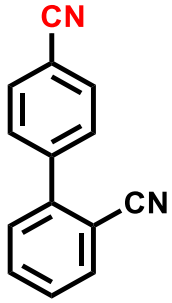

^{1}H NMR (400 MHz, Chloroform-*d*) δ 7.59 – 7.52 (m, 3H), 7.50 – 7.40 (m, 3H), 7.34 – 7.24 (m, 2H). **^{13}C NMR (101 MHz, Chloroform-*d*)** δ 143.33 , 142.53 , 133.99 , 133.20 , 132.54 , 129.93 , 129.59 , 128.80 , 118.40 , 118.03 , 112.66 , 111.25 . **HRMS (EI)** (m/z): [M^{+}] ($C_{14}H_8N_2^{+}$) calc. 204.0682; observed 204.0682. **Off-white solid.**

methyl 4'-cyano-[1,1'-biphenyl]-2-carboxylate[29]

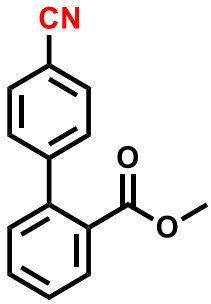

^{1}H NMR (400 MHz, Chloroform-*d*) δ 7.78 (dd, *J* = 7.7, 1.4 Hz, 1H), 7.54 (d, *J* = 8.3 Hz, 2H), 7.47 – 7.38 (m, 1H), 7.38 – 7.29 (m, 1H), 7.25 (d, *J* = 8.3 Hz, 2H), 7.16 (dd, *J* = 7.7, 1.3 Hz, 1H), 3.52 (s, 3H). **^{13}C NMR (101 MHz, Chloroform-*d*)** δ 167.93 , 146.39 , 141.09 , 131.79 , 131.77 , 130.52 , 130.45 , 130.07 , 129.19 , 128.29 , 118.89 , 111.10 , 52.11 . **HRMS (EI)** (m/z): [M^+] ($C_{15}H_{11}NO_2^+$) calc. 237.0784; observed 237.0786. **Colorless gum.**

[1,1'-biphenyl]-4,4'-dicarbonitrile[23]

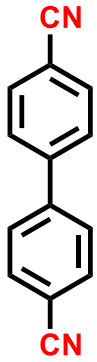

^{1}H NMR (400 MHz, Chloroform-*d*) δ 7.78 (d, *J* = 8.6 Hz, 4H), 7.69 (d, *J* = 8.6 Hz, 4H). **^{13}C NMR (101 MHz, Chloroform-*d*)** δ 146.76 , 132.91 , 127.95 , 118.41 , 112.48 . **HRMS (EI)** (m/z): [M^+] ($C_{14}H_8N_2^+$) calc. 204.0682; observed 204.0684. **White solid.**

4-(1H-indazole-1-carbonyl)benzonitrile[30]

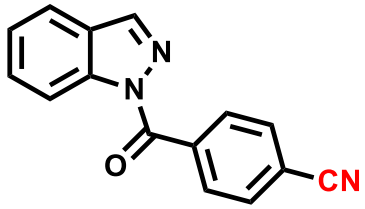

^{1}H NMR (400 MHz, Chloroform-*d*) δ 8.57 (dt, *J* = 8.4, 0.9 Hz, 1H), 8.22 (s, 1H), 8.16 (d, *J* = 8.4 Hz, 2H), 7.87 – 7.76 (m, 3H), 7.66 (ddd, *J* = 8.4, 7.2, 1.1 Hz, 1H), 7.46 (ddd, *J* = 8.0, 7.1, 0.9 Hz, 1H). **^{13}C NMR (101 MHz, Chloroform-*d*)** δ 166.57 , 141.22 , 139.96 , 137.36 , 131.74 , 131.38 , 130.03 , 126.28 , 125.45 , 121.21 , 118.06 , 115.93 , 115.53 . **HRMS (EI)** (m/z): [M^+] ($C_{15}H_9N_3O^+$) calc. 247.0740; observed 247.0749. **White solid.**

benzo[b]thiophene-3-carbonitrile[23]

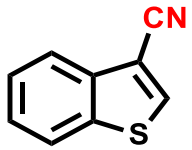

^{1}H NMR (400 MHz, Chloroform-*d*) δ 7.89 (s, 1H), 7.81 – 7.74 (m, 1H), 7.72 – 7.65 (m, 1H), 7.38 – 7.20 (m, 2H). **^{13}C NMR (101 MHz, Chloroform-*d*)** δ 138.52 , 137.54 , 137.30 , 126.21 , 126.01 , 122.86 , 122.58 , 114.34 , 107.17 . **HRMS (EI)** (m/z): [M^+] ($C_9H_5NS^+$) calc. 159.0137; observed 159.0133. **Brown solid.**

3-cyclopentylpropyl 4-cyanobenzoate

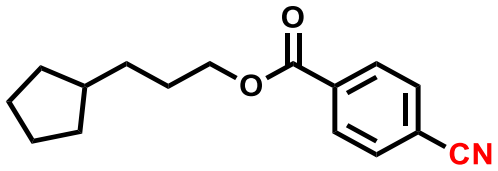

^{1}H NMR (400 MHz, Chloroform-*d*) δ 8.13 (d, *J* = 8.4 Hz, 2H), 7.74 (d, *J* = 8.4 Hz, 2H), 4.34 (t, *J* = 6.7 Hz, 2H), 1.86 – 1.70 (m, 5H), 1.66 – 1.36 (m, 6H), 1.17 – 1.03 (m, 2H). **^{13}C NMR (101 MHz, Chloroform-*d*)** δ 164.99 , 134.34 , 132.19 , 130.05 , 118.02 , 116.27 , 66.18 , 39.78 , 32.67 , 32.34 , 27.89 , 25.16 . **HRMS (APCI)** (m/z): [M+NH_4^+] ($C_{16}H_{19}NO_2$+NH_4^+) calc. 275.1754; observed 275.1760. **Colorless oil.**

(1R,2S,5R)-2-isopropyl-5-methylcyclohexyl 4-cyanobenzoate[31]

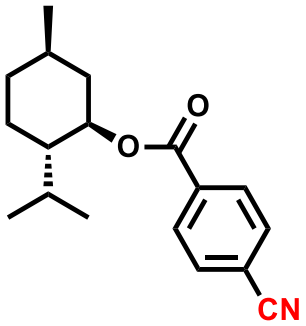

^{1}H NMR (400 MHz, Chloroform-*d*) δ 8.13 (d, *J* = 8.4 Hz, 2H), 7.73 (d, *J* = 8.4 Hz, 2H), 4.95 (td, *J* = 10.9, 4.4 Hz, 1H), 2.18 – 2.03 (m, 1H), 1.96 – 1.84 (m, 1H), 1.78 – 1.67 (m, 2H), 1.63 – 1.49 (m, 2H), 1.19 – 1.02 (m, 2H), 0.98 – 0.87 (m, 7H), 0.78 (d, *J* = 7.0 Hz, 3H). **^{13}C NMR (101 MHz, Chloroform-*d*)** δ 164.42 , 134.65 , 132.16 , 130.06 , 118.05 , 116.16 , 75.94 , 47.20 , 40.85 , 34.20 , 31.45 , 26.57 , 23.59 , 22.00 , 20.73 , 16.49 . **HRMS (APCI)** (m/z): [M+NH_4^+] ([$C_{18}H_{23}NO_2$+NH_4]$^+$) calc. 303.2067; observed 303.2068. **Yellow gum.**

((3aR,5R,5aS,8aS,8bR)-2,2,7,7-tetramethyltetrahydro-3aH-bis([1,3]dioxolo)[4,5-b:4',5'-d]pyran-5-yl)methyl 4-cyanobenzoate[32]

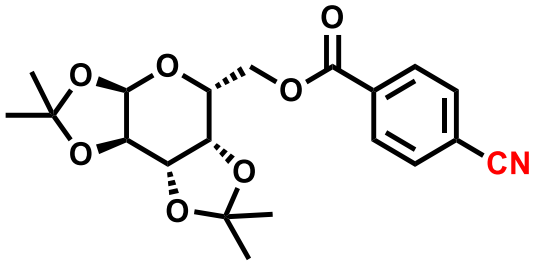

^{1}H NMR (400 MHz, Chloroform-*d*) δ 8.13 (d, *J* = 8.5 Hz, 2H), 7.72 (d, *J* = 8.5 Hz, 2H), 5.55 (d, *J* = 4.9 Hz, 1H), 4.64 (dd, *J* = 7.9, 2.5 Hz, 1H), 4.53 (dd, *J* = 11.6, 4.5 Hz, 1H), 4.45 (dd, *J* = 11.6, 7.8 Hz, 1H), 4.34 (dd, *J* = 5.0, 2.5 Hz, 1H), 4.30 (dd, *J* = 7.9, 1.9 Hz, 1H), 4.22 – 4.11 (m, 1H), 1.47 (d, *J* = 13.4 Hz, 6H), 1.33 (d, *J* = 7.6 Hz, 6H**). ^{13}C NMR (101 MHz, Chloroform-*d*)** δ 164.84 , 133.89 , 132.23 , 130.20 , 117.98 , 116.46 , 109.82 , 108.85 , 96.32 , 71.10 , 70.76 , 70.46 , 66.06 , 64.74 , 26.02 , 25.98 , 24.95 , 24.50 . **HRMS (ESI)** (m/z): $[M+H^+]$ ($[C_{20}H_{23}NO_7+H]^+$) calc. 390.1547; observed 390.1559. **Yellow gum.**

1,7,7-trimethylbicyclo[2.2.1]heptan-2-yl 4-cyanobenzoate

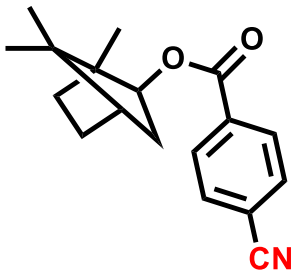

^{1}H NMR (400 MHz, Chloroform-*d*) δ 8.09 (d, *J* = 8.4 Hz, 2H), 7.73 (d, *J* = 8.5 Hz, 2H), 4.93 (dd, *J* = 7.4, 4.2 Hz, 1H), 1.97 – 1.85 (m, 2H), 1.85 – 1.70 (m, 2H), 1.67 – 1.55 (m, 1H), 1.28 – 1.12 (m, 2H), 1.10 (s, 3H), 0.91 (s, 3H), 0.89 (s, 3H). **^{13}C NMR (101 MHz, Chloroform-*d*)** δ 164.37 , 134.68 , 132.24 , 129.94 , 118.03 , 116.18 , 82.60 , 49.13 , 47.06 , 45.07 , 38.82 , 33.69 , 27.01 , 20.08 , 20.06 , 11.59 . **HRMS (APCI)** (m/z): $[M+NH_4^+]$ ($[C_{18}H_{21}NO_2+NH_4]^+$) calc. 301.1911; observed 301.1918. **White solid.**

2,2,3,3,4,4,5,5,6,6,7,7,8,8,9,9,10,10,11,11,12,12,12-tricosafluorododecyl 4-cyanobenzoate

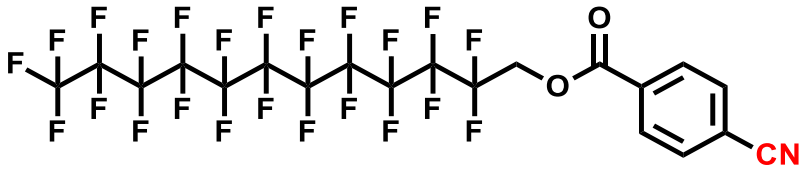

^{1}H NMR (400 MHz, Chloroform-*d*) δ 8.17 (d, *J* = 8.5 Hz, 2H), 7.79 (d, *J* = 8.4 Hz, 2H), 4.85 (t, *J* = 13.1 Hz, 2H).**^{13}C NMR (101 MHz, Chloroform-*d*)** δ 163.35 , 132.45 , 132.03 , 130.44 , 117.61 , 117.45 , 60.56 (t, *J* = 27.8 Hz). **^{19}F NMR (282 MHz, Chloroform-*d*)** δ -81.35 (t, *J* = 10.0 Hz, 3F), -119.41 – -120.36 (m, 2F), -121.97 – -122.76 (m, 12F), -123.19 – -123.37 (m, 2F), -123.58 – -123.80 (m, 2F), -126.26 – -126.97 (m, 2F). **HRMS (APCI)** (m/z): $[M+NH_4^+]$ ($[C_{20}H_6F_{23}NO_2+NH_4]^+$) calc. 747.0370; observed 747.0391. **White solid.**

(S)-dimethyl 2-((4-cyanobenzoyl)oxy)succinate

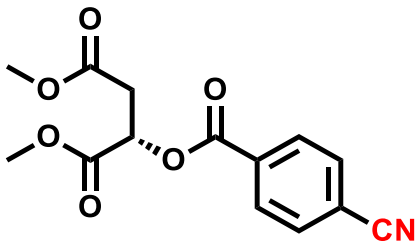

^{1}H NMR (400 MHz, Chloroform-*d*) δ 8.13 (d, *J* = 8.6 Hz, 2H), 7.74 (d, *J* = 8.7 Hz, 2H), 5.72 (dd, *J* = 6.8, 5.3 Hz, 1H), 3.78 (s, 3H), 3.71 (s, 3H), 3.07 – 3.00 (m, 2H). **^{13}C NMR (101 MHz, Chloroform-*d*)** δ 169.39 , 168.82 , 163.90 , 132.89 , 132.29 , 130.42 , 117.83 , 116.89 , 69.27 , 52.93 , 52.31 , 35.92 . **HRMS (APCI)** (m/z): $[M+NH_4^+]$ ($[C_{14}H_{13}NO_6+NH_4]^+$) calc. 309.1081; observed 309.1089. **Yellow gum.**

(S)-methyl 2-(4-cyanobenzamido)-3-methylbutanoate

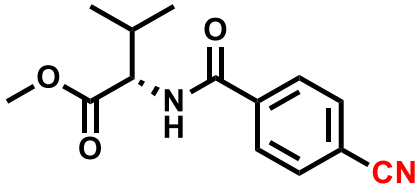

^{1}H NMR (400 MHz, Chloroform-*d*) δ 7.89 (d, *J* = 8.4 Hz, 2H), 7.73 (d, *J* = 8.6 Hz, 2H), 6.74 (d, *J* = 8.6 Hz, 1H), 4.75 (dd, *J* = 8.6, 4.9 Hz, 1H), 3.78 (s, 3H), 2.44 – 2.08 (m, 1H), 0.99 (dd, *J* = 7.9, 6.9 Hz, 6H). **^{13}C NMR (101 MHz, Chloroform-*d*)** δ 172.43 , 165.60 , 138.02 , 132.49 , 127.83 , 117.96 , 115.33 , 57.71 , 52.46 , 31.59 , 19.00 , 18.00 . **HRMS (ESI)** (m/z): [M+H^{+}] ([$C_{14}H_{16}N_2O_3$+H]$^{+}$) calc. 261.1234; observed 261.1238. **Off-white solid.**

4-cyano-N-(perfluorophenyl)benzamide[33]

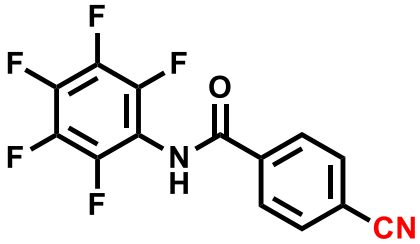

^{1}H NMR (400 MHz, DMSO-*d*$_6$) δ 10.85 (s, 1H), 8.15 (d, *J* = 8.4 Hz, 2H), 8.07 (d, *J* = 8.4 Hz, 2H). **^{13}C NMR (101 MHz, DMSO-*d*$_6$)** δ 164.71 , 153.11 – 151.07 (m), 145.22 – 143.67 (m), 139.64 – 138.22 (m), 136.69 , 134.29 – 132.51 (m), 130.10 – 128.57 (m), 118.57 , 115.30 , 113.35 – 112.62 (m). ^{19}F NMR (376 MHz, DMSO-d_6) δ -144.66 (d, *J* = 21.0 Hz, 2F), -156.39 (t, *J* = 22.9 Hz, 1F), -159.09 – -168.13 (m, 2F). **HRMS (EI)** (m/z): [M^{+}] ($C_{14}H_5N_2F_5O^{+}$) calc. 312.0316; observed 312.0308. **Colorless gum.**

(3S,5S,8R,9S,10S,13R,14S,17R)-10,13-dimethyl-17-((R)-6-methylheptan-2-yl)hexadecahydro-1H-cyclopenta[a]phenanthren-3-yl 4-cyanobenzoate

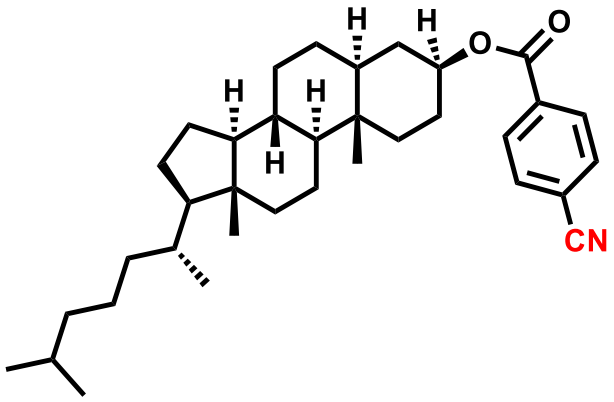

^{1}H NMR (400 MHz, Chloroform-*d*) δ 8.12 (d, *J* = 8.4 Hz, 2H), 7.72 (d, *J* = 8.4 Hz, 2H), 5.04 – 4.86 (m, 1H), 2.03 – 0.81 (m, 42H), 0.75 – 0.55 (m, 4H). **^{13}C NMR (101 MHz, Chloroform-*d*)** δ 164.43 , 134.78 , 132.12 , 130.06 , 118.08 , 116.14 , 75.47 , 56.43 , 56.30 , 54.24 , 44.71 , 42.62 , 40.00 , 39.54 , 36.77 , 36.20 , 35.83 , 35.53 , 35.51 , 34.05 , 32.00 , 28.65 , 28.27 , 28.04 , 27.53 , 24.24 , 23.87 , 22.85 , 22.59 , 21.26 , 18.71 , 12.31 , 12.11 . **HRMS (APCI)** (m/z): $[M+NH_4^+]$ ($[C_{35}H_{51}NO_2+NH_4]^+$) calc. 535.4258; observed 535.4255. **White solid.**

4-(5-(4-cyanophenyl)-3-(trifluoromethyl)-1H-pyrazol-1-yl)benzenesulfonamide[34]

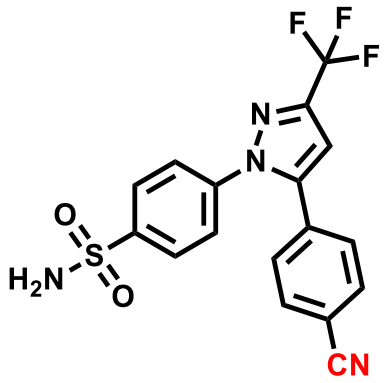

^{1}H NMR (300 MHz, Chloroform-*d*) δ 7.96 (d, *J* = 8.8 Hz, 2H), 7.69 (d, *J* = 8.7 Hz, 2H), 7.46 (d, *J* = 8.7 Hz, 2H), 7.37 (d, *J* = 8.6 Hz, 2H), 6.87 (s, 1H), 4.95 (s, 2H). **^{13}C NMR (101 MHz, Chloroform-*d*)** δ 144.56 (q, *J* = 39.0 Hz), 143.00 , 142.20 , 141.85 , 132.94 , 132.87 , 129.41 , 127.90 , 125.64 , 120.74 (q, *J* = 269.6 Hz), 117.82 , 113.47 , 107.51 . **^{19}F NMR (376 MHz, Chloroform-*d*)** δ -63.03 . **HRMS (ESI)** (m/z): $[M+H^+]$ ($[C_{17}H_{11}F_3N_4O_2S+H]^+$) calc. 393.0628; observed 393.0636. **Off-white solid.**

(2R,3S,4S,5R,6S)-6-(acetoxymethyl)-3-(4-cyanobenzamido)tetrahydro-2H-pyran-2,4,5-triyl triacetate

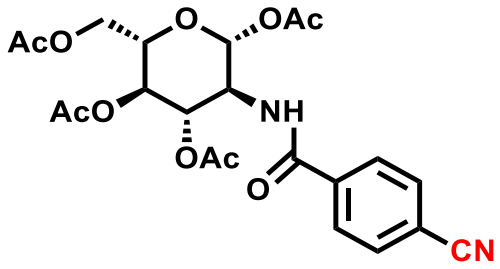

^{1}H NMR (400 MHz, Chloroform-*d*) δ 7.79 (d, *J* = 8.6 Hz, 2H), 7.71 (d, *J* = 8.6 Hz, 2H), 6.54 (d, *J* = 9.4 Hz, 1H), 5.81 (d, *J* = 8.7 Hz, 1H), 5.36 – 5.15 (m, 2H), 4.53 (dt, *J* = 10.4, 9.1 Hz, 1H), 4.29 (dd, *J* = 12.5, 4.7 Hz, 1H), 4.20 – 4.06 (m, 1H), 3.91 – 3.82 (m, 1H), 2.10 (s, 3H), 2.07 (s, 3H), 2.06 (s, 3H), 2.00 (s, 3H). **^{13}C NMR (101 MHz, Chloroform-*d*)** δ 171.63 , 170.69 , 169.58 , 169.25 , 165.57 , 137.34 , 132.62 , 127.66 , 117.78 , 115.64 , 92.72 , 73.14 , 72.67 , 67.63 , 61.69

, 53.79 , 20.86 , 20.74 , 20.65 , 20.60. **HRMS (ESI)** (m/z): [M+H$^+$] ([$C_{22}H_{24}N_2O_{10}$+H]$^+$) calc. 477.1504; observed 477.1505. **Brown solid.**

(R)-methyl 2-((S)-2-(4-cyanobenzamido)-3-methylbutanamido)-4-methylpentanoate

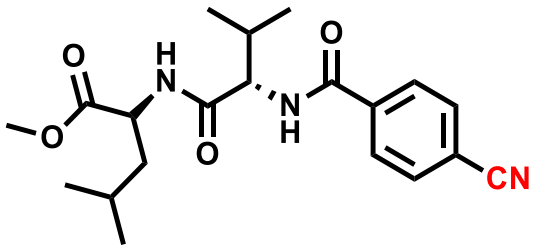

^{1}H NMR (400 MHz, Chloroform-*d*) δ 7.82 (d, *J* = 8.4 Hz, 2H), 7.60 (d, *J* = 8.4 Hz, 2H), 7.27 (d, *J* = 8.7 Hz, 1H), 6.86 (d, *J* = 7.8 Hz, 1H), 4.57 – 4.41 (m, 2H), 3.63 (s, 3H), 2.16 – 2.03 (m, 1H), 1.58 – 1.35 (m, 3H), 0.91 (dd, *J* = 9.7, 6.7 Hz, 6H), 0.74 (d, *J* = 6.1 Hz, 6H). **^{13}C NMR (101 MHz, Chloroform-*d*)** δ 173.00 , 171.20 , 165.65 , 137.85 , 132.38 , 127.96 , 117.94 , 115.29 , 58.94 , 52.32 , 51.02 , 41.00 , 31.74 , 24.81 , 22.64 , 21.81 , 19.08 , 18.48 . **HRMS (ESI)** (m/z): [M+H$^+$] ([$C_{20}H_{27}N_3O_4$+H]$^+$) calc. 374.2074; observed 374.2078. **Brown solid**

4-(pentafluorothio)benzonitrile[35]

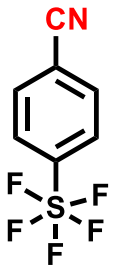

^{1}H NMR (400 MHz, Chloroform-*d*) δ 7.89 (d, *J* = 8.8 Hz, 2H), 7.79 (d, *J* = 9.6 Hz, 2H). **^{13}C NMR (101 MHz, Chloroform-*d*)** δ 157.62 – 155.08 (m), 132.72 , 128.44 – 125.04 (m), 116.90 , 115.87 . **White solid**

terephthalonitrile[25]

^{1}H NMR (400 MHz, Chloroform-*d*) δ 7.80 (s, 4H). **^{13}C NMR (101 MHz, Chloroform-*d*)** δ 132.80 , 117.01 , 116.73 . **White solid**

isophthalonitrile[25]

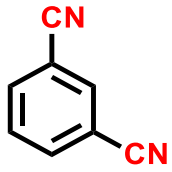

^{1}H NMR (400 MHz, Chloroform-*d*) δ 7.99 – 7.93 (m, 1H), 7.91 (d, *J* = 1.6 Hz, 1H), 7.89 (d, *J* = 1.6 Hz, 1H), 7.70 – 7.61 (m, 1H). **^{13}C NMR (101 MHz, Chloroform-*d*)** δ 136.00 , 135.43 , 130.35 , 116.60 , 114.19 . **White solid.**

3,5-dibromobenzonitrile[36]

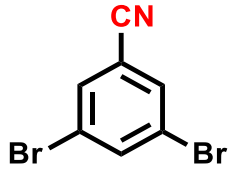

^{1}H NMR (400 MHz, Chloroform-*d*) δ 7.91 (t, *J* = 1.8 Hz, 1H), 7.74 (d, *J* = 1.7 Hz, 2H). **^{13}C NMR (101 MHz, Chloroform-*d*)** δ 138.84 , 133.45 , 123.60 , 115.92 , 115.47 . **White solid**.

2,6-dichlorobenzonitrile[37]

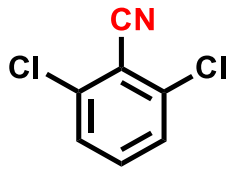

^{1}H NMR (400 MHz, Chloroform-*d*) δ 7.96 – 6.74 (m, 3H). **^{13}C NMR (101 MHz, Chloroform-*d*)** δ 138.51 , 133.86 , 128.17 , 114.44 , 113.35 . **White solid**.

4-nitrobenzonitrile[25]

^{1}H NMR (400 MHz, Chloroform-*d*) δ 8.36 (d, *J* = 8.8 Hz, 2H), 7.89 (d, *J* = 8.8 Hz, 2H). ^{13}C NMR (101 MHz, Chloroform-*d*) δ 150.04 , 133.48 , 124.30 , 118.35 , 116.79 . **Yellow solid.**

6. NMR Spectra

Jul24-2020.90.fid
KM05-551
rau_sPROTON_16 CDCl3 {C:\Bruker\TopSpin3.5pl7} AK_Koenig 46

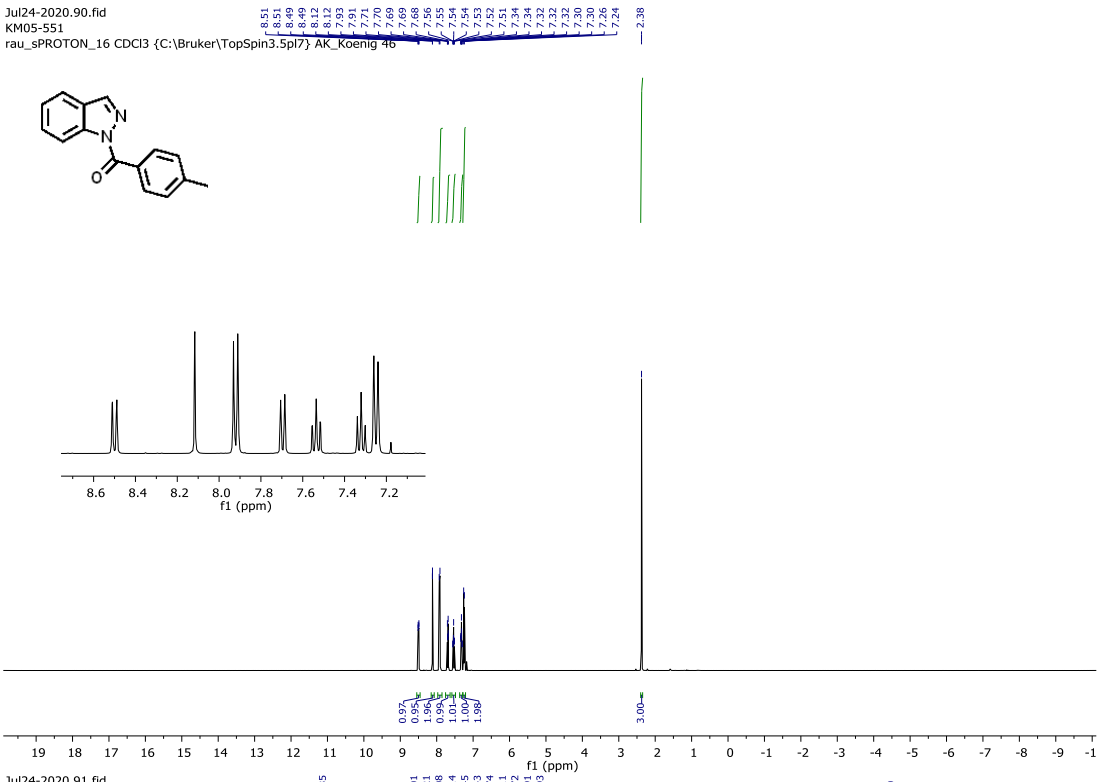

Jul24-2020.91.fid
KM05-551
rau_sC13CPD_256 CDCl3 {C:\Bruker\TopSpin3.5pl7} AK_Koenig 46

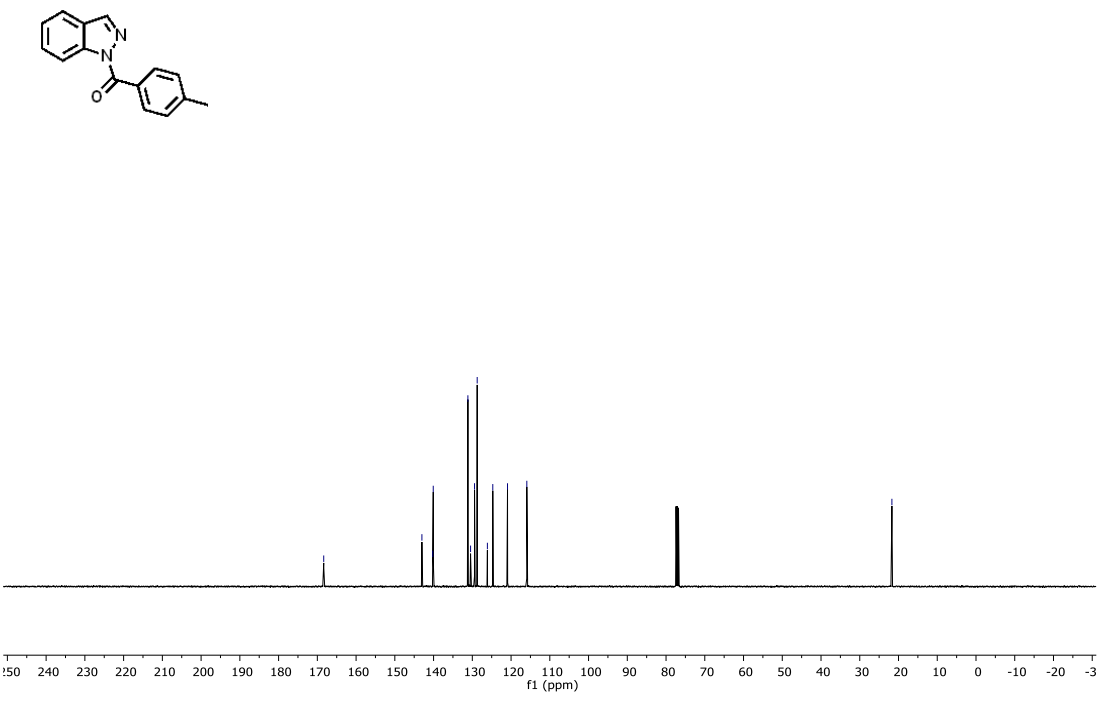

Jun11-2020.51.fid
KM05-494
rau_sPROTON_64 CDCl3 {C:\Bruker\TopSpin3.5pl7} AK_Koenig 59

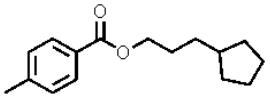

Jun11-2020.52.fid
KM05-494
rau_sC13CPD_256 CDCl3 {C:\Bruker\TopSpin3.5pl7} AK_Koenig 59

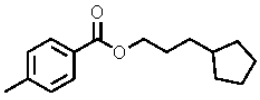

May27-2020.70.fid
KM05-431-F1
rau_sPROTON_64 CDCl3 {C:\Bruker\TopSpin3.5pl7} AK_Koenig 54

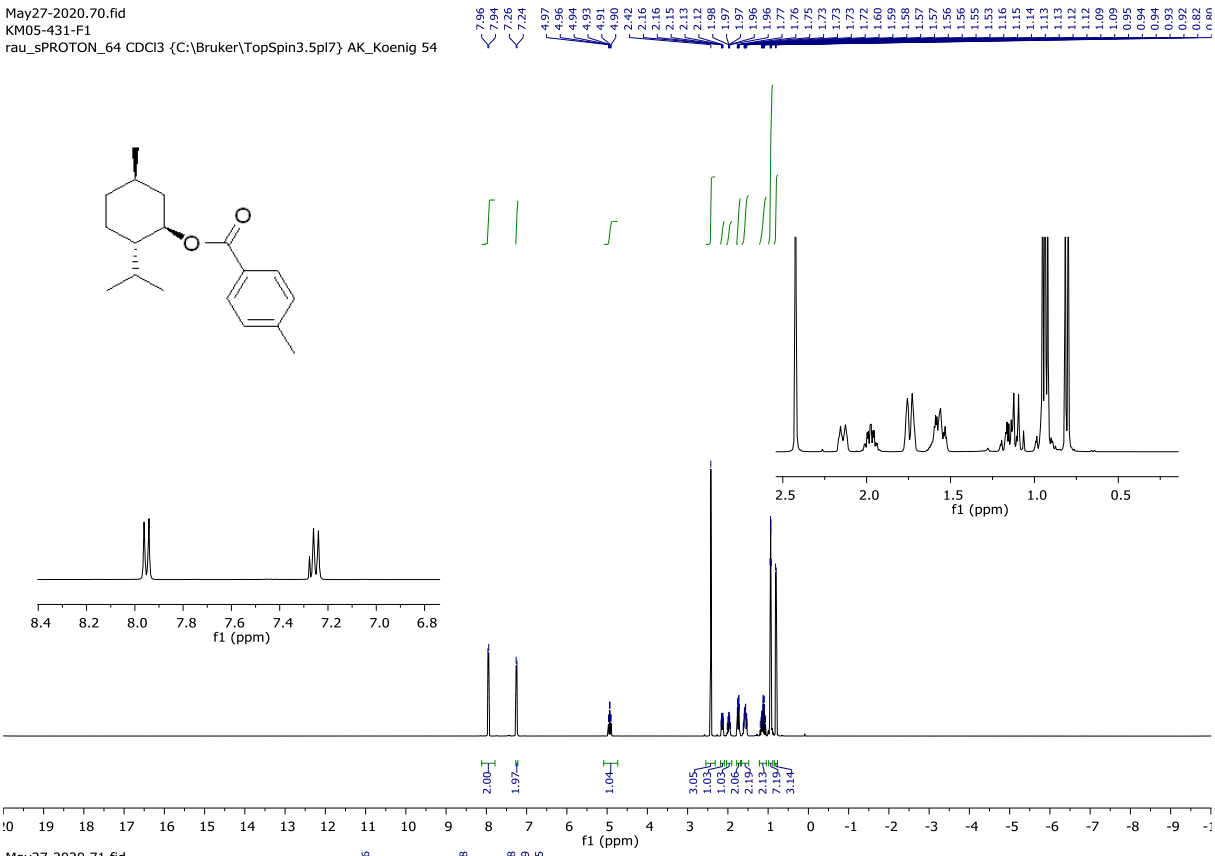

May27-2020.71.fid
KM05-431-F1
rau_sC13CPD_256 CDCl3 {C:\Bruker\TopSpin3.5pl7} AK_Koenig 54

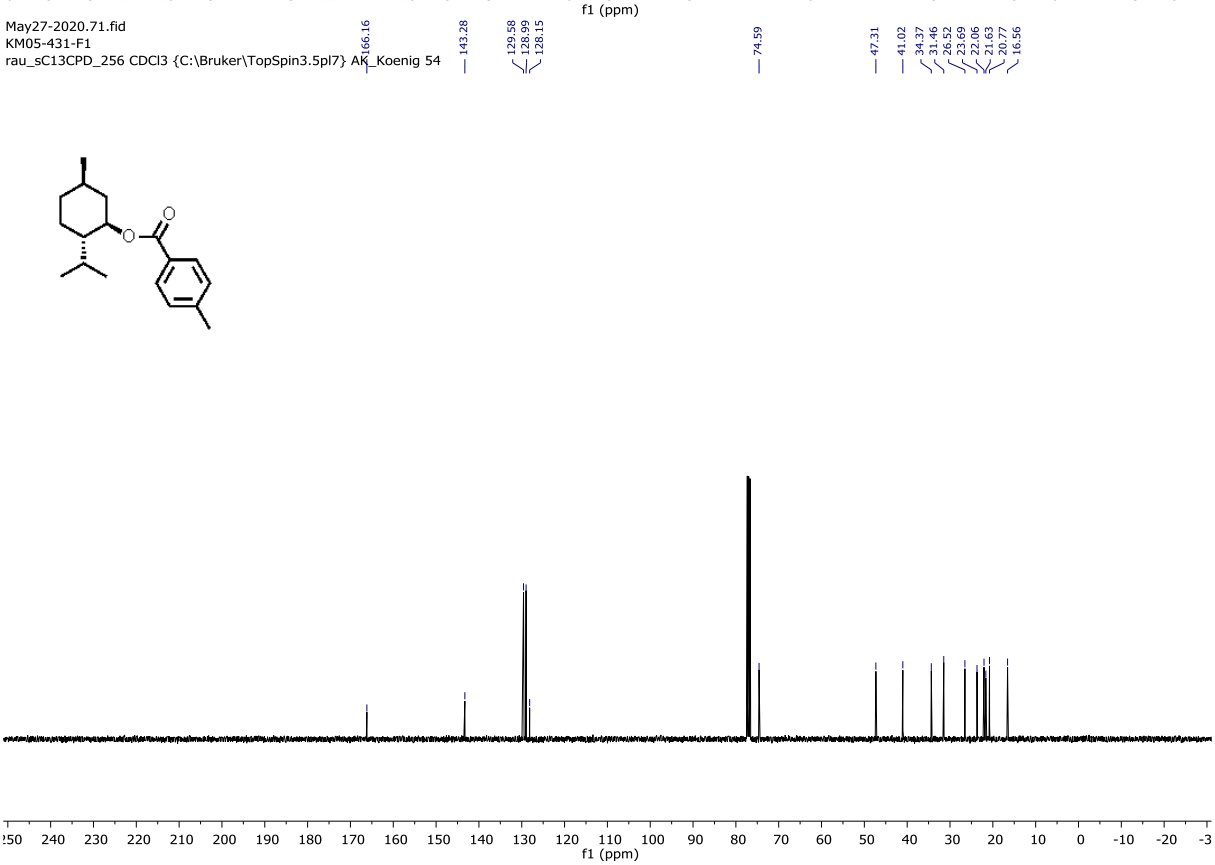

Jun11-2020.11.fid
KM05-490
rau_sPROTON_64 CDCl3 {C:\Bruker\TopSpin3.5pl7} AK_Koenig 55

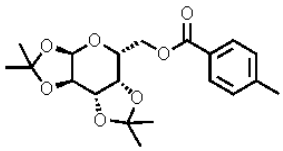

Jun11-2020.12.fid
KM05-490
rau_sC13CPD_256 CDCl3 {C:\Bruker\TopSpin3.5pl7} AK_Koenig 55

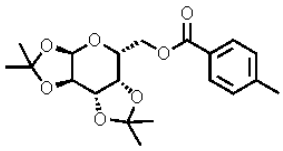

Jun12-2020.13.fid
KM05-491-F1
rau_sPROTON_64 CDCl3 {C:\Bruker\TopSpin3.5pl7} AK_Koenig 4

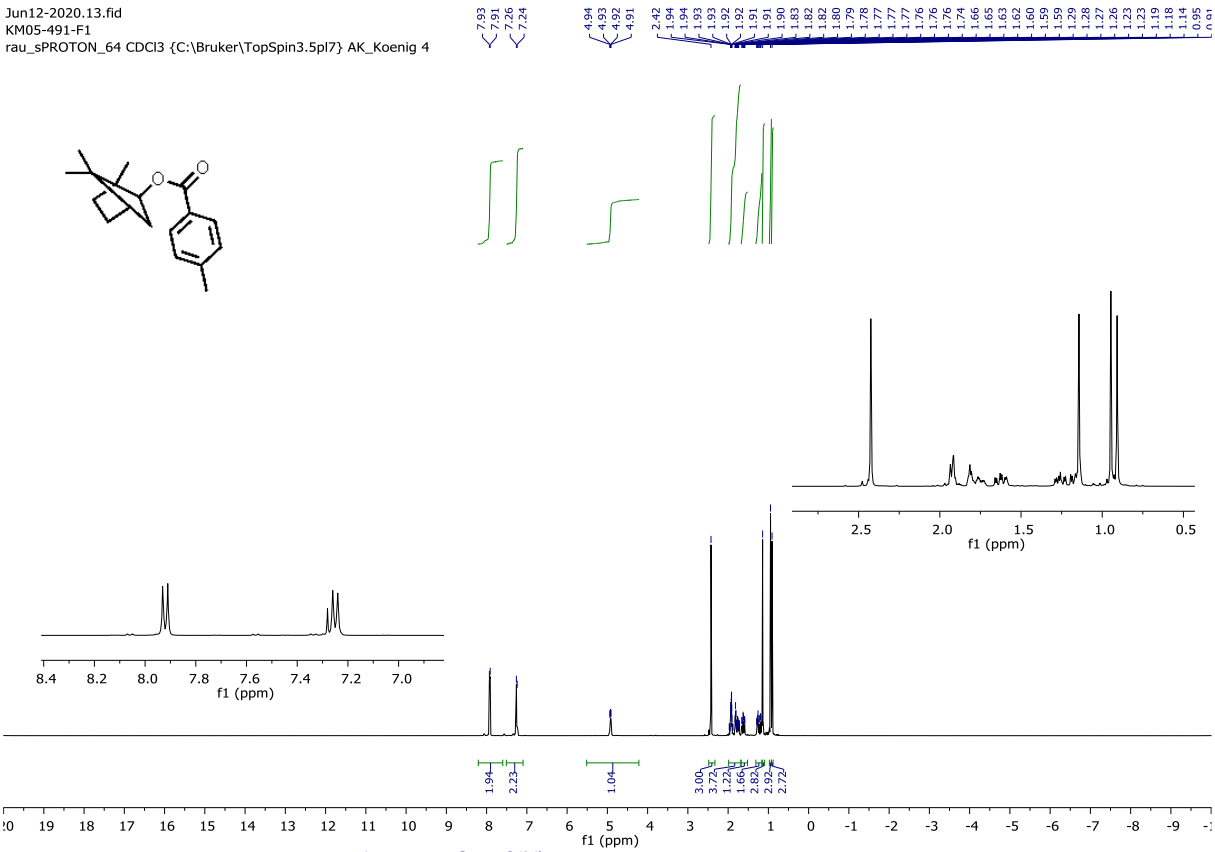

Jun12-2020.14.fid
KM05-491-F1
rau_sC13CPD_256 CDCl3 {C:\Bruker\TopSpin3.5pl7} AK_Koenig 4

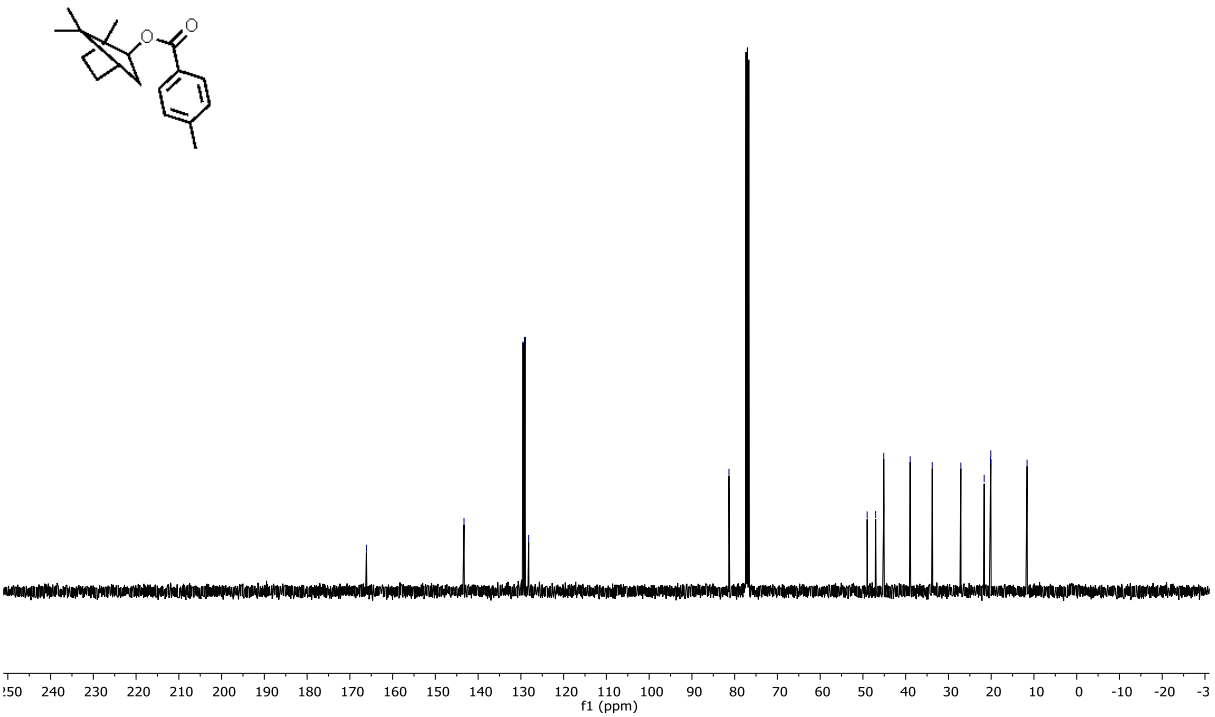

Jun12-2020.73.fid
KM05-495
rau_sPROTON_64 CDCl3 {C:\Bruker\TopSpin3.5pl7} AK_Koenig 13

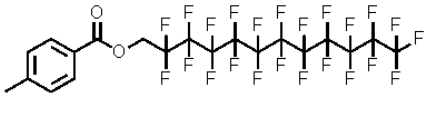

Jun12-2020.74.fid
KM05-495
rau_sC13CPD_256 CDCl3 {C:\Bruker\TopSpin3.5pl7} AK_Koenig 13

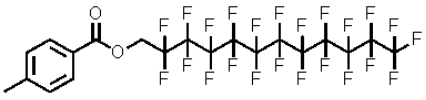

Jun30-2020.82.fid
KM05-495
rau_F19CPD CDCl3 {C:\Bruker\TOPSPIN2.1PL3} AK_Koenig 54

-81.28
-81.31
-81.35

-119.80
-119.82
-119.85
-122.27
-122.27
-122.40
-123.25
-123.25
-123.66
-123.72
-123.72
-126.61
-126.63
-126.66
-126.67
-126.68
-126.71

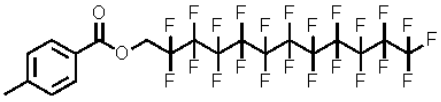

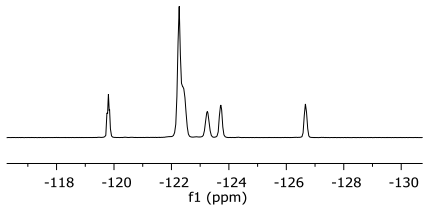

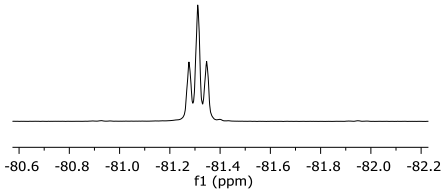

Jun12-2020.81.fid
KM05-496
rau_sPROTON_64 CDCl3 {C:\Bruker\TopSpin3.5pl7} AK_Koenig 14

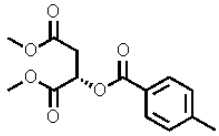

Jun12-2020.82.fid
KM05-496
rau_sC13CPD_256 CDCl3 {C:\Bruker\TopSpin3.5pl7} AK_Koenig 14

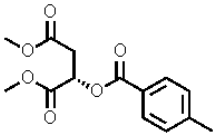

Jun12-2020.93.fid
KM05-498
rau_sPROTON_64 CDCl3 {C:\Bruker\TopSpin3.5pl7} AK_Koenig 15

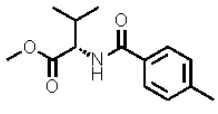

Jun12-2020.94.fid
KM05-498
rau_sC13CPD_256 CDCl3 {C:\Bruker\TopSpin3.5pl7} AK_Koenig 15

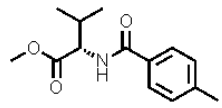

May27-2020.90.fid
KM05-432-F1
rau_sPROTON_64 CDCl3 {C:\Bruker\TopSpin3.5pl7} AK_Koenig 56

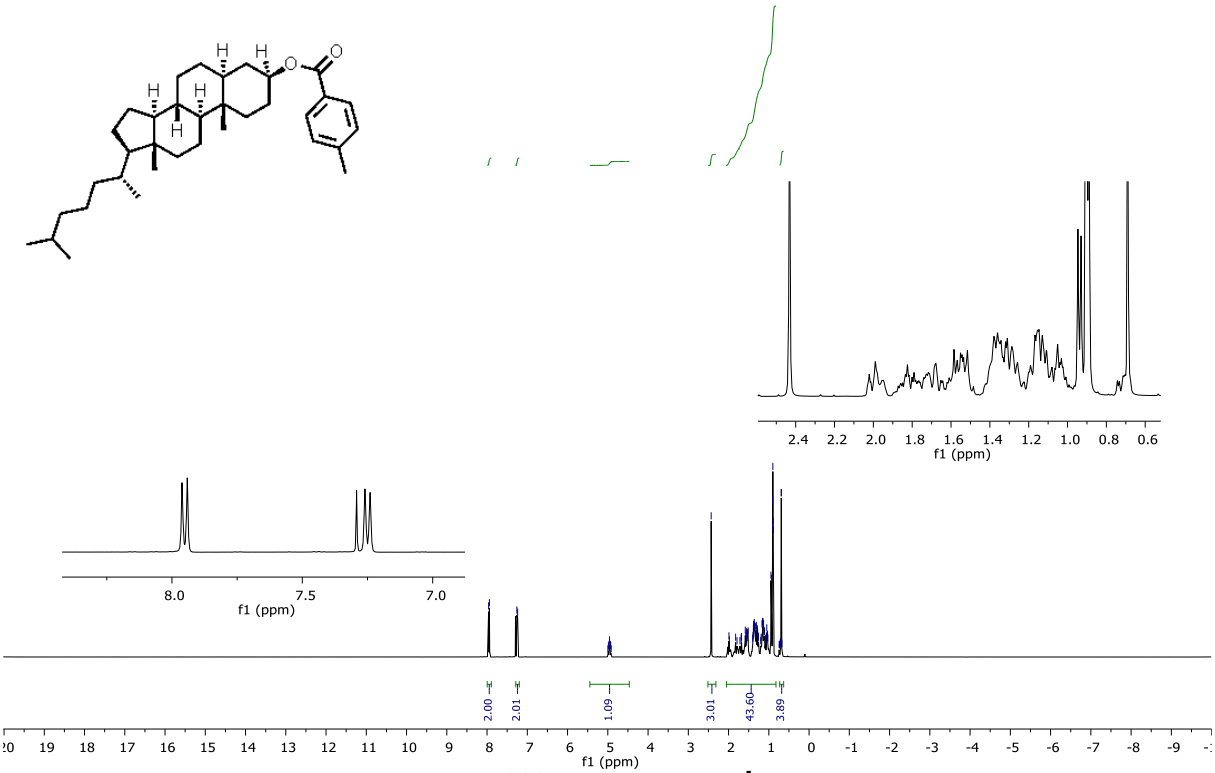

May27-2020.91.fid
KM05-432-F1
rau_sC13CPD_256 CDCl3 {C:\Bruker\TopSpin3.5pl7} AK_Koenig 56

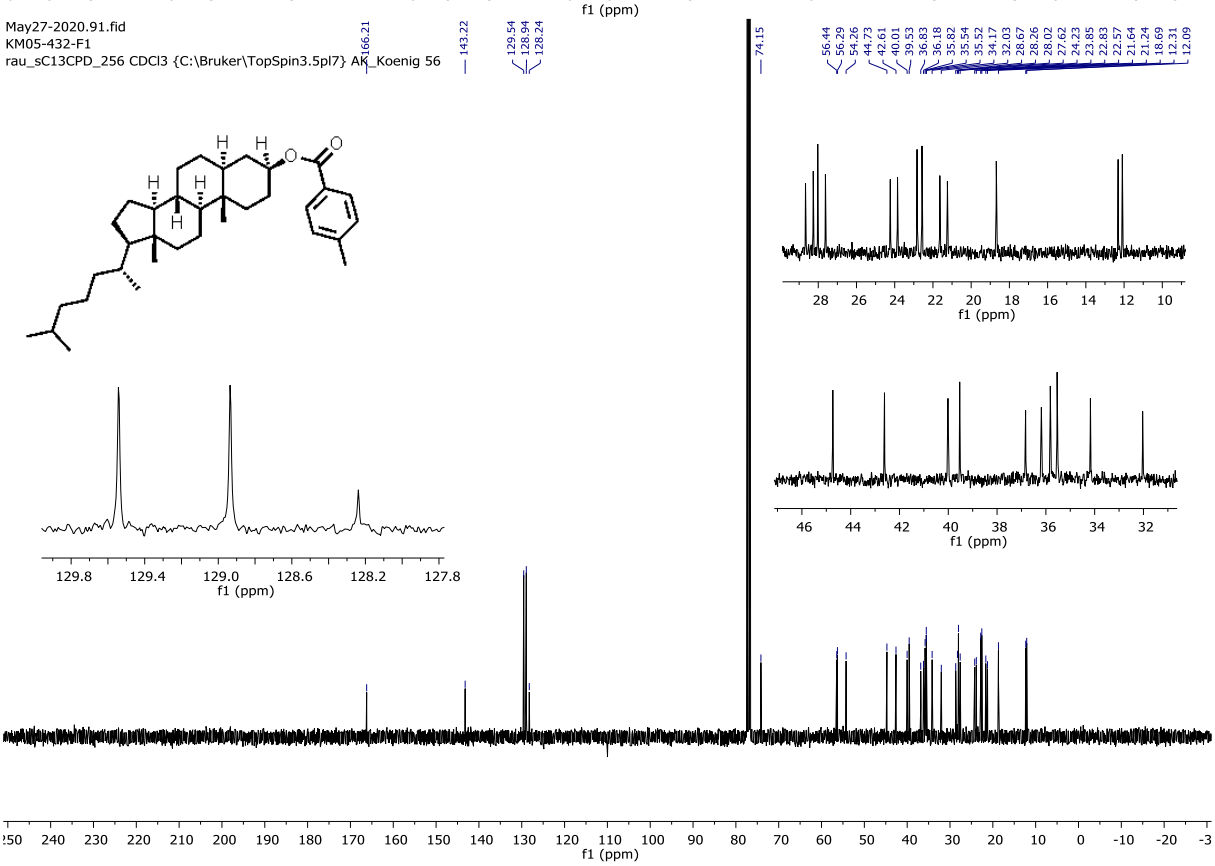

Jul03-2020.90.fid
KM05-549
rau_sPROTON_64 CDCl3 {C:\Bruker\TopSpin3.5pl7} AK_Koenig 53

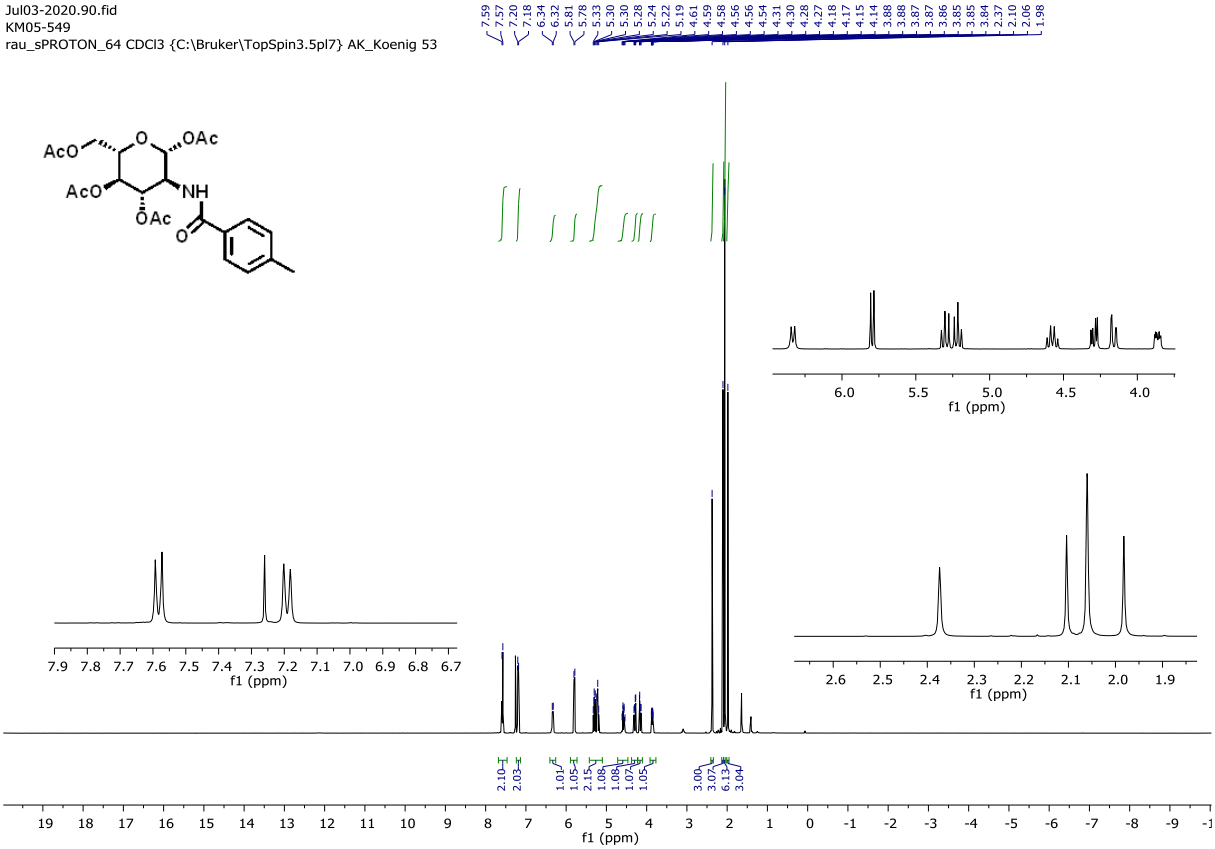

Jul03-2020.91.fid
KM05-549
rau_sC13CPD_256 CDCl3 {C:\Bruker\TopSpin3.5pl7} AK_Koenig 53

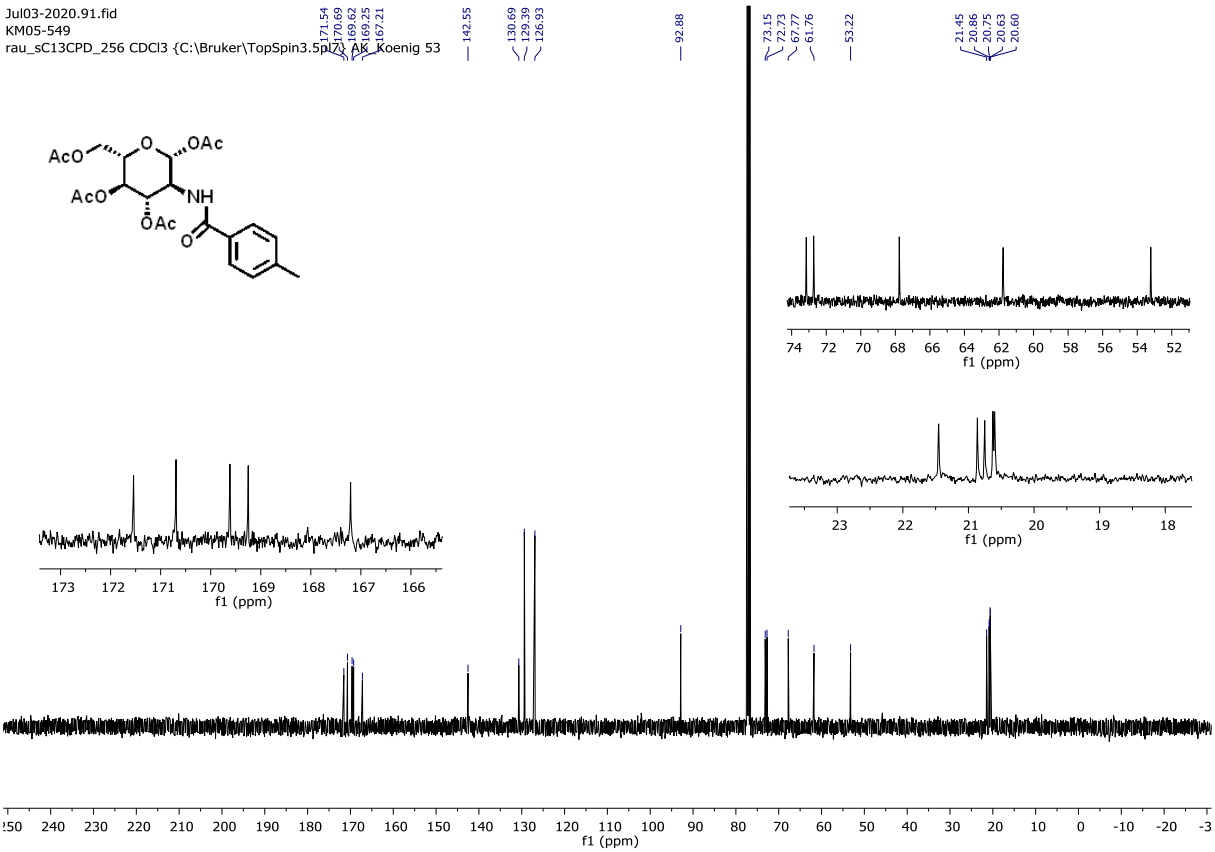

Jun24-2020.10.fid
KM05-535
rau_sPROTON_16 CDCl3 {C:\Bruker\TopSpin3.0} AK_Koenig 7

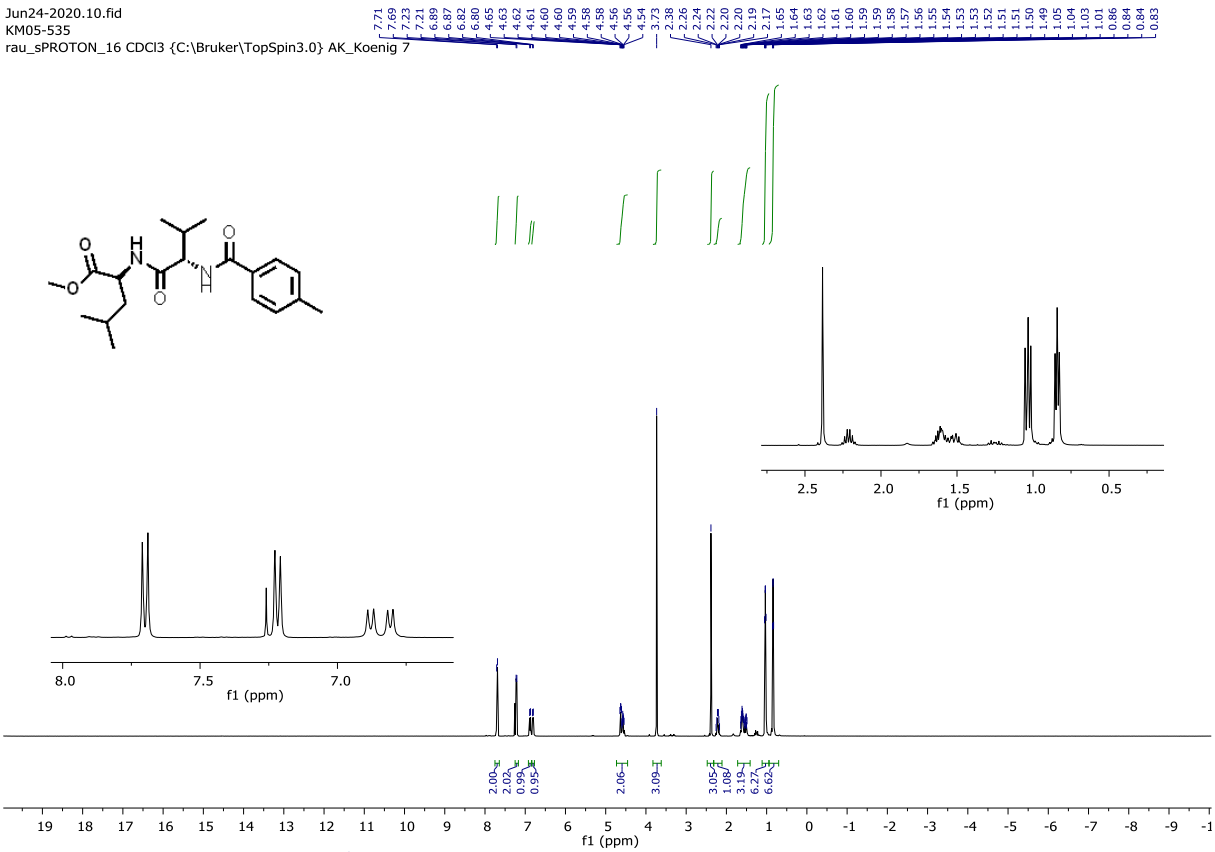

Jun24-2020.11.fid
KM05-535
rau_sC13CPD_256 CDCl3 {C:\Bruker\TopSpin3.0} AK_Koenig 7

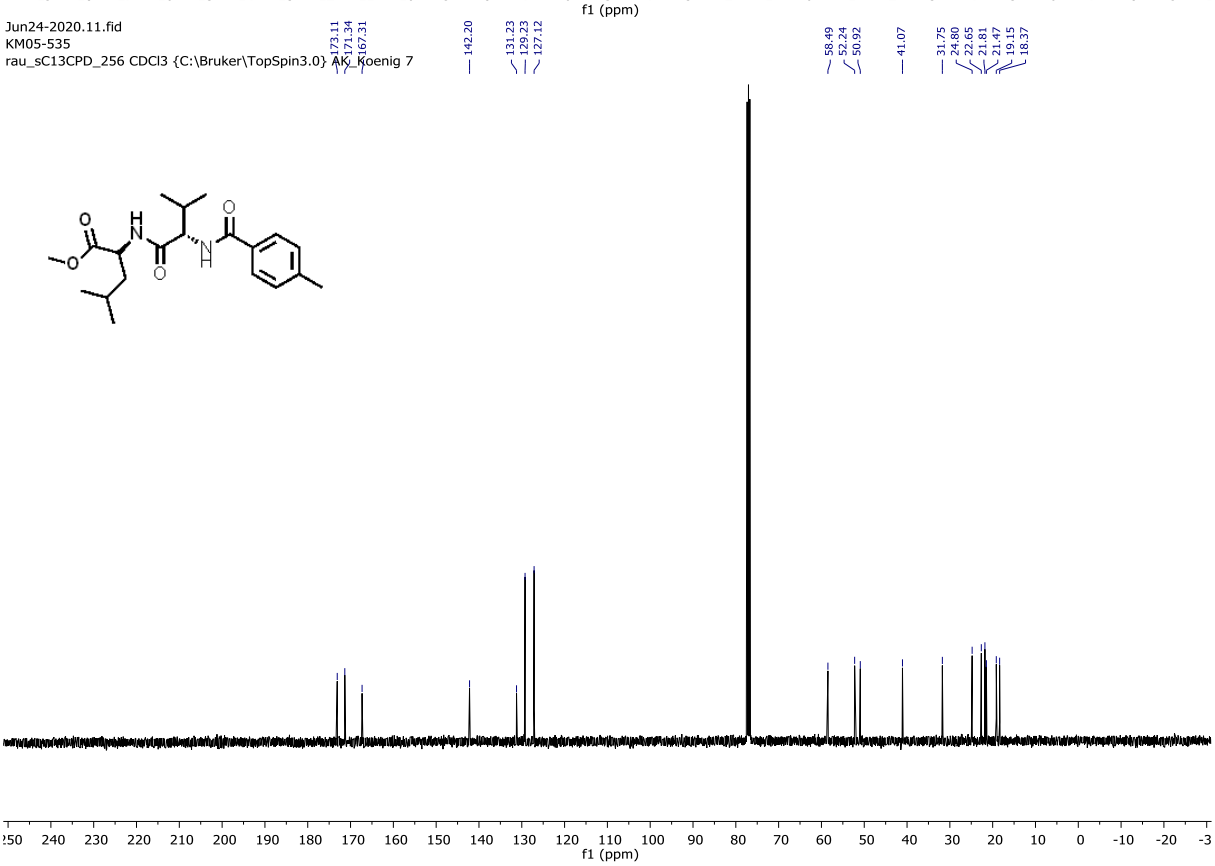

May27-2020.60.fid
KM05-4-ome-oxime
rau_sPROTON_64 CDCl3 {C:\Bruker\TopSpin3.5pl7} AK_Koenig 53

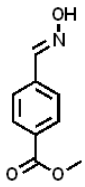

May27-2020.61.fid
KM05-4-ome-oxime
rau_sC13CPD_256 CDCl3 {C:\Bruker\TopSpin3.5pl7} AK_Koenig 53

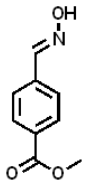

Jul23-2020.20.fid
KM05-617
rau_sPROTON_16 DMSO {C:\Bruker\TopSpin3.5pl7} AK_Koenig 16

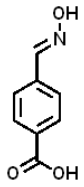

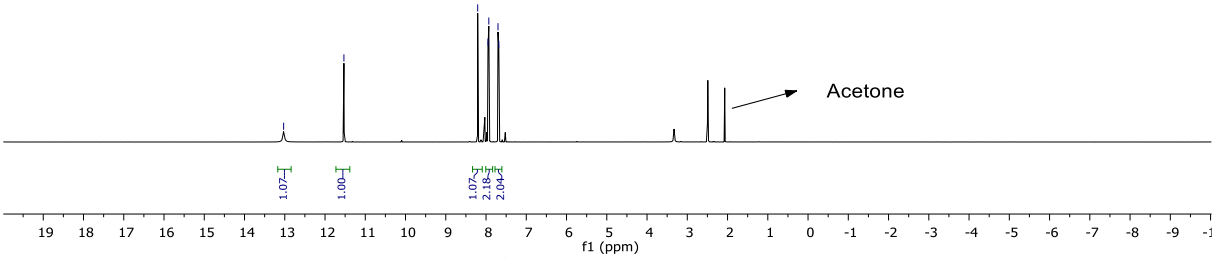

Jul23-2020.21.fid
KM05-617
rau_sC13CPD_256 DMSO {C:\Bruker\TopSpin3.5pl7} AK_Koenig 16

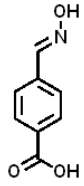

Jul23-2020.40.fid
KM05-619
rau_sPROTON_16 DMSO {C:\Bruker\TopSpin3.5pl7} AK_Koenig 18

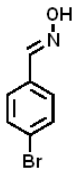

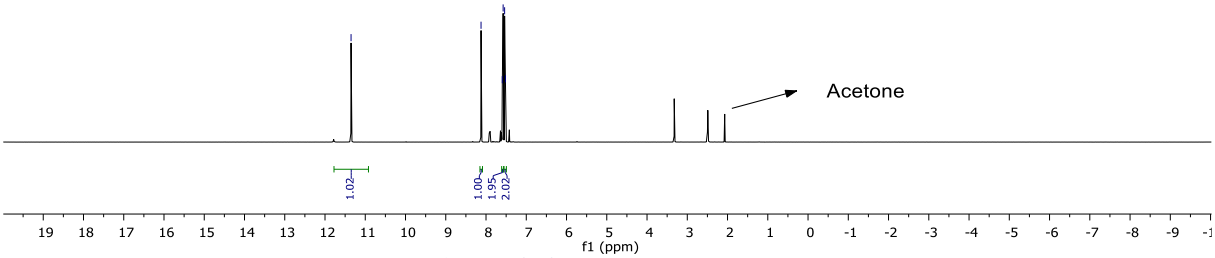

Jul23-2020.41.fid
KM05-619
rau_sC13CPD_256 DMSO {C:\Bruker\TopSpin3.5pl7} AK_Koenig 18

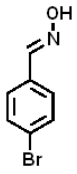

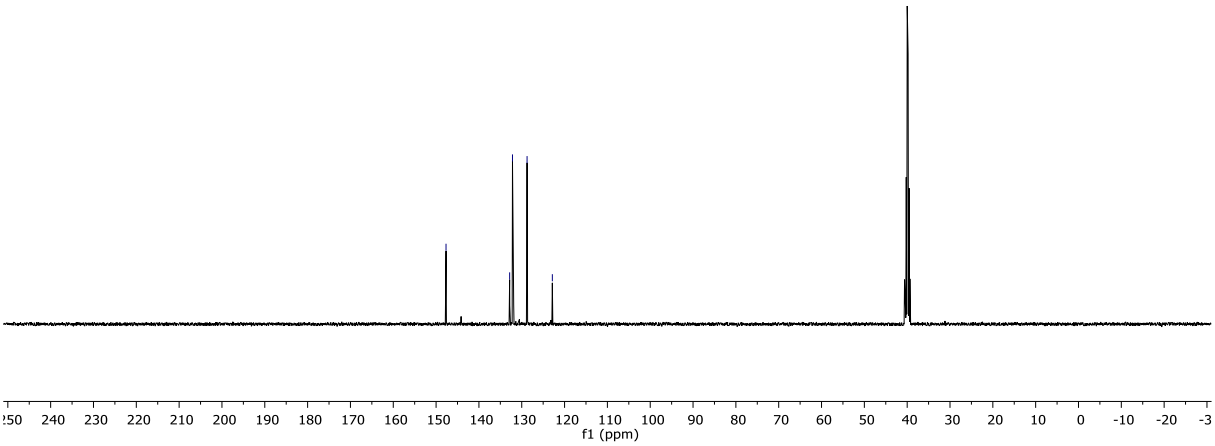

Jul23-2020.30.fid
KM05-618
rau_sPROTON_16 DMSO {C:\Bruker\TopSpin3.5pl7} AK_Koenig 17

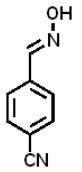

Jul23-2020.31.fid
KM05-618
rau_sC13CPD_256 DMSO {C:\Bruker\TopSpin3.5pl7} AK_Koenig 17

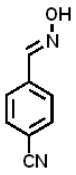

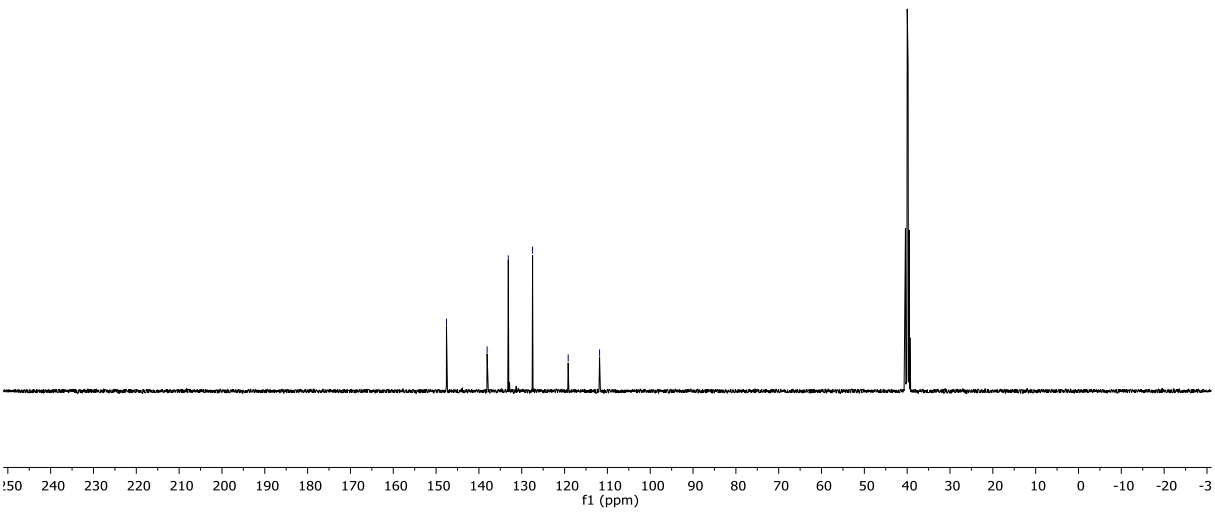

Jun26-2020.70.fid
KM05-399A
rau_sPROTON_16 CDCl3 {C:\Bruker\TopSpin3.0} AK_Koenig 39

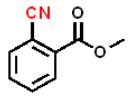

Jun26-2020.71.fid
KM05-399A
rau_sC13CPD_256 CDCl3 {C:\Bruker\TopSpin3.0} AK_Koenig 39

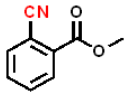

Jun26-2020.80.fid
KM05-400
rau_sPROTON_16 CDCl3 {C:\Bruker\TopSpin3.0} AK_Koenig 40

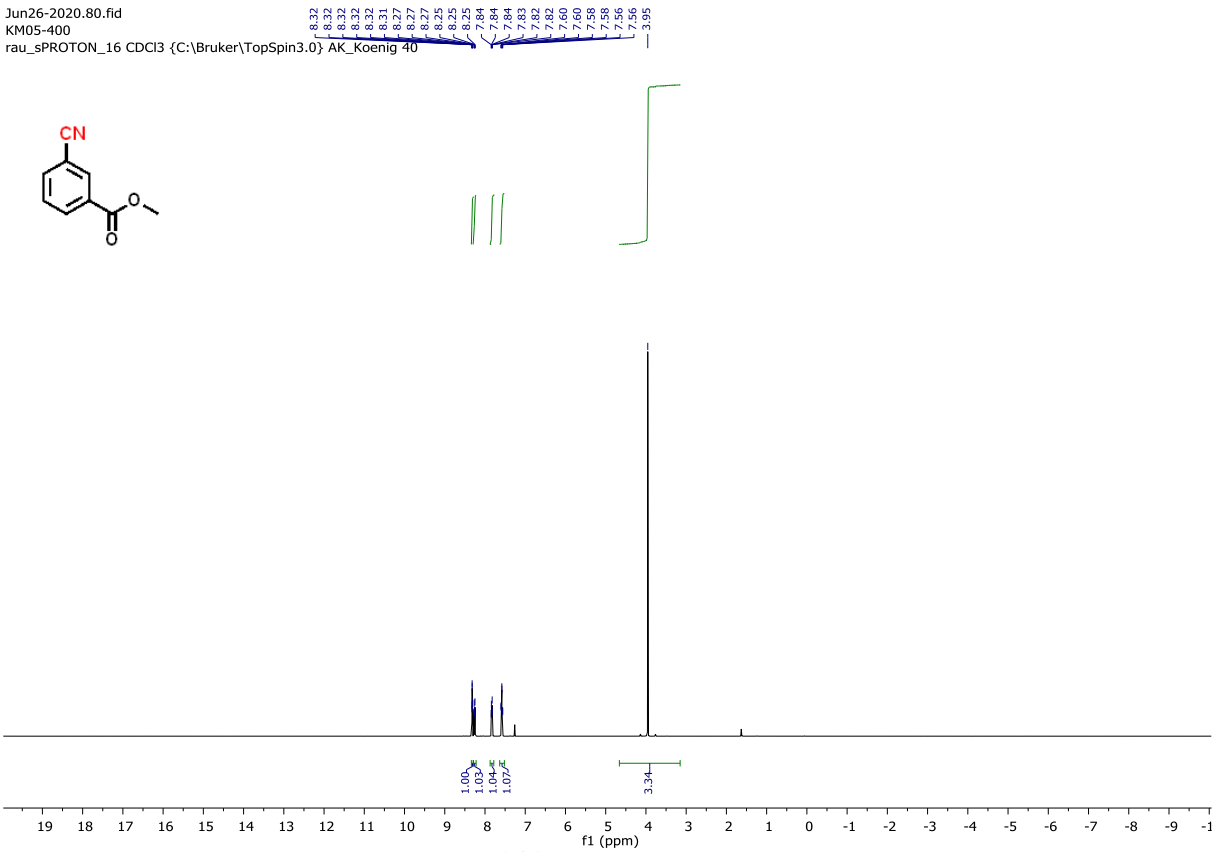

Jun26-2020.81.fid
KM05-400
rau_sC13CPD_256 CDCl3 {C:\Bruker\TopSpin3.0} AK_Koenig 40

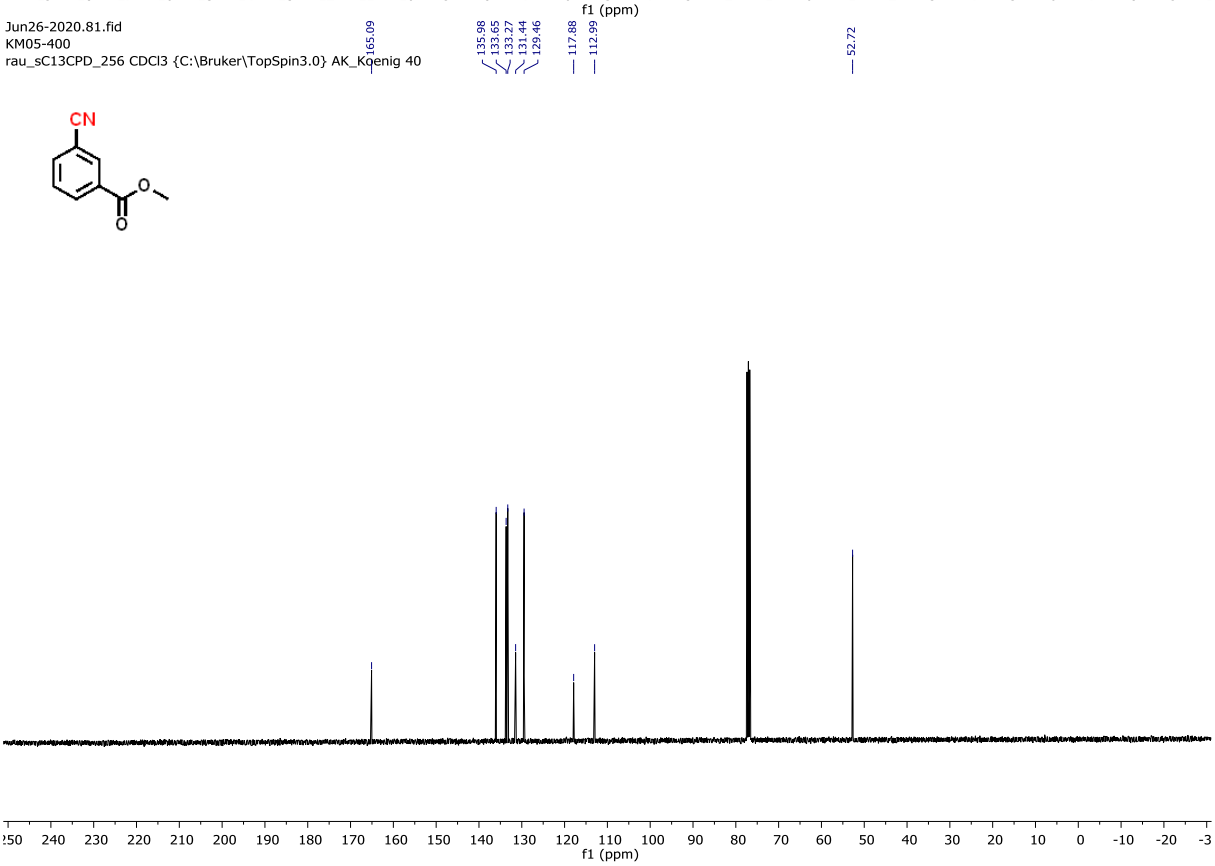

Jun26-2020.40.fid
KM05-284
rau_sPROTON_16 CDCl3 {C:\Bruker\TopSpin3.0} AK_Koenig 36

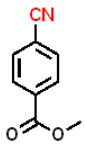

Jun26-2020.41.fid
KM05-284
rau_sC13CPD_256 CDCl3 {C:\Bruker\TopSpin3.0} AK_Koenig 36

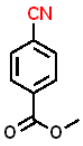

Jun26-2020.60.fid
KM05-392
rau_sPROTON_16 CDCl3 {C:\Bruker\TopSpin3.0} AK_Koenig 38

Jun26-2020.61.fid
KM05-392
rau_sC13CPD_256 CDCl3 {C:\Bruker\TopSpin3.0} AK_Koenig 38

Jul14-2020.130.fid
KM05-423
rau_sPROTON_16 DMSO {C:\Bruker\TopSpin3.5pl7} AK_Koenig 56

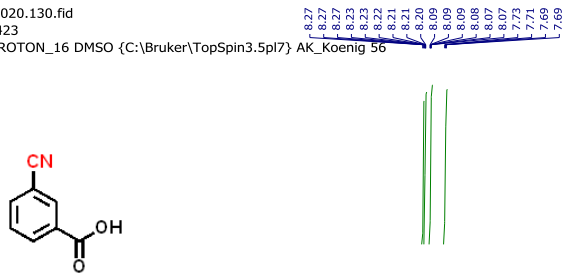

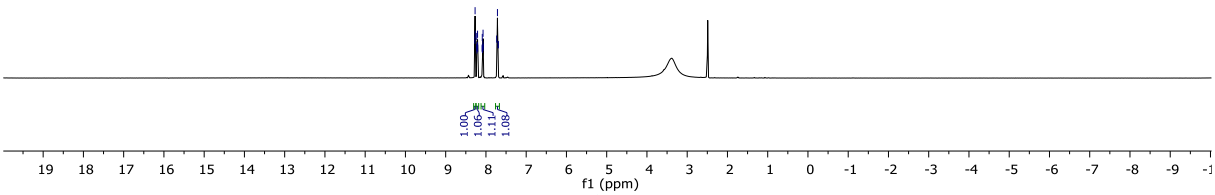

Jul14-2020.131.fid
KM05-423
rau_sC13CPD_256 DMSO {C:\Bruker\TopSpin3.5pl7} AK_Koenig 56

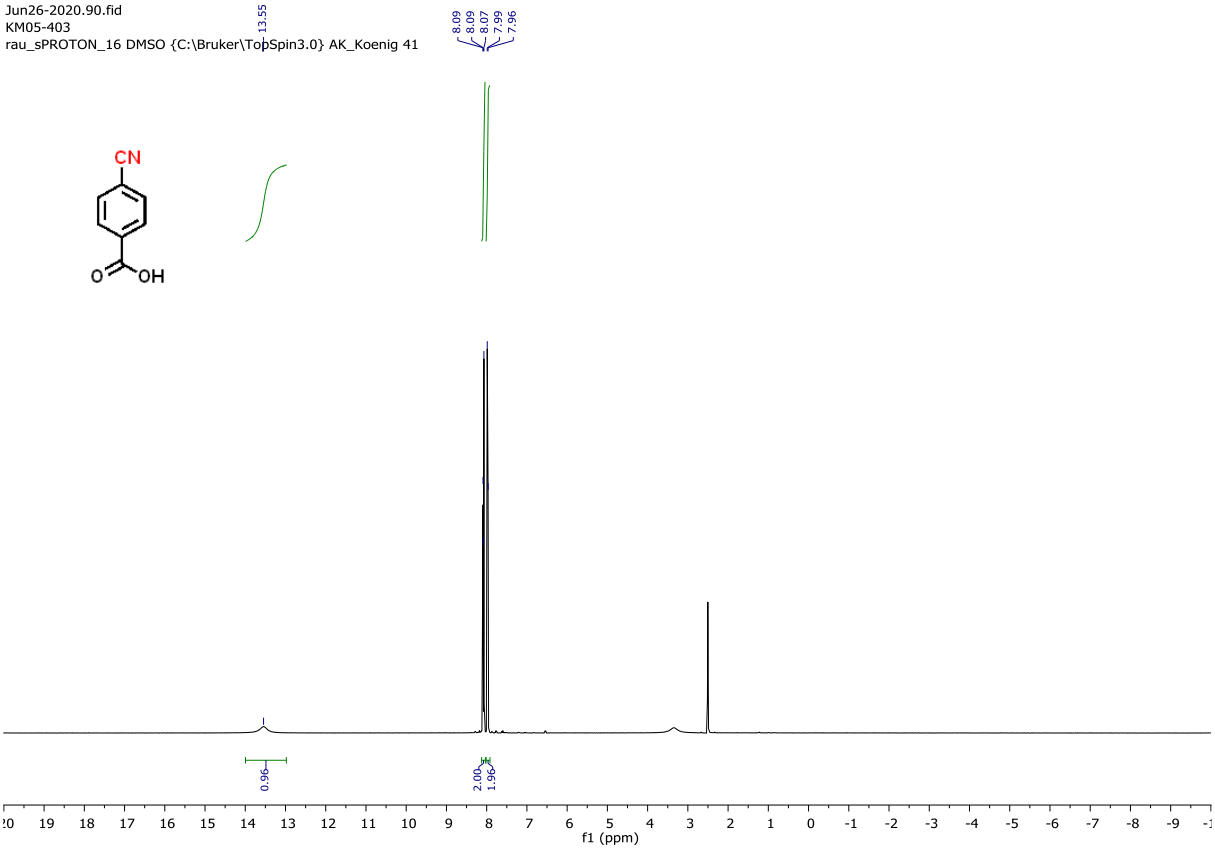
Jun26-2020.90.fid
KM05-403
rau_sPROTON_16 DMSO {C:\Bruker\TopSpin3.0} AK_Koenig 41
13.55
8.09
8.09
8.07
7.99
7.96
CN
O
OH
0.96
2.00
1.96
f1 (ppm)

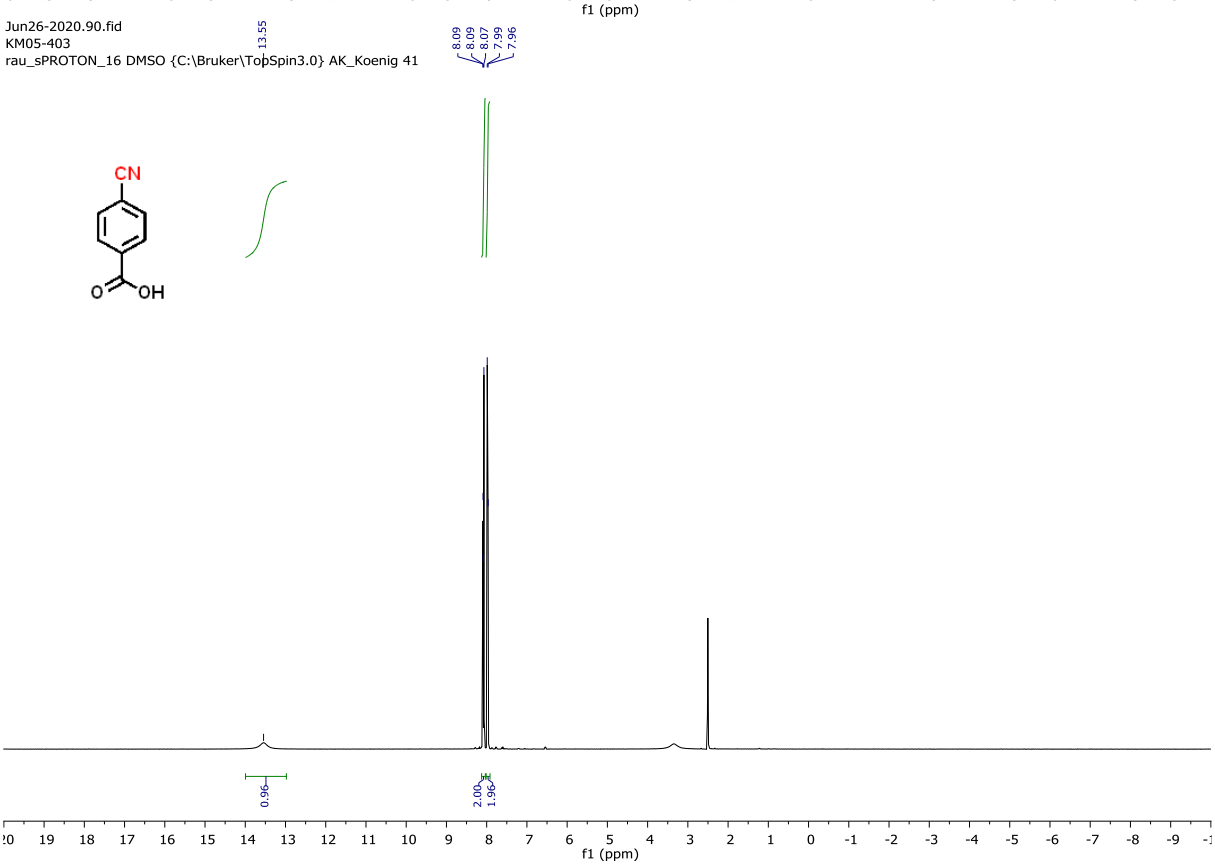
Jun26-2020.90.fid
KM05-403
rau_sPROTON_16 DMSO {C:\Bruker\TopSpin3.0} AK_Koenig 41
13.55
8.09
8.09
8.07
7.99
7.96
CN
O
OH
0.96
2.00
1.96
f1 (ppm)

Jul27-2020.60.fid
KM05-434A
rau_sPROTON_16 DMSO {C:\Bruker\TopSpin3.5pl7} AK_Koenig 17

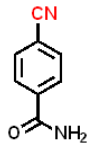

Jul27-2020.61.fid
KM05-434A
rau_sC13CPD_256 DMSO {C:\Bruker\TopSpin3.5pl7} AK_Koenig 17

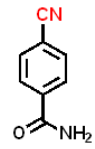

Jun26-2020.100.fid
KM05-411A
rau_sPROTON_16 CDCl3 {C:\Bruker\TopSpin3.0} AK_Koenig 42

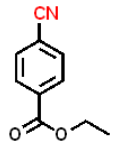

Jun26-2020.101.fid
KM05-411A
rau_sC13CPD_256 CDCl3 {C:\Bruker\TopSpin3.0} AK_Koenig 42

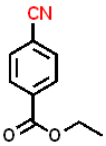

Jun26-2020.130.fid
KM05-462
rau_sPROTON_16 CDCl3 {C:\Bruker\TopSpin3.0} AK_Koenig 45

Jun26-2020.131.fid
KM05-462
rau_sC13CPD_256 CDCl3 {C:\Bruker\TopSpin3.0} AK_Koenig 45

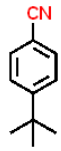

Jun26-2020.200.fid
KM05-524
rau_sPROTON_16 CDCl3 {C:\Bruker\TopSpin3.0} AK_Koenig 52

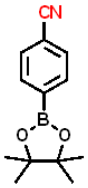

Jun26-2020.201.fid
KM05-524
rau_sC13CPD_256 CDCl3 {C:\Bruker\TopSpin3.0} AK_Koenig 52

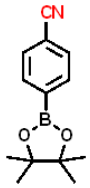

Jun26-2020.150.fid
KM05-482
rau_sPROTON_16 CDCl3 {C:\Bruker\TopSpin3.0} AK_Koenig 47

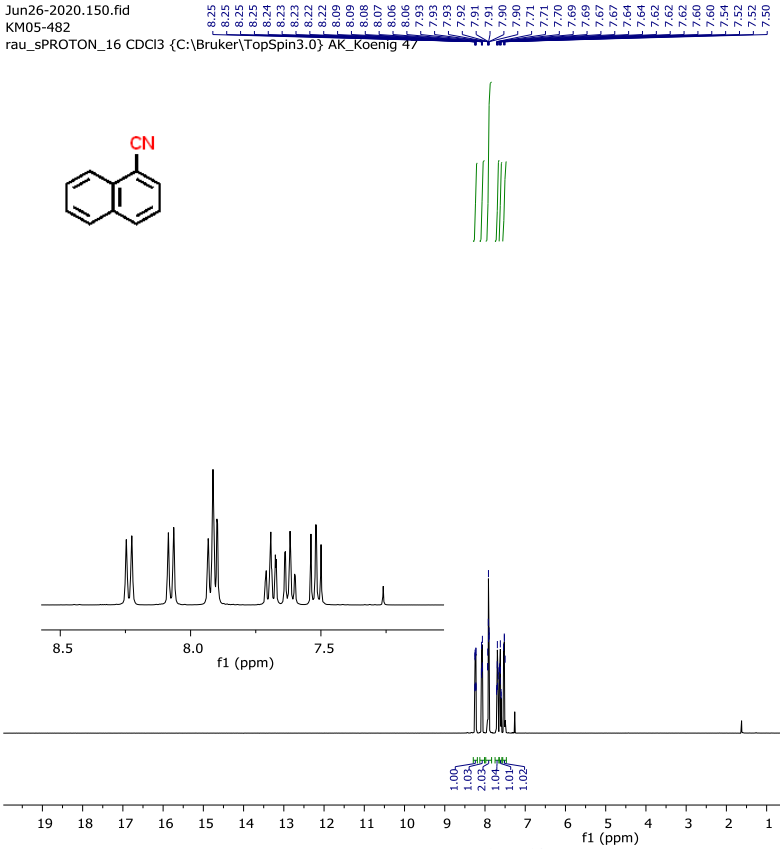

Jun26-2020.151.fid
KM05-482
rau_sC13CPD_256 CDCl3 {C:\Bruker\TopSpin3.0} AK_Koenig 47

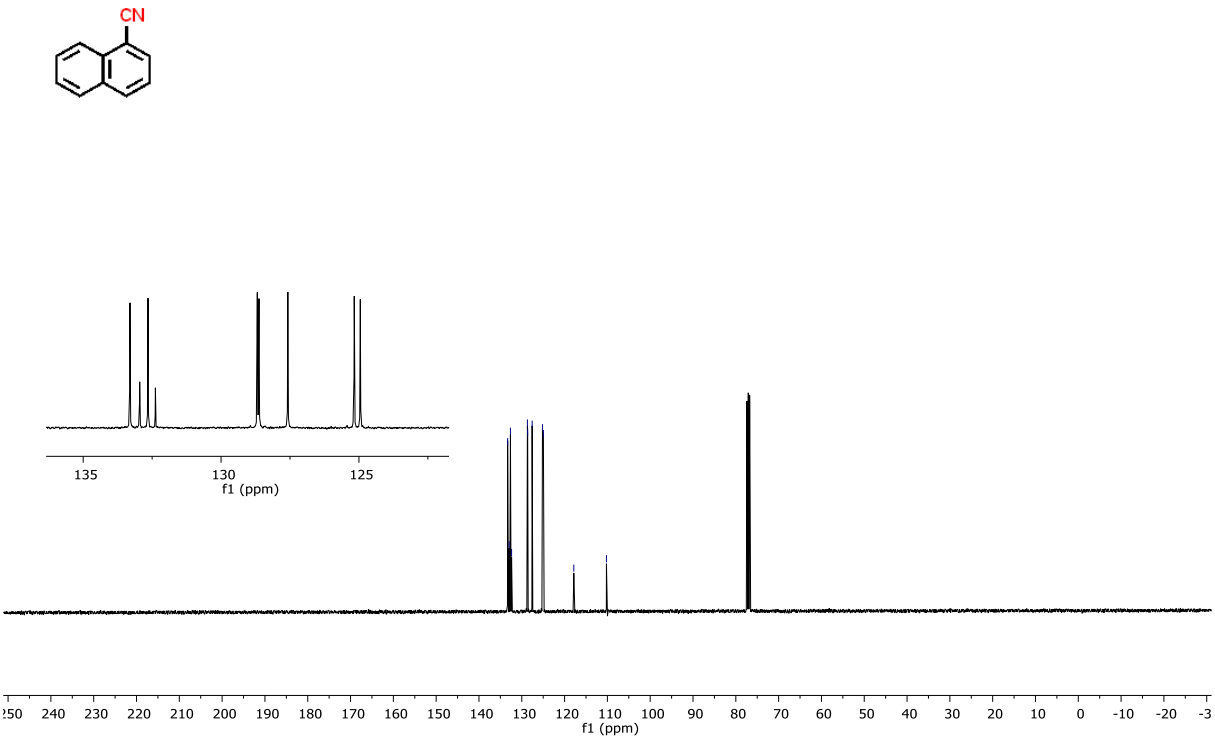

Jun26-2020.50.fid
KM05-306
rau_sPROTON_16 CDCl3 {C:\Bruker\TopSpin3.0} AK_Koenig 37

Jun26-2020.51.fid
KM05-306
rau_sC13CPD_256 CDCl3 {C:\Bruker\TopSpin3.0} AK_Koenig 37

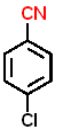

Jun26-2020.160.fid
KM05-483
rau_sPROTON_16 CDCl3 {C:\Bruker\TopSpin3.0} AK_Koenig 48

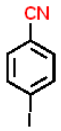

Jun26-2020.161.fid
KM05-483
rau_sC13CPD_256 CDCl3 {C:\Bruker\TopSpin3.0} AK_Koenig 48

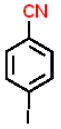

Jun26-2020.180.fid
KM05-510
rau_sPROTON_16 CDCl3 {C:\Bruker\TopSpin3.0} AK_Koenig 50

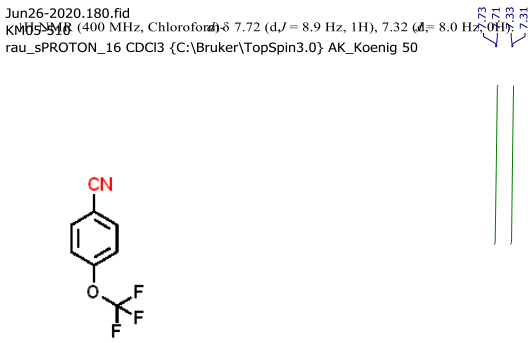

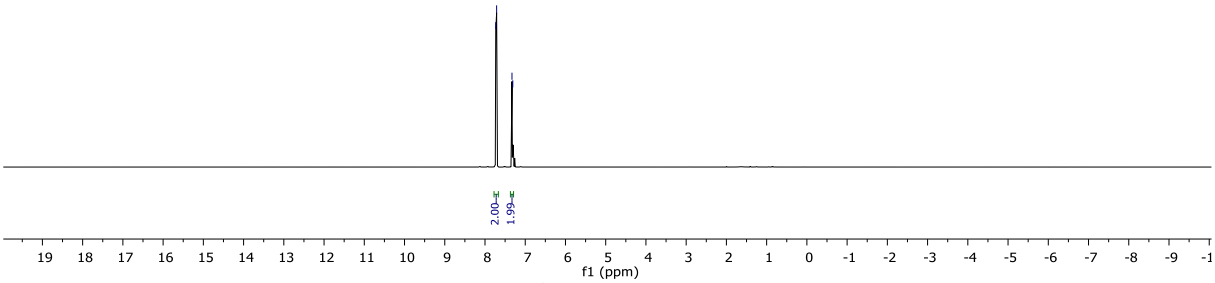

Jun26-2020.181.fid
KM05-510
rau_sC13CPD_256 CDCl3 {C:\Bruker\TopSpin3.0} AK_Koenig 50

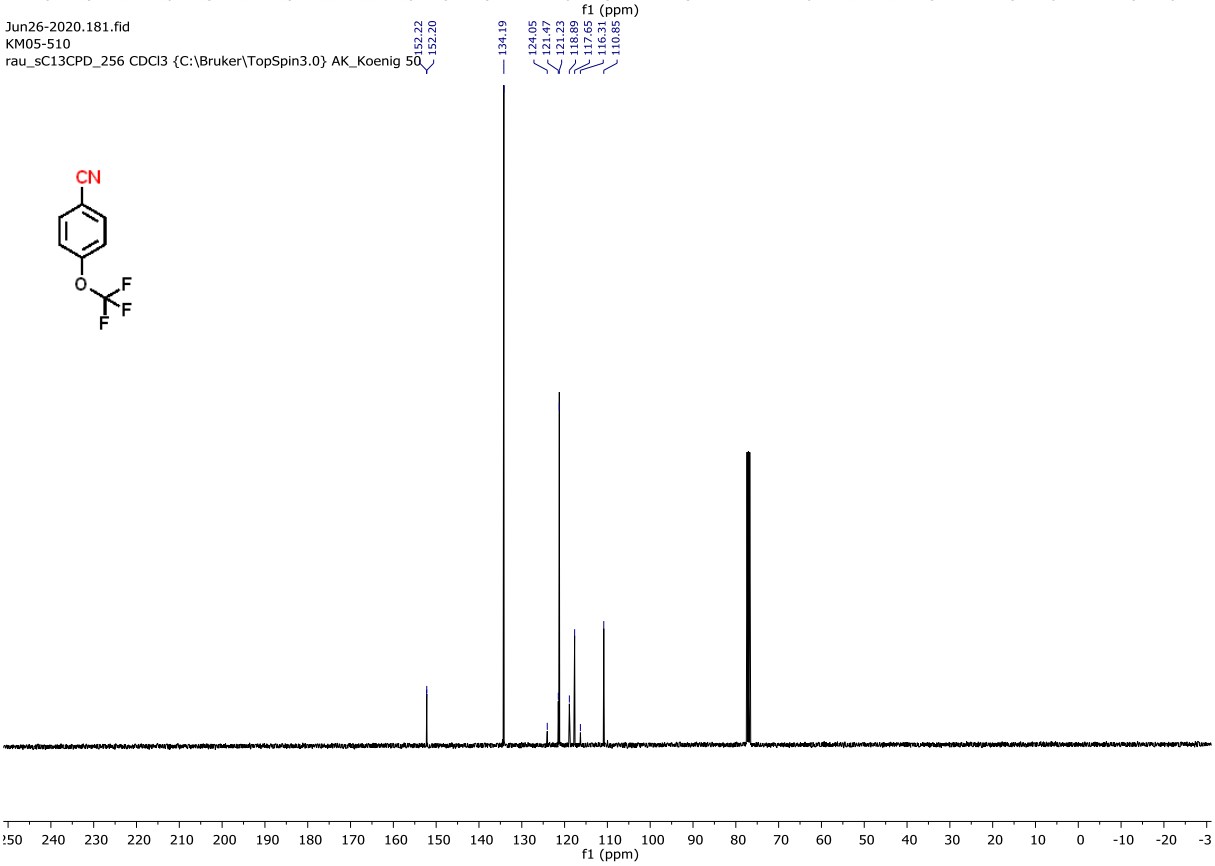

Jun26-2020.182.fid
KM05-510
rau_sF19CPD CDCl3 {C:\Bruker\TopSpin3.0} AK_Koenig 50

-58.30

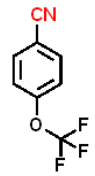

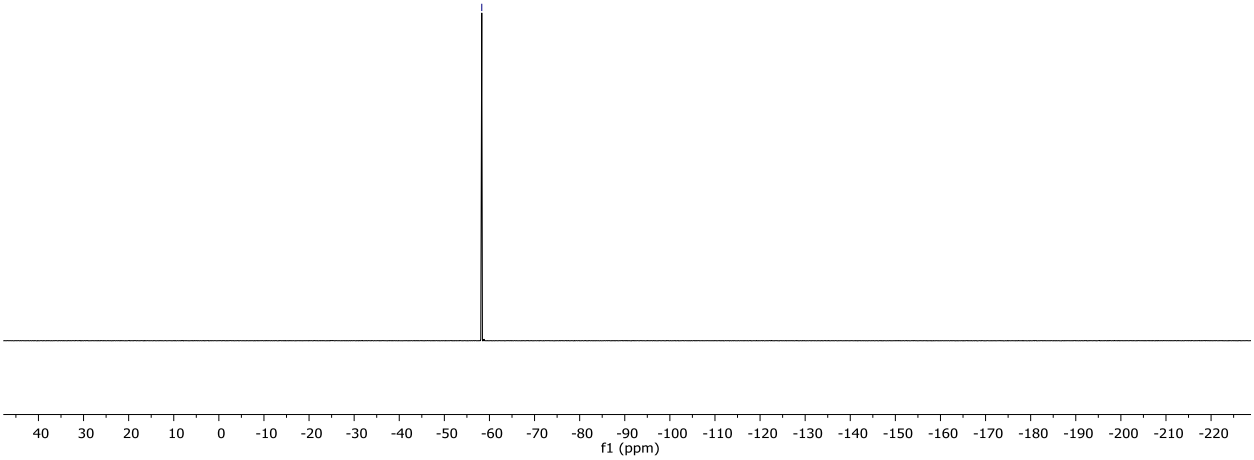

Jul03-2020.40.fid
KM05-419
rau_sPROTON_64 CDCl3 {C:\Bruker\TopSpin3.5pl7} AK_Koenig 48

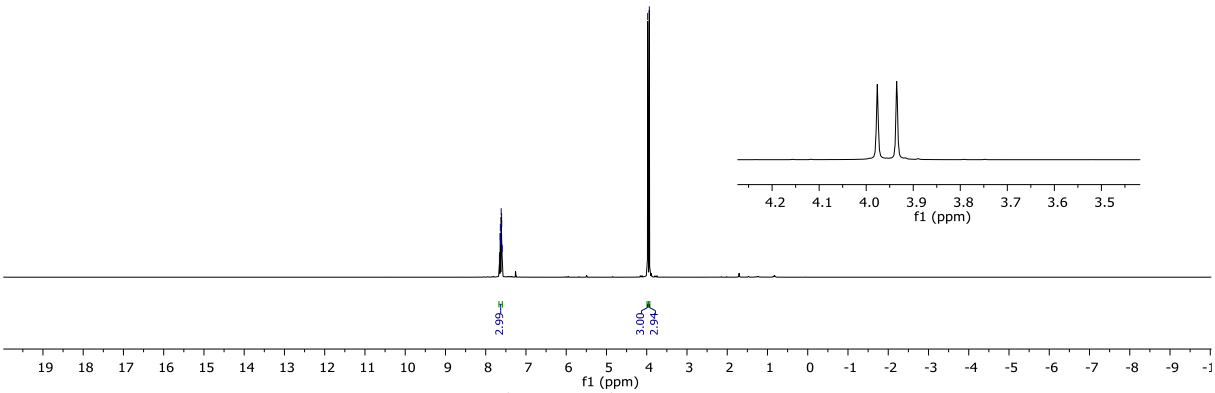

Jul03-2020.41.fid
KM05-419
rau_sC13CPD_256 CDCl3 {C:\Bruker\TopSpin3.5pl7} AK_Koenig 48

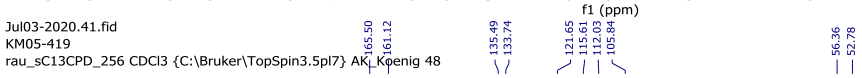

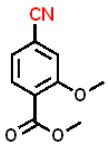

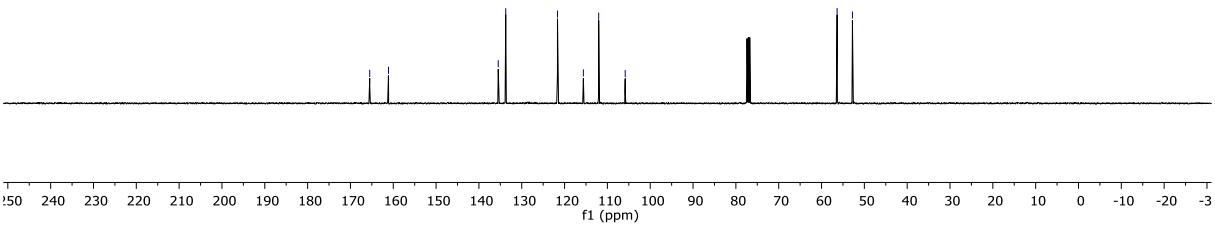

Jun26-2020.170.fid
KM05-488
rau_sPROTON_16 CDCl3 {C:\Bruker\TopSpin3.0} AK_Koenig 49

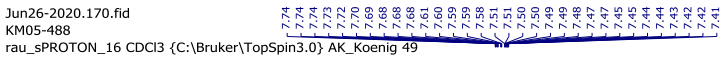

Jun26-2020.171.fid
KM05-488
rau_sC13CPD_256 CDCl3 {C:\Bruker\TopSpin3.0} AK_Koenig 49

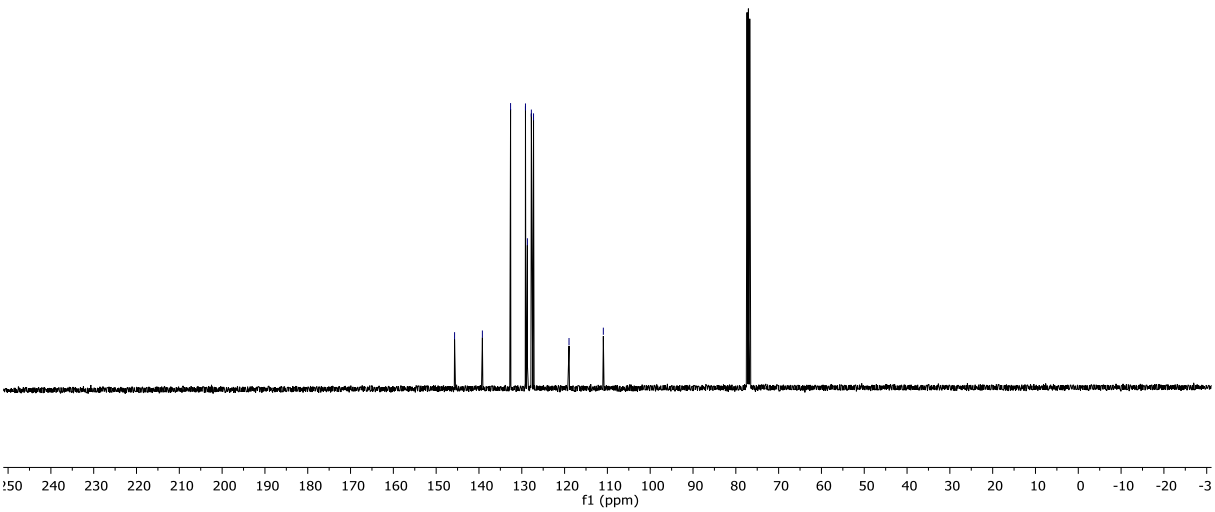

Jun26-2020.190.fid
KM05-523
rau_sPROTON_16 CDCl3 {C:\Bruker\TopSpin3.0} AK_Koenig 51

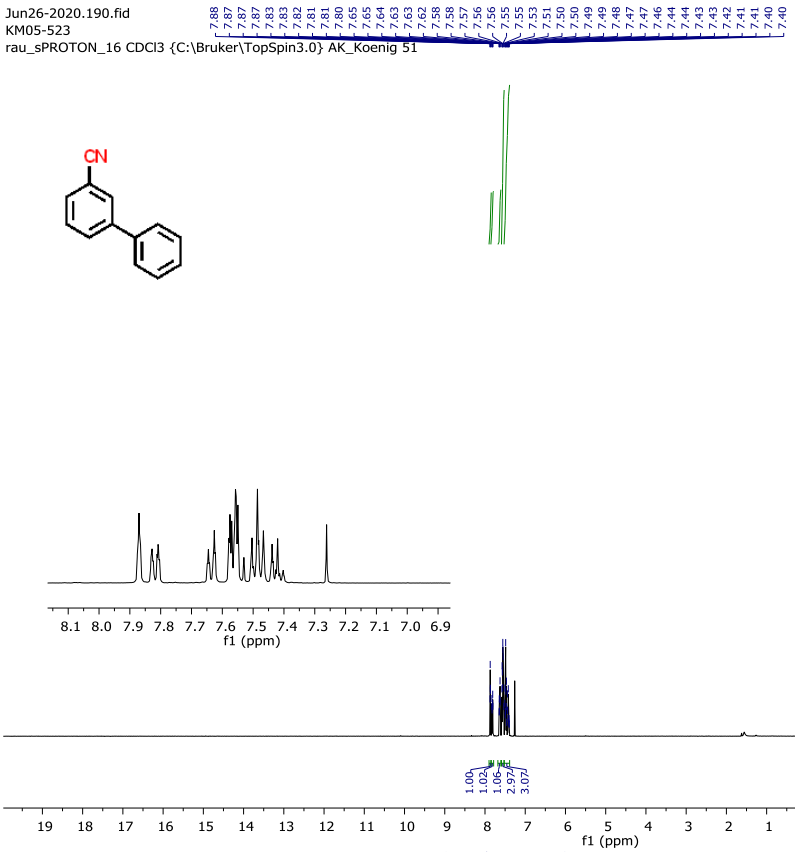

Jun26-2020.191.fid
KM05-523
rau_sC13CPD_256 CDCl3 {C:\Bruker\TopSpin3.0} AK_Koenig 51

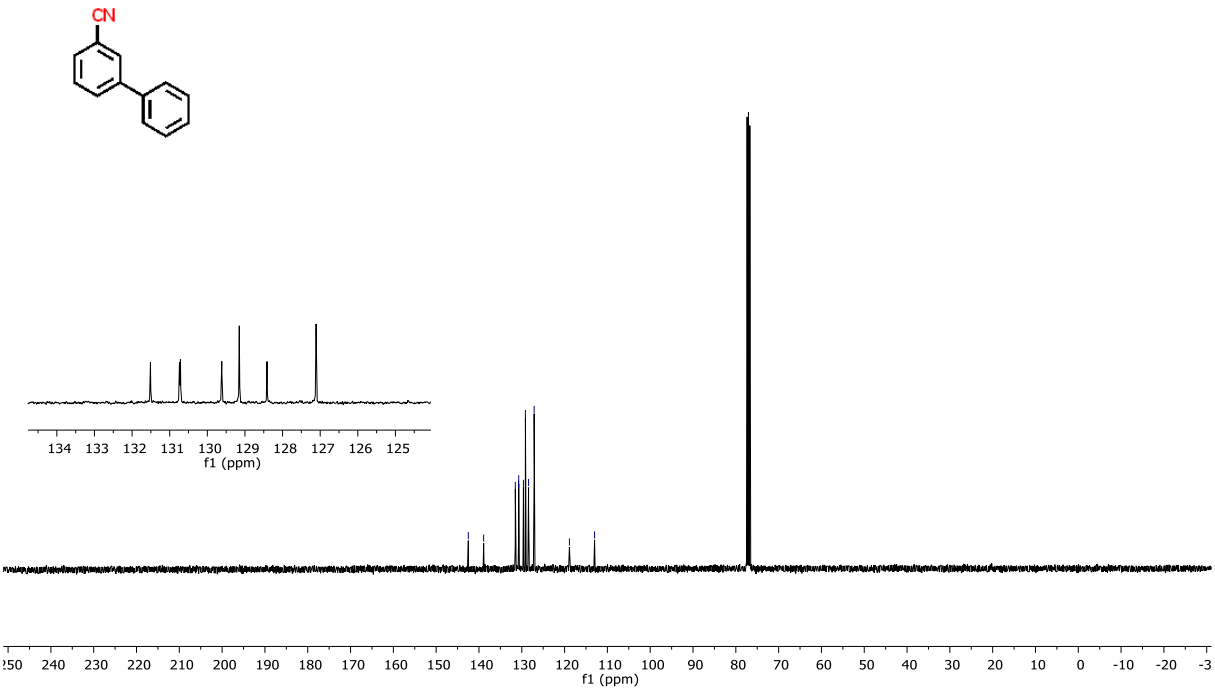

Jun26-2020.50.fid
KM05-511
rau_sPROTON_16 CDCl3 {C:\Bruker\TopSpin3.5pl7} AK_Koenig 52

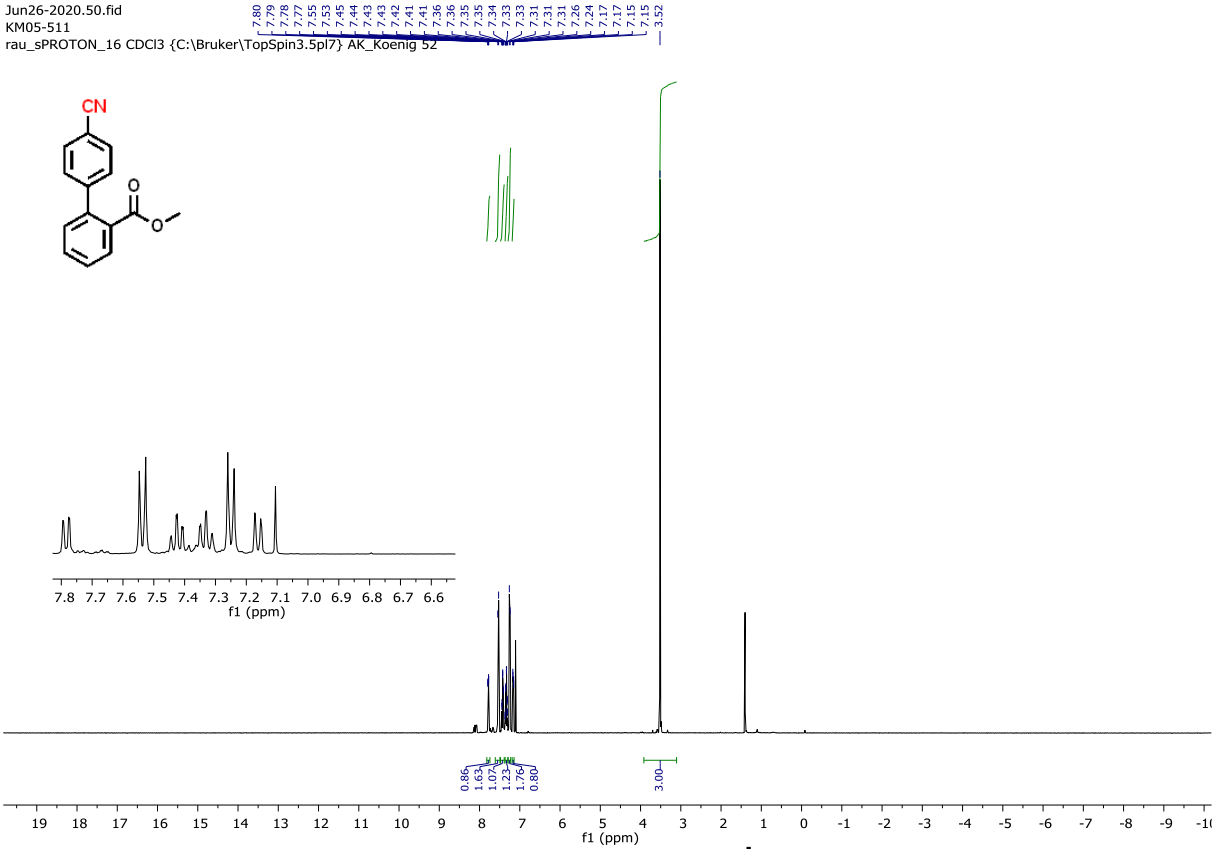

Jun26-2020.51.fid
KM05-511
rau_sC13CPD_256 CDCl3 {C:\Bruker\TopSpin3.5pl7} AK_Koenig 52

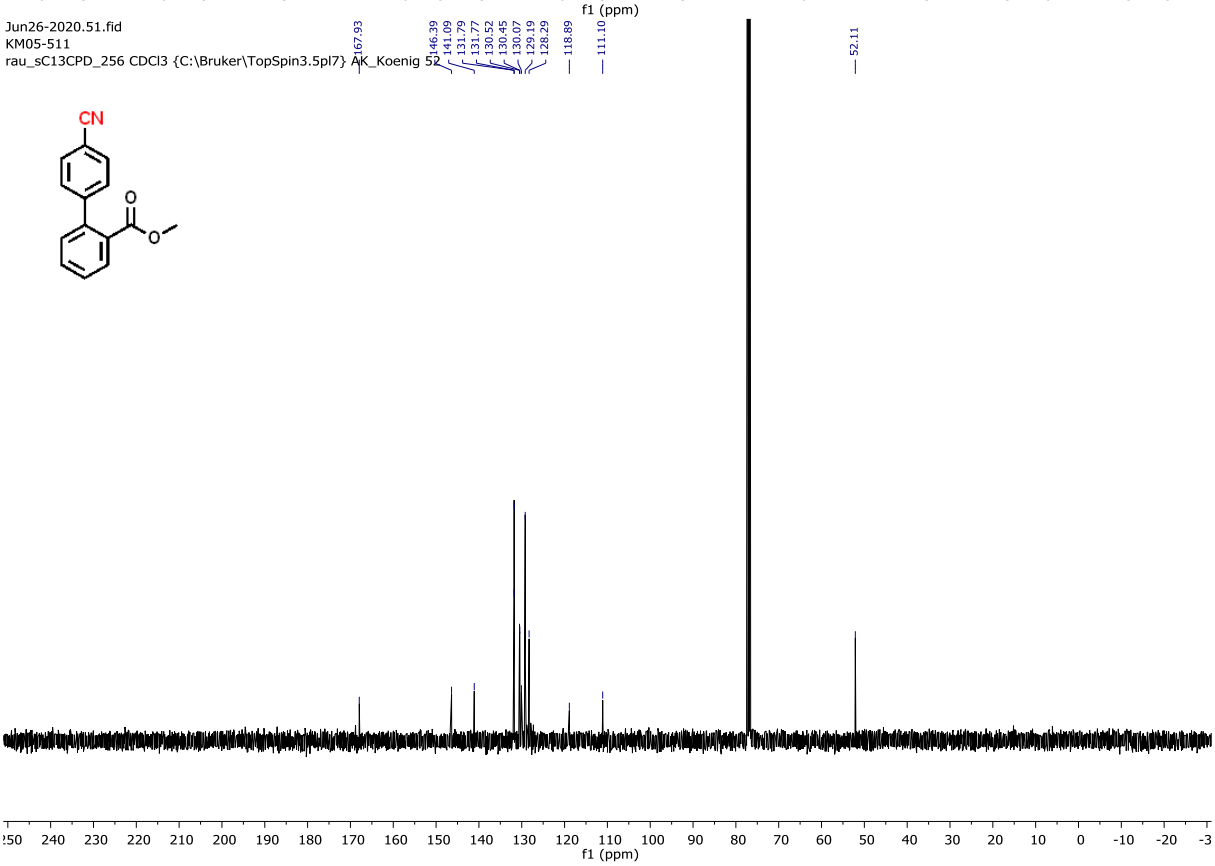

Jun12-2020.12.fid
KM05-499
rau_sPROTON_64 CDCl3 {C:\Bruker\TopSpin3.5pl7} AK_Koenig 18

7.58 7.57 7.55 7.54 7.53 7.48 7.48 7.46 7.46 7.44 7.44 7.43 7.42 7.42 7.31 7.31 7.29 7.29 7.28 7.27 7.27 7.26 7.26

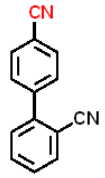

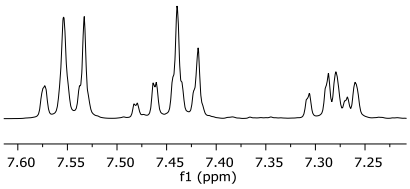

2.82
2.93
2.00

19 18 17 16 15 14 13 12 11 10 9 8 7 6 5 4 3 2 1 0 -1 -2 -3 -4 -5 -6 -7 -8 -9 -10
f1 (ppm)

Jun12-2020.13.fid
KM05-499
rau_sC13CPD_256 CDCl3 {C:\Bruker\TopSpin3.5pl7} AK_Koenig 18

143.33 142.53 133.99 133.20 132.54 129.93 129.59 128.80 118.40 118.03 112.66 111.25

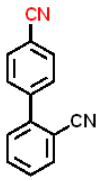

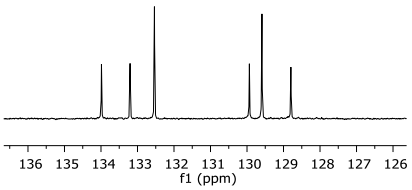

250 240 230 220 210 200 190 180 170 160 150 140 130 120 110 100 90 80 70 60 50 40 30 20 10 0 -10 -20 -3
f1 (ppm)

Jul07-2020.30.fid
KM05-439
rau_sPROTON_64 CDCl3 {C:\Bruker\TopSpin3.0} AK_Koenig 28

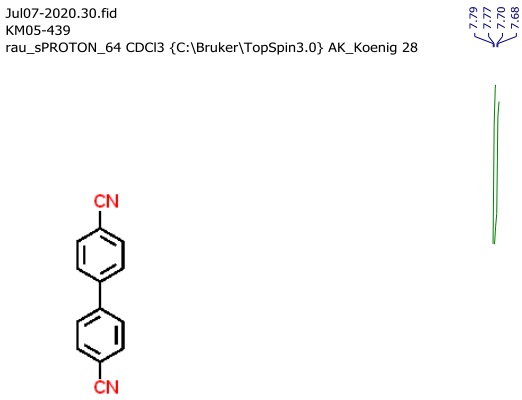

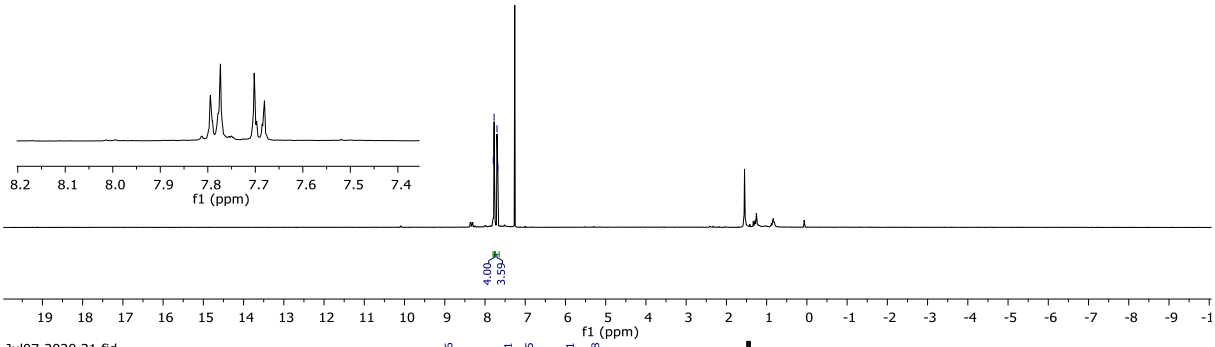

Jul07-2020.31.fid
KM05-439
rau_sC13CPD_256 CDCl3 {C:\Bruker\TopSpin3.0} AK_Koenig 28

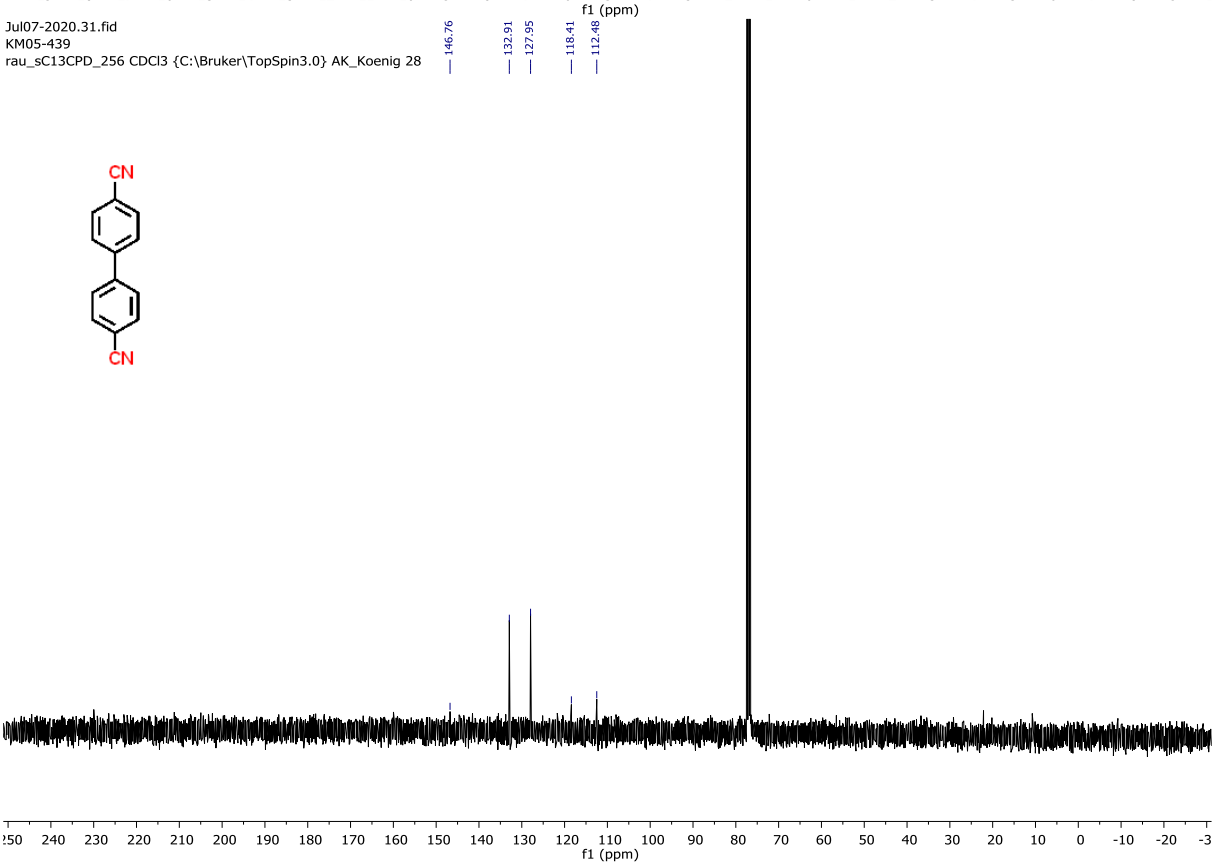

Jul15-2020.120.fid
KM05-587
rau_sPROTON_16 CDCl3 {C:\Bruker\TopSpin3.0} AK_Koenig 22

8.58 8.58 8.58 8.56 8.56 8.55 8.22 8.17 8.15 7.83 7.82 7.82 7.81 7.80 7.80 7.68 7.68 7.67 7.66 7.66 7.65 7.64 7.48 7.48 7.46 7.46 7.46 7.44 7.44

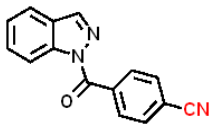

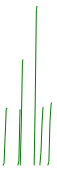

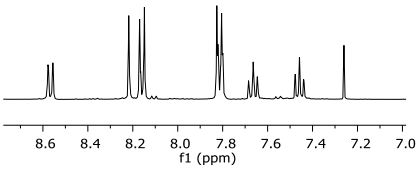

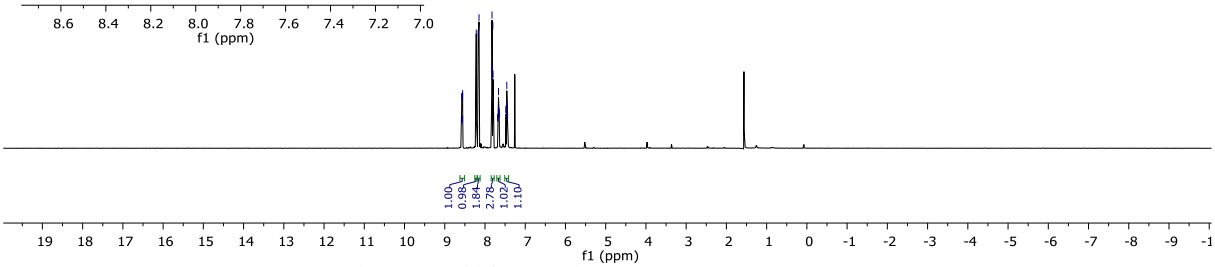

Jul15-2020.121.fid
KM05-587
rau_sC13CPD_256 CDCl3 {C:\Bruker\TopSpin3.0} AK_Koenig 22

166.57

141.22 139.96 137.36 131.74 131.38 130.03 126.28 125.45 121.21 118.06 115.93 115.53

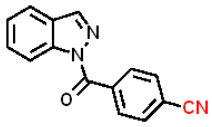

Jun30-2020.80.fid
KM05-529
rau_sPROTON_64 CDCl3 {C:\Bruker\TopSpin3.5pl7} AK_Koenig 40

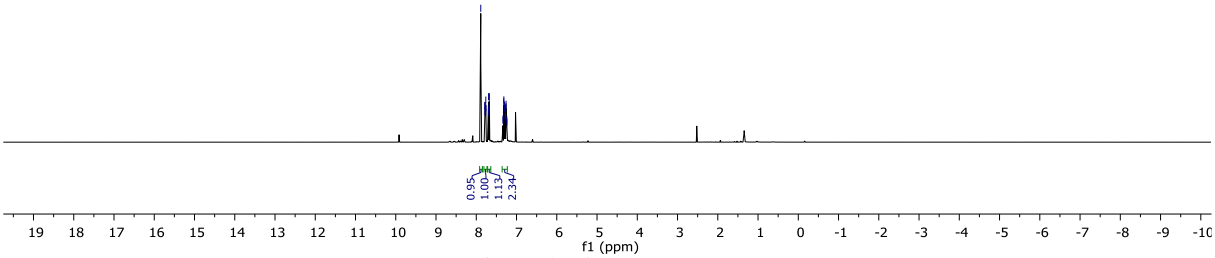

Jun30-2020.82.fid
KM05-529
rau_sC13CPD_256 CDCl3 {C:\Bruker\TopSpin3.5pl7} AK_Koenig 40

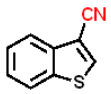

Jun26-2020.10.fid
KM05-505
rau_sPROTON_16 CDCl3 {C:\Bruker\TopSpin3.5pl7} AK_Koenig 48

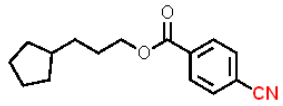

Jun26-2020.11.fid
KM05-505
rau_sC13CPD_256 CDCl3 {C:\Bruker\TopSpin3.5pl7} AK_Koenig 48

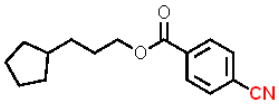

Jun08-2020.20.fid
KM05-476
rau_sPROTON_64 CDCl3 {C:\Bruker\TopSpin3.5pl7} AK_Koenig 27

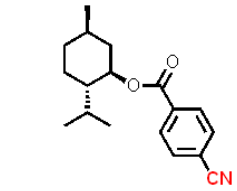

Jun08-2020.21.fid
KM05-476
rau_sC13CPD_256 CDCl3 {C:\Bruker\TopSpin3.5pl7} AK_Koenig 27

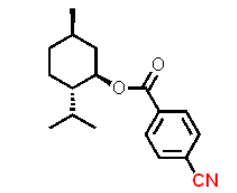

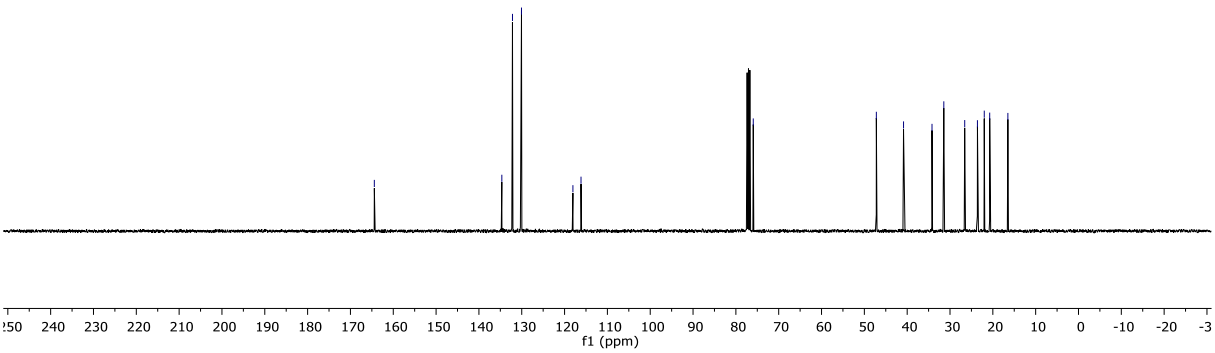

Jun23-2020.40.fid
KM05-502
rau_sPROTON_64 CDCl3 {C:\Bruker\TopSpin3.0} AK_Koenig 22

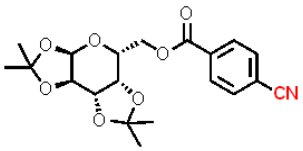

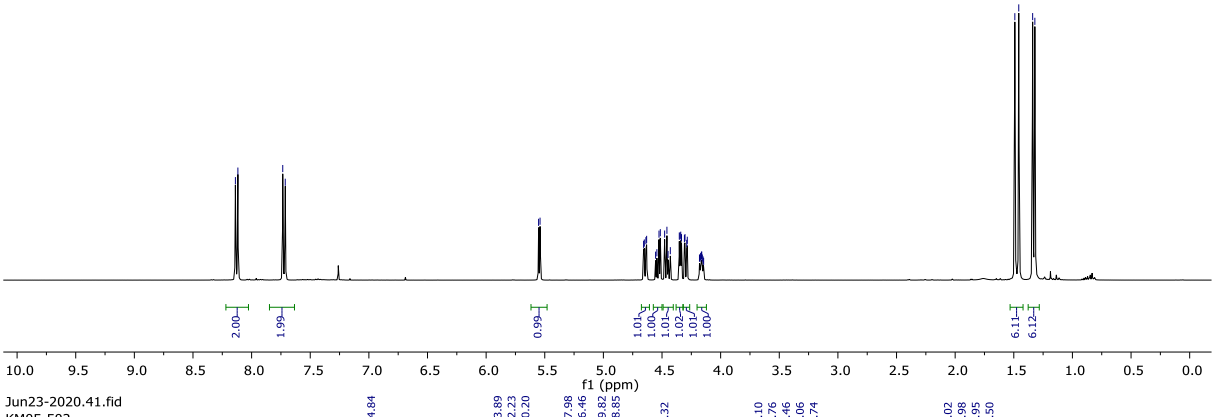

Jun23-2020.41.fid
KM05-502
rau_sC13CPD_256 CDCl3 {C:\Bruker\TopSpin3.0} AK_Koenig 22

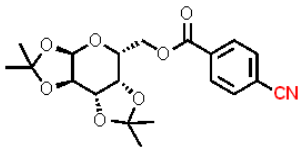

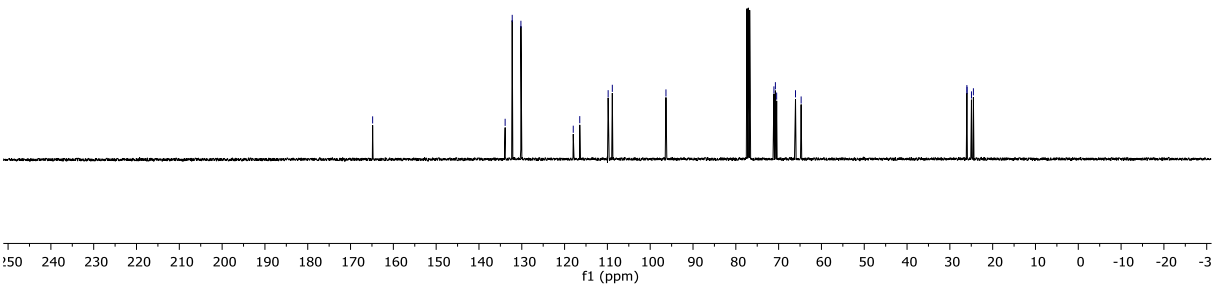

Jun25-2020.80.fid
KM05-503
rau_sPROTON_16 CDCl3 {C:\Bruker\TopSpin3.5pl7} AK_Koenig 47

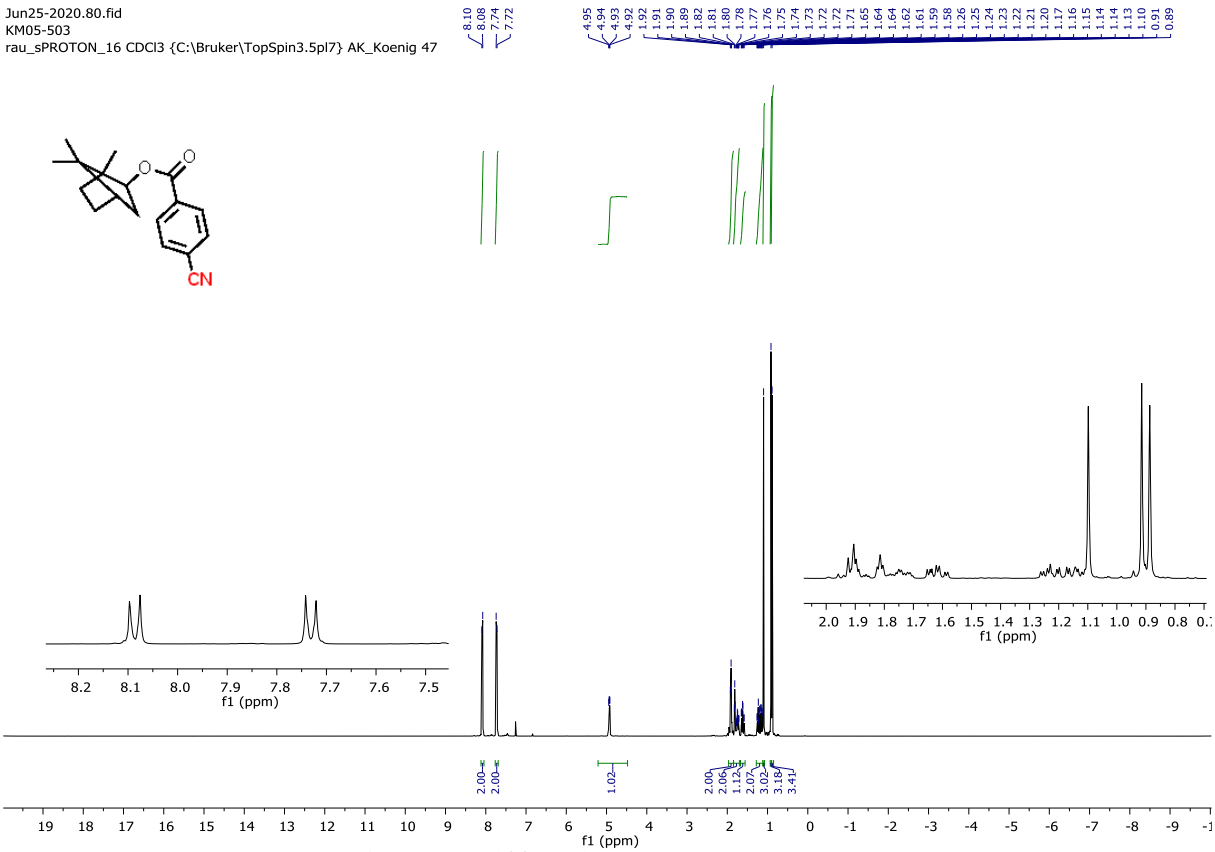

Jun25-2020.81.fid
KM05-503
rau_sC13CPD_256 CDCl3 {C:\Bruker\TopSpin3.5pl7} AK_Koenig 47

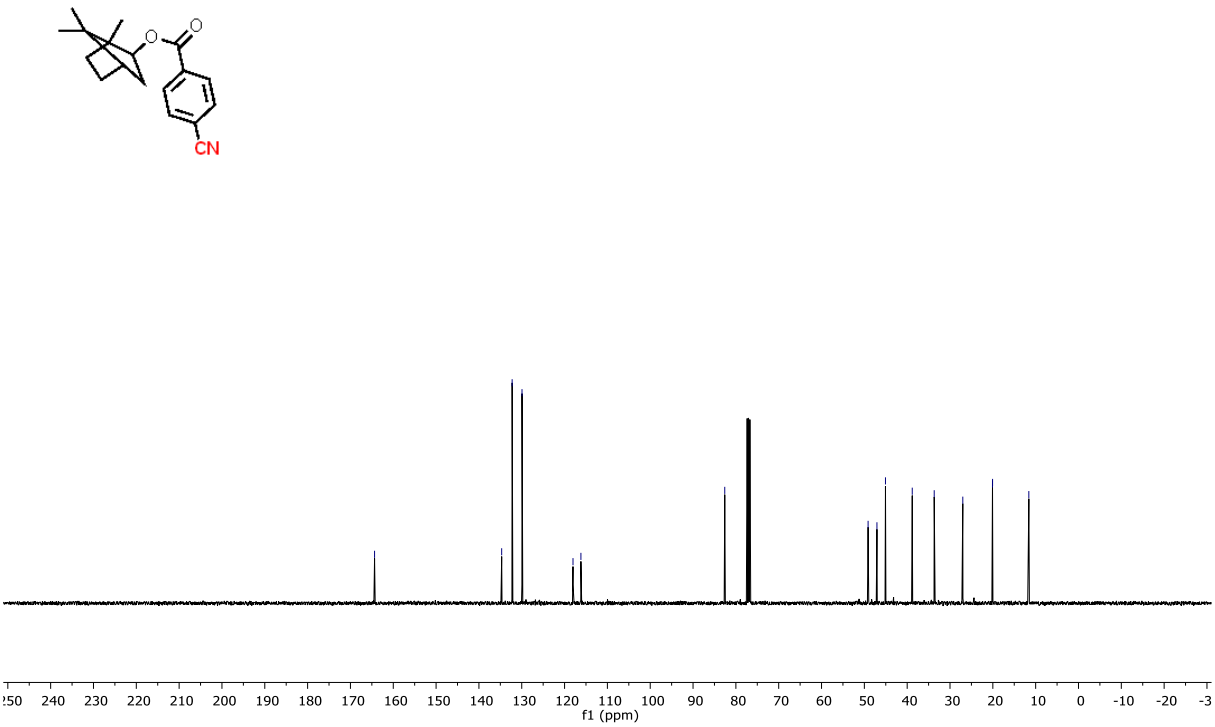

Jun26-2020.20.fid
KM05-506
rau_sPROTON_16 CDCl3 {C:\Bruker\TopSpin3.5pl7} AK_Koenig 49

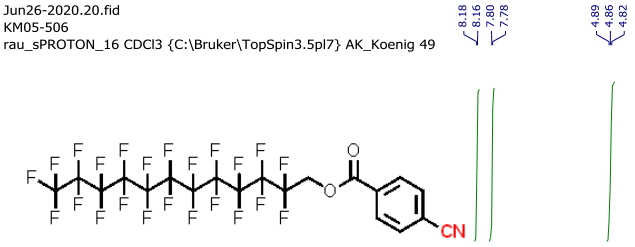

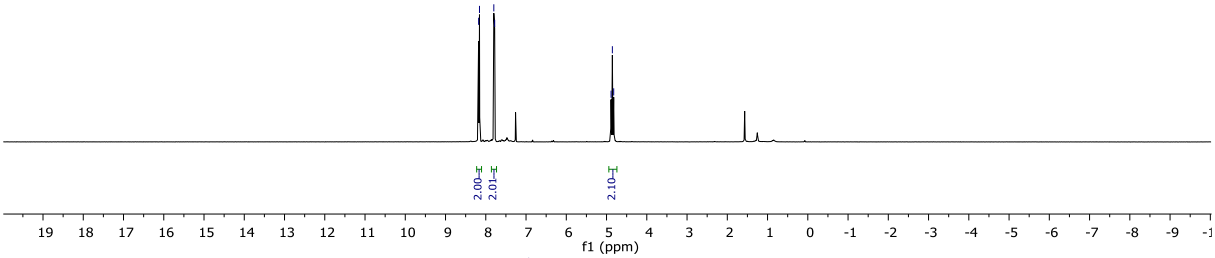

Jun26-2020.21.fid
KM05-506
rau_sC13CPD_256 CDCl3 {C:\Bruker\TopSpin3.5pl7} AK_Koenig 49

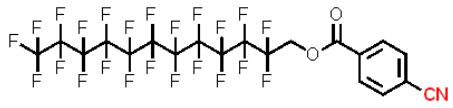

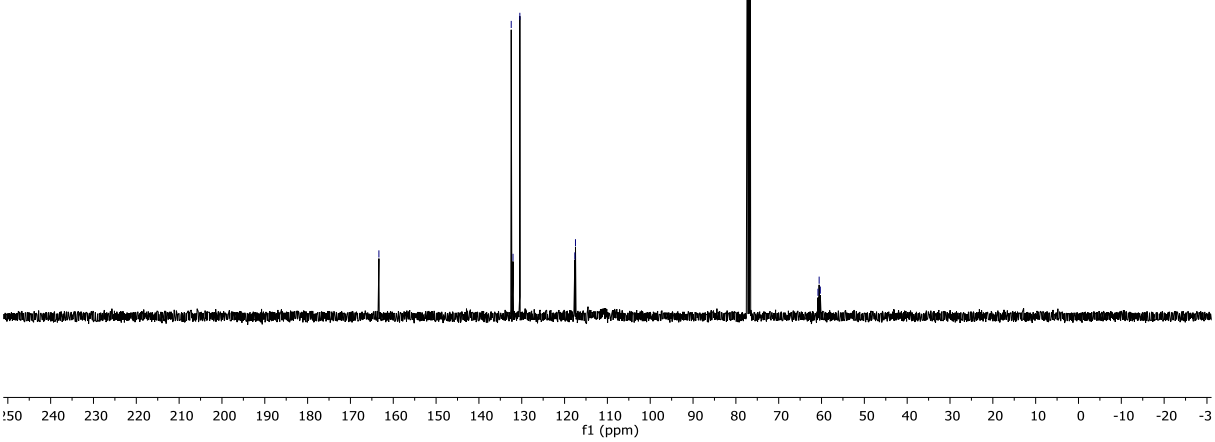

Jun30-2020.92.fid
KM05-506
rau_F19CPD CDCl3 {C:\Bruker\TOPSPIN2.1PL3} AK_Koenig 55

-81.31
-81.35
-81.38

-119.79
-119.83
-119.85
-119.88
-122.29
-122.29
-122.46
-123.28
-123.28
-123.68
-123.68
-126.64
-126.66
-126.69
-126.70
-126.71
-126.74

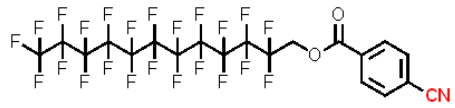

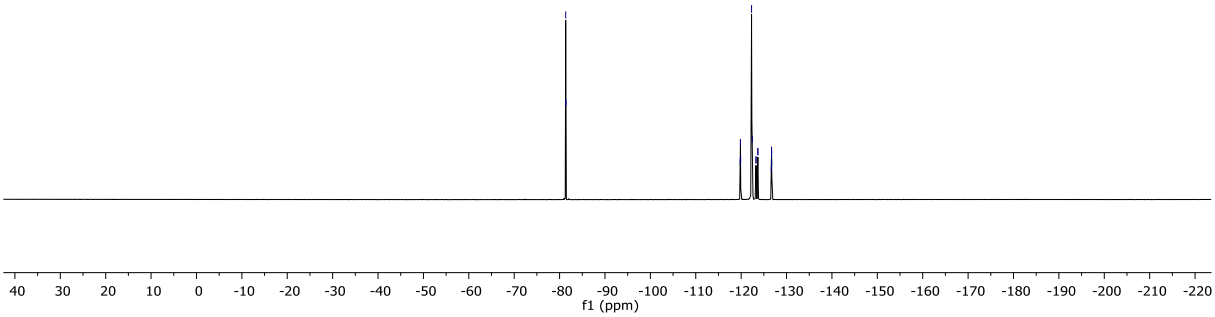

Jun26-2020.30.fid
KM05-507
rau_sPROTON_16 CDCl3 {C:\Bruker\TopSpin3.5pl7} AK_Koenig 50

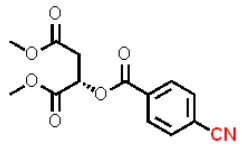

Jun26-2020.31.fid
KM05-507
rau_sC13CPD_256 CDCl3 {C:\Bruker\TopSpin3.5pl7} AK_Koenig 50

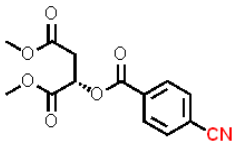

Jun23-2020.50.fid
KM05-509
rau_sPROTON_64 CDCl3 {C:\Bruker\TopSpin3.0} AK_Koenig 23

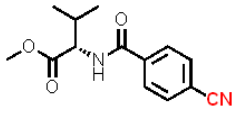

Jun23-2020.51.fid
KM05-509
rau_sC13CPD_256 CDCl3 {C:\Bruker\TopSpin3.0} AK_Koenig 23

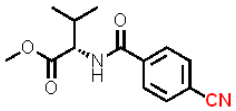

Jul17-2020.100.fid
KM05-590-F2
rau_sPROTON_16 DMSO {C:\Bruker\TopSpin3.0} AK_Koenig 37

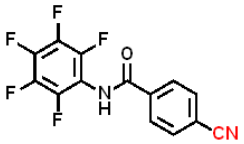

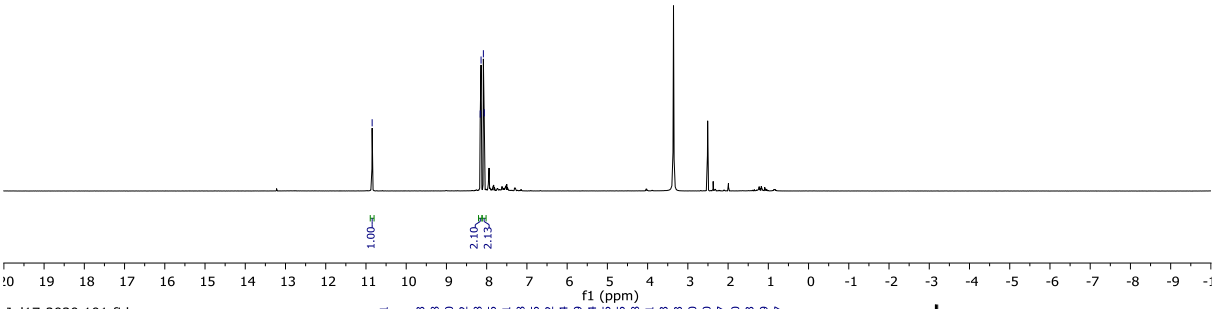

Jul17-2020.101.fid
KM05-590-F2
rau_sC13CPD_256 DMSO {C:\Bruker\TopSpin3.0} AK_Koenig 37

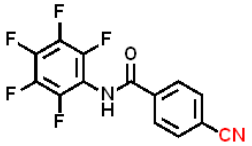

Jul17-2020.102.fid
KM05-590-F2
rau_sF19CPD DMSO {C:\Bruker\TopSpin3.0} AK_Koenig 37

-144.63
-144.68
-156.32
-156.39
-156.45
-162.59
-162.64
-162.65
-162.70

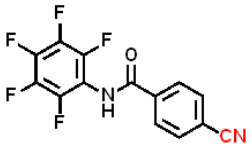

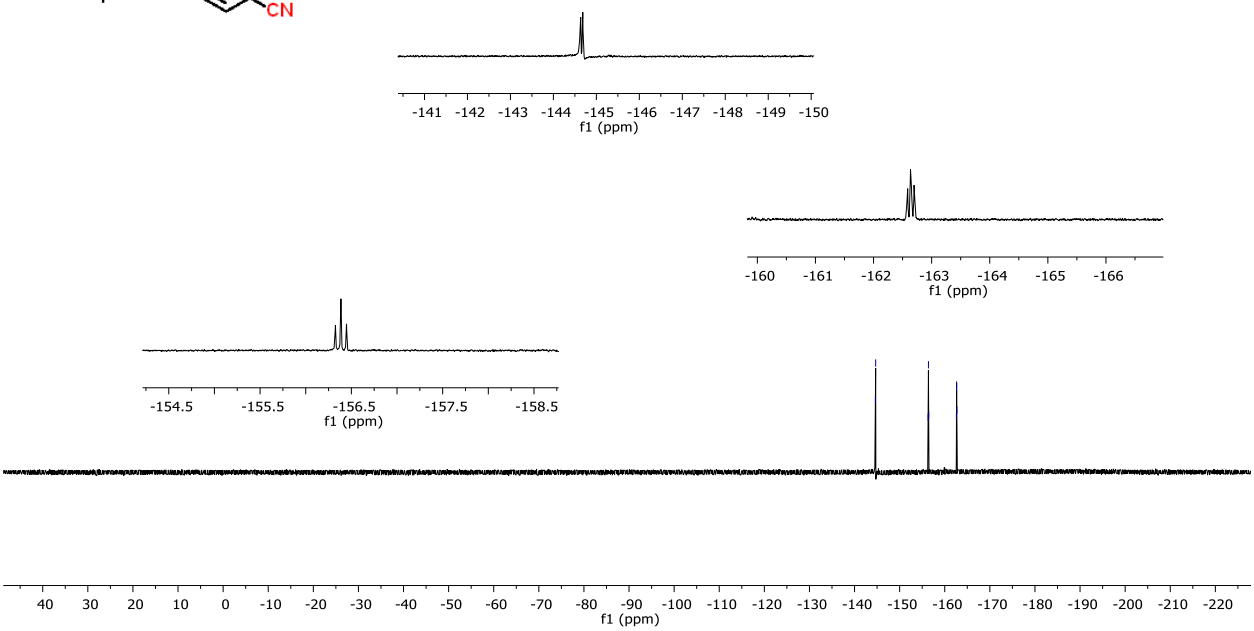

Jul28-2020.40.fid
KM05-501
rau_sPROTON_16 CDCl3 {C:\Bruker\TopSpin3.0} AK_Koenig 19

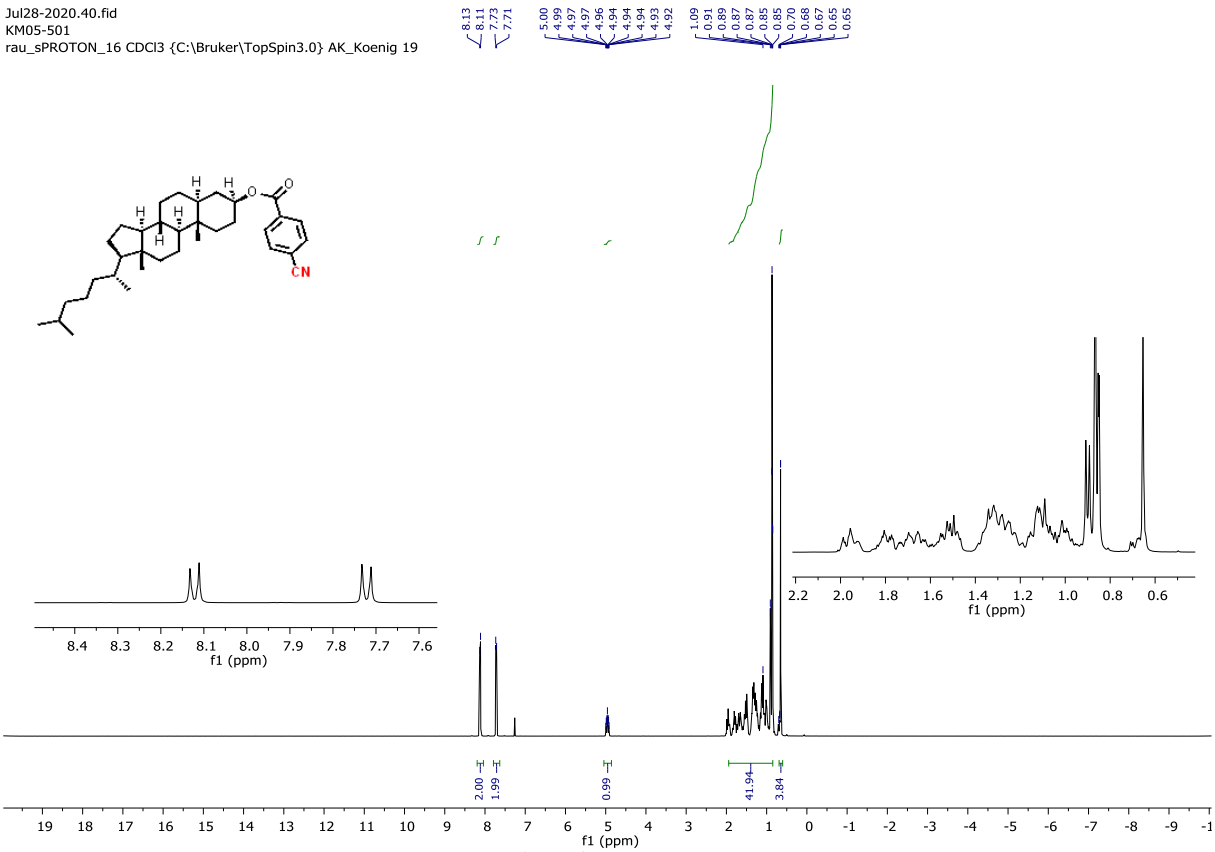

Jul28-2020.41.fid
KM05-501
rau_sC13CPD_256 CDCl3 {C:\Bruker\TopSpin3.0} AK_Koenig 19

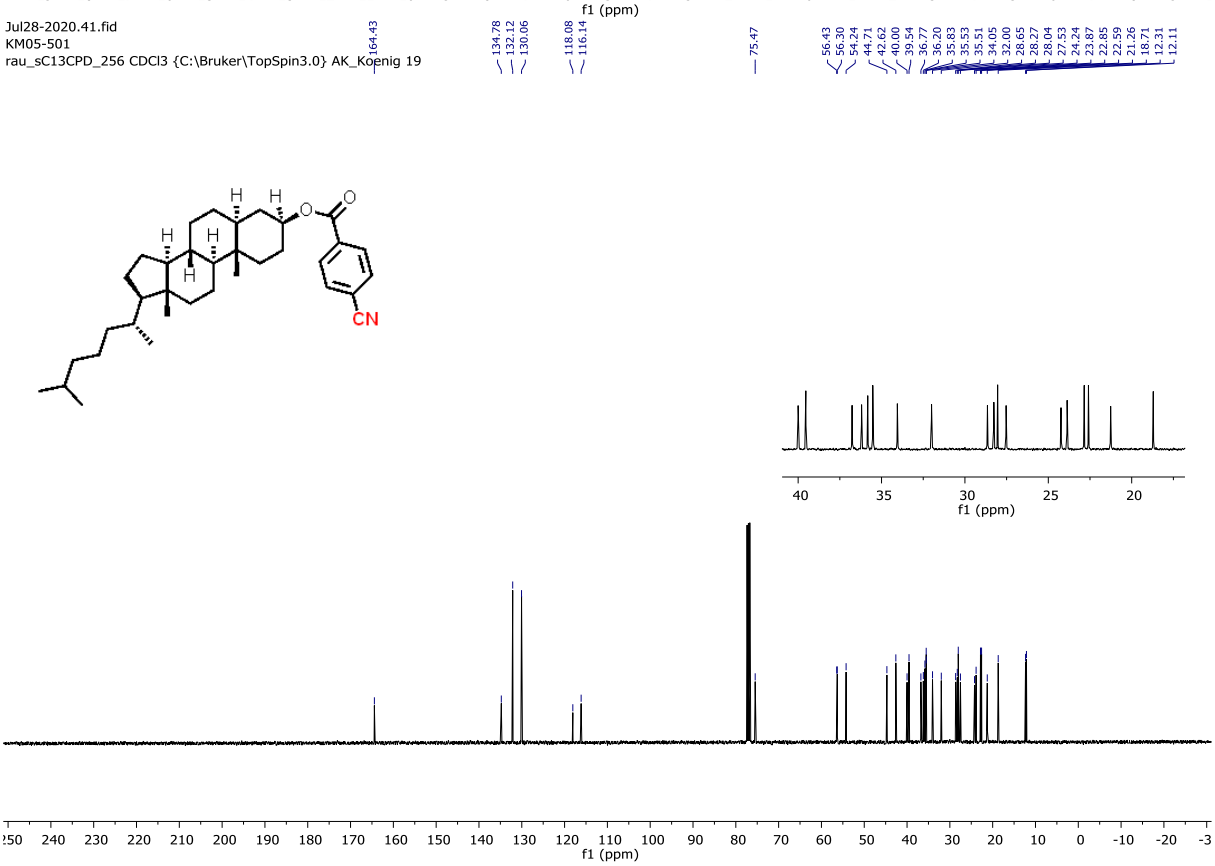

Jun30-2020.100.fid
KM05-513
rau_PROTONLF_16 CDCl3 {C:\Bruker\TOPSPIN2.1PL3} AK_Koenig 56

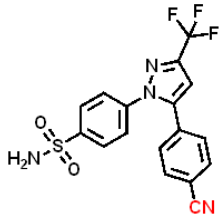

Jul28-2020.10.fid
KM05-513-CDCl3
rau_sC13CPD_1k CDCl3 {C:\Bruker\TopSpin3.0} AK_Koenig 7

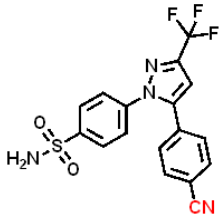

Jul01-2020.32.fid
KM05-513
rau_sF19CPD CDCl3 {C:\Bruker\TopSpin3.0} AK_Koenig 18

-63.03

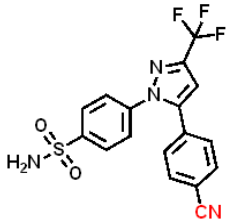

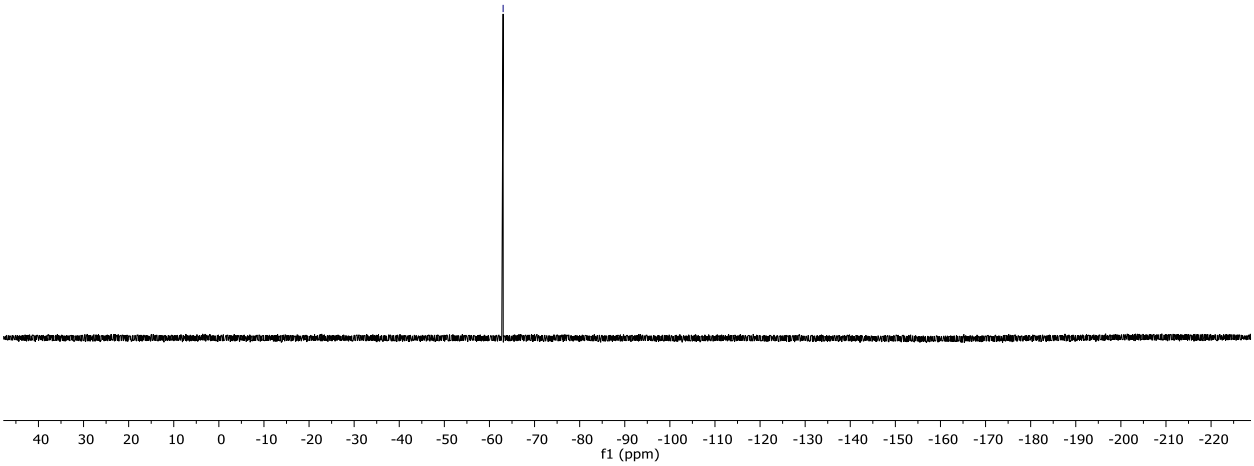

Jul13-2020.100.fid
KM05-580
rau_sPROTON_64 CDCl3 {C:\Bruker\TopSpin3.5pl7} AK_Koenig 39

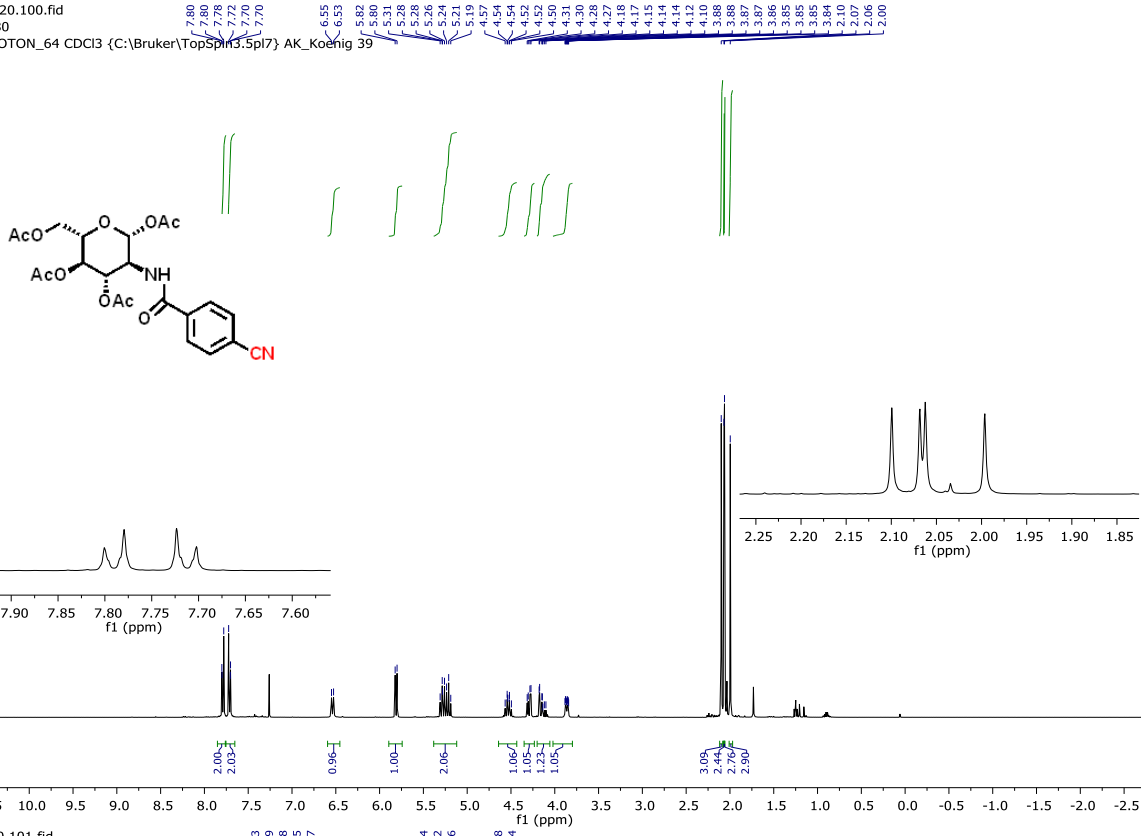

Jul13-2020.101.fid
KM05-580
rau_sC13CPD_256 CDCl3 {C:\Bruker\TopSpin3.5pl7} AK_Koenig 39

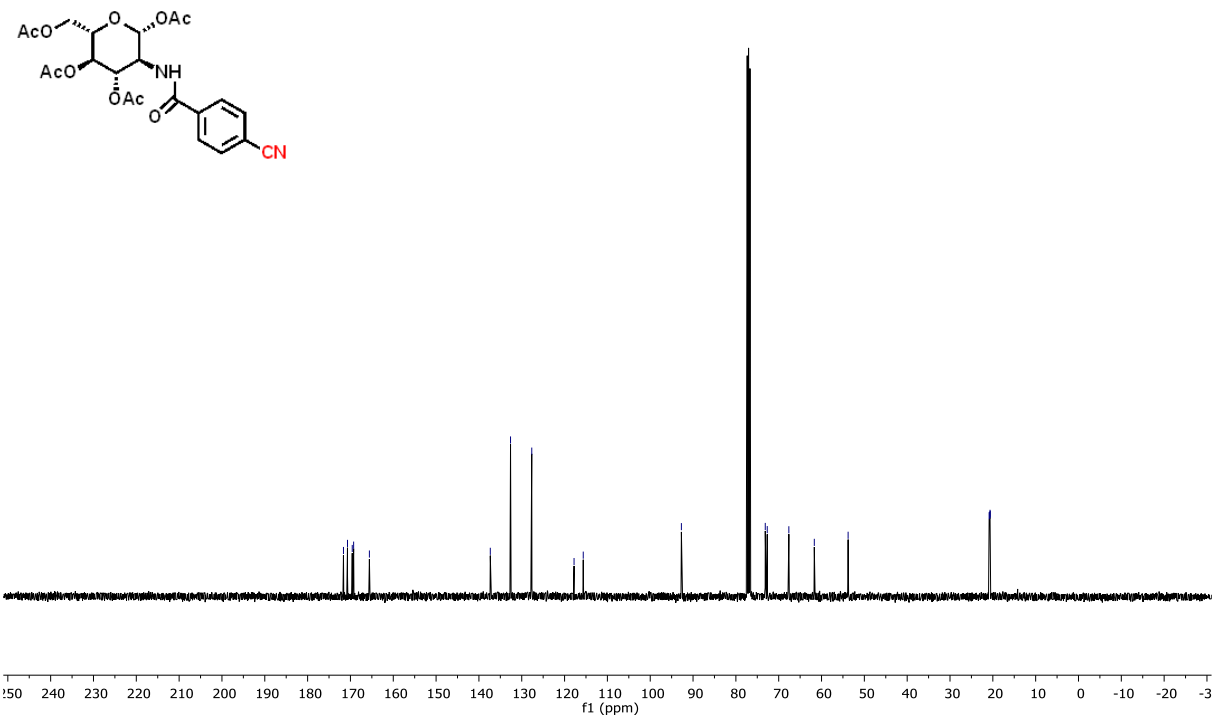

Jul03-2020.60.fid
KM05-540
rau_sPROTON_64 CDCl3 {C:\Bruker\TopSpin3.5pl7} AK_Koenig 50

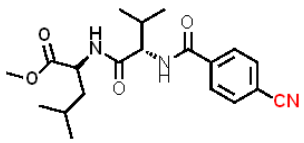

Jul03-2020.61.fid
KM05-540
rau_sC13CPD_256 CDCl3 {C:\Bruker\TopSpin3.5pl7} AK_Koenig 50

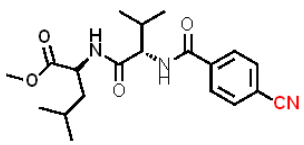

Jul24-2020.100.fid
KM05-599
rau_sPROTON_16 CDCl3 {C:\Bruker\TopSpin3.5pl7} AK_Koenig 47

Jul24-2020.101.fid
KM05-599
rau_sC13CPD_256 CDCl3 {C:\Bruker\TopSpin3.5pl7} AK_Koenig 47

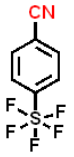

Jul23-2020.70.fid
KM05-597
rau_sPROTON_16 CDCl3 {C:\Bruker\TopSpin3.5pl7} AK_Koenig 41

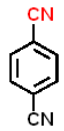

Jul23-2020.71.fid
KM05-597
rau_sC13CPD_256 CDCl3 {C:\Bruker\TopSpin3.5pl7} AK_Koenig 41

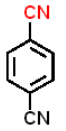

Jul21-2020.120.fid
KM05-612
rau_sPROTON_16 CDCl3 {C:\Bruker\TopSpin3.5pl7} AK_Koenig 28

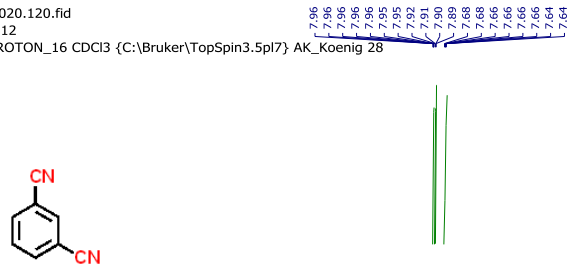

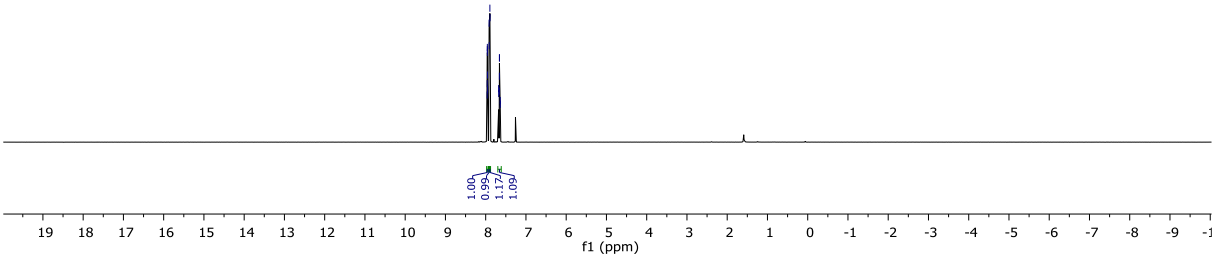

Jul21-2020.121.fid
KM05-612
rau_sC13CPD_256 CDCl3 {C:\Bruker\TopSpin3.5pl7} AK_Koenig 28

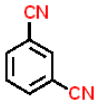

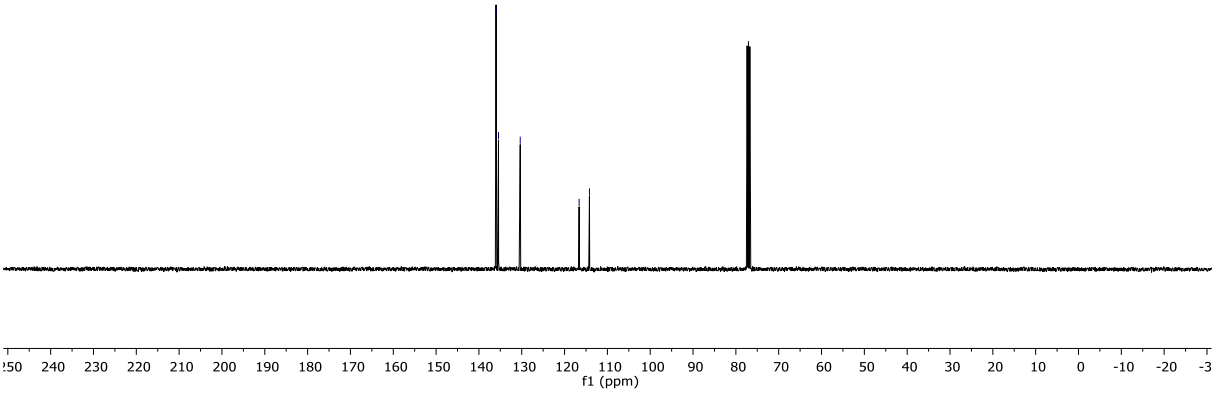

Jul21-2020.100.fid
KM05-609
rau_sPROTON_16 CDCl3 {C:\Bruker\TopSpin3.5pl7} AK_Koenig 26

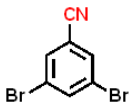

Jul27-2020.40.fid
KM05-609
rau_sC13CPD_256 CDCl3 {C:\Bruker\TopSpin3.5pl7} AK_Koenig 15

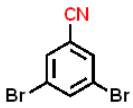

Jul21-2020.110.fid
KM05-610
rau_sPROTON_16 CDCl3 {C:\Bruker\TopSpin3.5pl7} AK_Koenig 27

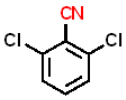

Jul27-2020.50.fid
KM05-610
rau_sC13CPD_256 CDCl3 {C:\Bruker\TopSpin3.5pl7} AK_Koenig 16

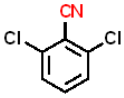

Jul23-2020.80.fid
KM05-604
rau_sPROTON_16 CDCl3 {C:\Bruker\TopSpin3.5pl7} AK_Koenig 42

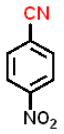

Jul23-2020.81.fid
KM05-604
rau_sC13CPD_256 CDCl3 {C:\Bruker\TopSpin3.5pl7} AK_Koenig 42

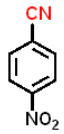

7. References

1. NMR nomenclature: nuclear spin properties and conventions for chemical shifts. IUPAC recommendations 2001. Prepared for publication by Robin K. Harris, Edwin D. Becker, Sonia M. Cabral de Menezes, Robin Goodfellow and Pierre Granger Magn. Reson. Chem. 2002; 40: 489–505. **2002,** *40*, 622-622, doi:10.1002/mrc.1079
2. Fulmer, G. R.; Miller, A. J. M.; Sherden, N. H.; Gottlieb, H. E.; Nudelman, A.; Stoltz, B. M.; Bercaw, J. E.; Goldberg, K. I., NMR Chemical Shifts of Trace Impurities: Common Laboratory Solvents, Organics, and Gases in Deuterated Solvents Relevant to the Organometallic Chemist. *Organometallics* **2010,** *29*, 2176-2179, doi:10.1021/om100106e
3. Shen, Y.; Gu, Y.; Martin, R., sp3 C–H Arylation and Alkylation Enabled by the Synergy of Triplet Excited Ketones and Nickel Catalysts. *J. Am. Chem. Soc.* **2018,** *140*, 12200-12209, doi:10.1021/jacs.8b07405
4. Simoni, D.; Rondanin, R.; Baruchello, R.; Rizzi, M.; Grisolia, G.; Eleopra, M.; Grimaudo, S.; Cristina, A. D.; Pipitone, M. R.; Bongiorno, M. R.; Aricò, M.; Invidiata, F. P.; Tolomeo, M., Novel Terphenyls and 3,5-Diaryl Isoxazole Derivatives Endowed with Growth Supporting and Antiapoptotic Properties. *J. Med. Chem.* **2008,** *51*, 4796-4803, doi:10.1021/jm800388m
5. Romero, N. A.; Margrey, K. A.; Tay, N. E.; Nicewicz, D. A., Site-selective arene C-H amination via photoredox catalysis. *Science* **2015,** *349*, 1326-1330, doi:10.1126/science.aac9895 %J Science
6. Pavlishchuk, V. V.; Addison, A. W., Conversion constants for redox potentials measured versus different reference electrodes in acetonitrile solutions at 25°C. *Inorg. Chim. Acta* **2000,** *298*, 97-102, doi:https://doi.org/10.1016/S0020-1693(99)00407-7
7. Ovian, J. M.; Kelly, C. B.; Pistritto, V. A.; Leadbeater, N. E., Accessing N-Acyl Azoles via Oxoammonium Salt-Mediated Oxidative Amidation. *Org. Lett.* **2017,** *19*, 1286-1289, doi:10.1021/acs.orglett.7b00060
8. Dai, P.-F.; Ning, X.-S.; Wang, H.; Cui, X.-C.; Liu, J.; Qu, J.-P.; Kang, Y.-B., Cleavage of C(aryl)−CH3 Bonds in the Absence of Directing Groups under Transition Metal Free Conditions. *Angew. Chem. Int. Ed.* **2019,** *58*, 5392-5395, doi:10.1002/anie.201901783
9. Wybon, C. C. D.; Mensch, C.; Hollanders, K.; Gadais, C.; Herrebout, W. A.; Ballet, S.; Maes, B. U. W., Zn-Catalyzed tert-Butyl Nicotinate-Directed Amide Cleavage as a Biomimic of Metallo-Exopeptidase Activity. *ACS Catal.* **2018,** *8*, 203-218, doi:10.1021/acscatal.7b02599
10. Tu, G.; Yan, Y.; Chen, X.; Lv, Q.; Wang, J.; Li, S., Synthesis and Antiproliferative Assay of 1,3,4-Oxadiazole and 1,2,4-Triazole Derivatives in Cancer Cells. *Drug discoveries & therapeutics* **2013,** *7*, 58-65, doi:10.5582/ddt.2013.v7.2.58
11. Lam, K.; Markó, I. E., Using Toluates as Simple and Versatile Radical Precursors. *Org. Lett.* **2008,** *10*, 2773-2776, doi:10.1021/ol800944p
12. Kong, H.; Chen, W.; Lu, H.; Yang, Q.; Dong, Y.; Wang, D.; Zhang, J., Synthesis of NAG-thiazoline-derived inhibitors for β-N-acetyl-d-hexosaminidases. *Carbohydr. Res.* **2015,** *413*, 135-144, doi:https://doi.org/10.1016/j.carres.2015.06.004
13. Kasprzak, A.; Bystrzejewski, M.; Koszytkowska-Stawinska, M.; Poplawska, M., Grinding-induced functionalization of carbon-encapsulated iron nanoparticles. *Green Chem.* **2017,** *19*, 3510-3514, doi:10.1039/C7GC00282C
14. Vo, Q. V.; Trenerry, C.; Rochfort, S.; Wadeson, J.; Leyton, C.; Hughes, A. B., Synthesis and anti-inflammatory activity of aromatic glucosinolates. *Biorg. Med. Chem.* **2013,** *21*, 5945-5954, doi:https://doi.org/10.1016/j.bmc.2013.07.049
15. Schwarz, L.; Girreser, U.; Clement, B., Synthesis and Characterization of para-Substituted N,N′-Dihydroxybenzamidines and Their Derivatives as Model Compounds for a Class of Prodrugs. *Eur. J. Org. Chem* **2014,** *2014*, 1961-1975, doi:10.1002/ejoc.201301622
16. Li, J.; Okuda, Y.; Zhao, J.; Mori, S.; Nishihara, Y., Skeletal Rearrangement of Cyano-Substituted Iminoisobenzofurans into Alkyl 2-Cyanobenzoates Catalyzed by B(C6F5)3. *Org. Lett.* **2014,** *16*, 5220-5223, doi:10.1021/ol5026519
17. Sridhar, A.; Swarnalakshmi, S.; Selvaraj, M., Oxidative Esterification of Aromatic Aldehydes Using Polymer-Supported Green Bromine. *Synlett* **2016,** *27*, 1344-1348, doi:10.1055/s-0035-1561347
18. Fang, W.-Y.; Qin, H.-L., Cascade Process for Direct Transformation of Aldehydes (RCHO) to Nitriles (RCN) Using Inorganic Reagents NH2OH/Na2CO3/SO2F2 in DMSO. *J. Org. Chem.* **2019,** *84*, 5803-5812, doi:10.1021/acs.joc.8b03164

19. Liu, Y.-Y.; Liang, D.; Lu, L.-Q.; Xiao, W.-J., Practical heterogeneous photoredox/nickel dual catalysis for C–N and C–O coupling reactions. *Chem. Commun.* **2019,** *55*, 4853-4856, doi:10.1039/C9CC00987F
20. Ma, C.; Zhao, C.-Q.; Xu, X.-T.; Li, Z.-M.; Wang, X.-Y.; Zhang, K.; Mei, T.-S., Nickel-Catalyzed Carboxylation of Aryl and Heteroaryl Fluorosulfates Using Carbon Dioxide. *Org. Lett.* **2019,** *21*, 2464-2467, doi:10.1021/acs.orglett.9b00836
21. Liu, M.; Li, C.-J., Catalytic Fehling's Reaction: An Efficient Aerobic Oxidation of Aldehyde Catalyzed by Copper in Water. *Angew. Chem. Int. Ed.* **2016,** *55*, 10806-10810, doi:10.1002/anie.201604847
22. Mane, R. S.; Bhanage, B. M., Pd/C-catalyzed facile synthesis of primary aromatic amides by aminocarbonylation of aryl iodides using ammonia surrogates. *RSC Adv.* **2015,** *5*, 76122-76127, doi:10.1039/C5RA15831A
23. Mills, L. R.; Graham, J. M.; Patel, P.; Rousseaux, S. A. L., Ni-Catalyzed Reductive Cyanation of Aryl Halides and Phenol Derivatives via Transnitrilation. *J. Am. Chem. Soc.* **2019,** *141*, 19257-19262, doi:10.1021/jacs.9b11208
24. Wang, L.; Li, J.; Cui, X.; Wu, Y.; Zhu, Z.; Wu, Y., Cyclopalladated Ferrocenylimine as Efficient Catalyst for the Syntheses of Arylboronate Esters. *Adv. Synth. Catal.* **2010,** *352*, 2002-2010, doi:10.1002/adsc.201000085
25. Liu, J.; Zheng, H.-X.; Yao, C.-Z.; Sun, B.-F.; Kang, Y.-B., Pharmaceutical-Oriented Selective Synthesis of Mononitriles and Dinitriles Directly from Methyl(hetero)arenes: Access to Chiral Nitriles and Citalopram. *J. Am. Chem. Soc.* **2016,** *138*, 3294-3297, doi:10.1021/jacs.6b00180
26. Shu, Z.; Ye, Y.; Deng, Y.; Zhang, Y.; Wang, J., Palladium(II)-Catalyzed Direct Conversion of Methyl Arenes into Aromatic Nitriles. *Angew. Chem., Int. Ed.* **2013,** *52*, 10573-10576, doi:10.1002/anie.201305731
27. Varga, N.; Sutkeviciute, I.; Guzzi, C.; McGeagh, J.; Petit-Haertlein, I.; Gugliotta, S.; Weiser, J.; Angulo, J.; Fieschi, F.; Bernardi, A., Selective Targeting of Dendritic Cell-Specific Intercellular Adhesion Molecule-3-Grabbing Nonintegrin (DC-SIGN) with Mannose-Based Glycomimetics: Synthesis and Interaction Studies of Bis(benzylamide) Derivatives of a Pseudomannobioside. *Chem. Eur. J.* **2013,** *19*, 4786-4797, doi:10.1002/chem.201202764
28. Nagaki, A.; Hirose, K.; Moriwaki, Y.; Mitamura, K.; Matsukawa, K.; Ishizuka, N.; Yoshida, J., Integration of borylation of aryllithiums and Suzuki–Miyaura coupling using monolithic Pd catalyst. *Catal. Sci. Technol.* **2016,** *6*, 4690-4694, doi:10.1039/C5CY02098K
29. Ahmed, J.; Chakraborty, S.; Jose, A.; P, S.; Mandal, S. K., Integrating Organic Lewis Acid and Redox Catalysis: The Phenalenyl Cation in Dual Role. *J. Am. Chem. Soc.* **2018,** *140*, 8330-8339, doi:10.1021/jacs.8b04786
30. Morioka, T.; Nakatani, S.; Sakamoto, Y.; Kodama, T.; Ogoshi, S.; Chatani, N.; Tobisu, M., Nickel-catalyzed decarbonylation of N-acylated N-heteroarenes. *Chem. Sci.*, **2019,** *10*, 6666-6671, doi:10.1039/C9SC02035G
31. Krasik, P., Synthesis of sterically hindered esters via titanium catalyzed transesterification. *Tetrahedron Lett.* **1998,** *39*, 4223-4226, doi:https://doi.org/10.1016/S0040-4039(98)00790-4
32. Shigeno, M.; Hayashi, K.; Nozawa-Kumada, K.; Kondo, Y., Phosphazene Base tBu-P4 Catalyzed Methoxy–Alkoxy Exchange Reaction on (Hetero)Arenes. *Chem. Eur. J.* **2019,** *25*, 6077-6081, doi:10.1002/chem.201900498
33. Jin, L.-M.; Lu, H.; Cui, Y.; Lizardi, C. L.; Arzua, T. N.; Wojtas, L.; Cui, X.; Zhang, X. P., Selective radical amination of aldehydic C(sp2)–H bonds with fluoroaryl azides via Co(ii)-based metalloradical catalysis: synthesis of N-fluoroaryl amides from aldehydes under neutral and nonoxidative conditions. *Chem. Sci.*, **2014,** *5*, 2422-2427, doi:10.1039/C4SC00697F
34. Ellis-Sawyer, K.; Bragg, R. A.; Bushby, N.; Elmore, C. S.; Hickey, M. J., Isotope labelling by reduction of nitriles: Application to the synthesis of isotopologues of tolmetin and celecoxib. *J Label Compd Radiopharm.* **2017,** *60*, 213-220, doi:10.1002/jlcr.3492
35. Okazaki, T.; Laali, K. K.; Bunge, S. D.; Adas, S. K., 4-(Pentafluorosulfanyl)benzenediazonium Tetrafluoroborate: A Versatile Launch Pad for the Synthesis of Aromatic SF5 Compounds via Cross Coupling, Azo Coupling, Homocoupling, Dediazoniation, and Click Chemistry. *Eur. J. Org. Chem.* **2014,** *2014*, 1630-1644, doi:10.1002/ejoc.201301538
36. Gurjar, J.; Bater, J.; Fokin, V. V., Sulfuryl Fluoride Mediated Conversion of Aldehydes to Nitriles. *Chem. Eur. J.* **2019,** *25*, 1906-1909, doi:10.1002/chem.201805175
37. Murugesan, K.; Senthamarai, T.; Sohail, M.; Sharif, M.; Kalevaru, N. V.; Jagadeesh, R. V., Stable and reusable nanoscale Fe2O3-catalyzed aerobic oxidation process for the selective synthesis of nitriles and primary amides. *Green Chem.* **2018,** *20*, 266-273, doi:10.1039/c7gc02627g